UMS
UNIVERSITI MALAYSIA SABAH

BORNEO SCIENCE

The Journal of Science and Technology

ONLINE ISSN : 2231-9085 | ISSN : 1394- 4339

BORNEO SCIENCE

A JOURNAL OF SCIENCE AND TECHNOLOGY

BORNEO SCIENCE is a journal of science and technology published twice a year. It publishes original articles on all aspects of research in science and technology of general or regional interest particularly related to Borneo. Manuscripts submitted must not have been published, accepted for publication, or be under consideration elsewhere. Borneo Science welcomes all categories of papers: full research papers, short communications, papers describing novel methods, review papers and book reviews. Views expressed in the articles do not represent those of the Editorial Board and the University.

BORNEO *SCIENCE* *merupakan jurnal sains dan teknologi yang diterbitkan dwitahunan. Jurnal ini menerbitkan artikel asli dalam kesemua bidang sains dan teknologi secara umum mahupun dalam kepentingan serantau, terutamanya yang berkaitan dengan Borneo. Manuskrip yang dihantar bukan yang telah diterbitkan, telah diterima untuk diterbitkan, atau sedang dipertimbangkan untuk diterbitkan. Borneo Science mengalu-alukan semua jenis kertas kerja sama ada hasil penyelidikan, komunikasi pendek, penjelasan suatu kaedah, ulasan kertas kerja atau ulasan buku. Pandangan yang ditulis dalam artikel Borneo Science tidak menggambarkan pendapat Sidang Editor dan Universiti.*

DOI: https://doi.org/10.51200/bsj.v40i1

BORNEO SCIENCE
A JOURNAL OF SCIENCE AND TECHNOLOGY

BORNEO SCIENCE

A JOURNAL OF SCIENCE AND TECHNOLOGY

ONLINE ISSN 2231-9085 | ISSN 1394-4339

BORNEO SCIENCE

A JOURNAL OF SCIENCE AND TECHNOLOGY
JURNAL SAINS DAN TELNOLOGI

Volume 40 Issue 1

March 2019

CONTENT
KANDUNGAN

Page
Muka Surat

ORIGINAL ARTICLES

BorneoScience
The Journal of Science & Technology
Volume 40 Issue 1 : March 2019
Online ISSN : 2231-9085 | ISSN : 1394-4339

MECHANICAL PERFORMANCE OF ACETATE LACQUER FROM *ACACIA MANGIUM*

Melissa Sharmah Gilbert Jesuet, Ismawati Palle & Liew Kang Chiang

Wood Technology and Industry Program, Faculty of Science and Natural Resources (Forestry Complex), Universiti Malaysia Sabah, Jalan UMS, 88400 Kota Kinabalu, Sabah, Malaysia

*Corresponding author ; melissa.gilbert@ums.edu.my

Received 11st February 2019; accepted 11st February 2019
Available online 29th March 2019
Doi: https://doi.org/10.51200/bsj.v40i1.

ABSTRACT. *Cellulose comprises about 40–50 % of the composition of wood, making it one of the most abundant organic polymers on earth. Cellulose is very versatile in terms of application, with a wide array of products fabricated, including the chemically modified cellulose derivatives. One of the more prominent and multifaceted derivatives is the cellulose acetate, in which have been used predominantly as cigarette filters, membrane filters, and coating. In this study, the intermediate product, Acacia mangium-produced cellulose acetate was modified into lacquer to produce a feasible wood coating product. The lacquer underwent a series of tests such as impact, abrasion, adhesion, and hardness to evaluate its mechanical performance. The results of the coating were compared to a similarly formulated acetate lacquer that was produced using commercial cellulose acetate instead as a control. Based on the result, it is shown that Acacia mangium-produced cellulose acetate lacquer shows a better impact resistance with a rating of 4 as opposed to the commercial cellulose acetate with a rating of 3 with moderate cracking, with an approximate 6% better abrasion resistance and higher hardness rating class. Meanwhile, the commercial cellulose acetate lacquer presents a better adhesion performance with only 5% flaking compared to the 15% flaking of Acacia mangium-produced cellulose acetate lacquer. The Acacia mangium-produced cellulose acetate lacquer indicates a novel benefit from the presence of impurities from the intermediate Acacia mangium-produced cellulose acetate product such as the plasticizing hemicellulose acetate, as well as the hydrophobic lignin.*

KEYWORDS. Cellulose acetate, lacquer, wood coating, mechanical properties

INTRODUCTION

Wood has long been utilized primarily as structural components in buildings and furniture. Due to the hygroscopic nature of wood, humidity is one of the conditions avoided for a prolonged utilization but to no avail other than with additional treatments or coating layers. One of the more decorated but functional type of coating is lacquer, a protective coating made out of cellulose esters or resin through the evaporation of solvent, or formerly as a resinous varnish obtained from *Rhus verniciflua* which originated in Japan (Ma *et al*., 2014).

Lacquers are predominantly produced from nitrocellulose, a modified cellulose product where the free hydroxyl groups were substituted from nitro groups from the reagent. Similarly, cellulose esters such as cellulose acetate (CA) are also being developed into lacquers for wood coating. CA has a concomitant resemblance to the nitrocellulose, but with a low to none flammability hazard. CA and other cellulose derivatives are produced from renewable materials such as wood pulp and cotton, making them renewable materials and an environmentally friendly, material-wise, bio-based product (Egot & Alguno, 2018; Cheng *et al*., 2010). In this study, lacquer was produced from *Acacia mangium*-based cellulose acetate (AMCA) and evaluated based on the mechanical performance, which includes the impact, hardness, adhesion, and abrasion test. The properties of the AMCA lacquer will then be compared to the commercial cellulose acetate (CCA) lacquer based on the cellulose acetate coating compositions by Swain et al. (1940), to determine the differences of performance based on the purity of raw materials used in the production of the intermediate AMCA and CCA.

MATERIALS AND METHODS

2.1 Materials

The cellulose acetate produced from *Acacia mangium* pulp was produced from a previously developed acetylation process (Gilbert & Palle, 2013). The commercial cellulose acetate, ethyl acetate, and acetone were obtained from Sigma Aldrich, while the melamine formaldehyde was supplied from Norsechem (Sabah) Sdn. Bhd.

2.2 Lacquer Formulation and Application

The compound for the lacquer was loosely based on the Unites States Patent no. 2426379 by Swain *et al*. (1940). Both types of lacquer; the AMCA and CCA lacquer, followed the same mixture of cellulose acetate, ethyl acetate, acetone, and melamine formaldehyde. It follows a ratio of 1:9 between MF and the cellulose acetate stock solution. The stock solution meanwhile, follows a ratio of 1:5:1 that comprises of cellulose acetate, acetone, and ethyl acetate, respectively, still based on the aforementioned patent. The lacquer solution was then heated at 135˚ C oven for half an hour and left to cool. The lacquer was then applied on *Acacia mangium* blocks (30 x 10 x 1 cm) via brushing technique.

2.3 Mechanical Testing

Standardized double layer of lacquer was applied on the *A. mangium* blocks. A series of performance-intensive mechanical testing was measured on both AMCA and CCA applied lacquer that includes impact resistance, adhesion, abrasion, and hardness test.

2.3.1 Impact Resistance

For this test, the ball drop test was executed. A 1.0 kg ball of steel was dropped onto the surface of the coating from a height of 1.0 meter. Impacts from the ball were evaluated based on the Indian Standard 5807 Part 6 (2002) as in Table 1.

Table 1: Impact Test Rating Code Description

Rating (Code)	Description
1	More than 25% of finish removed from the area of indentation
2	Cracking extending outside the area of the indentation and/or slightly flaking of the finish
3	Moderate or severe cracking confined of the area of indentation
4	Slight cracking e.g: One or two circular around the edge of indentation
5	No surface cracking

(Source: Indian Standard (IS) 5807 Part 6: 1980)

2.3.2 Adhesion

For the adhesion test, the crosscut method based on ASTM D3359 (1997) was used where a lattice pattern is cut into the coating, penetrating fully into the film and substrate. Each line of six (6) must be 1–2 mm apart, where the outcome of the cross-cut test is evaluated based on the principal classifying paint film adhesion in Figure 1.

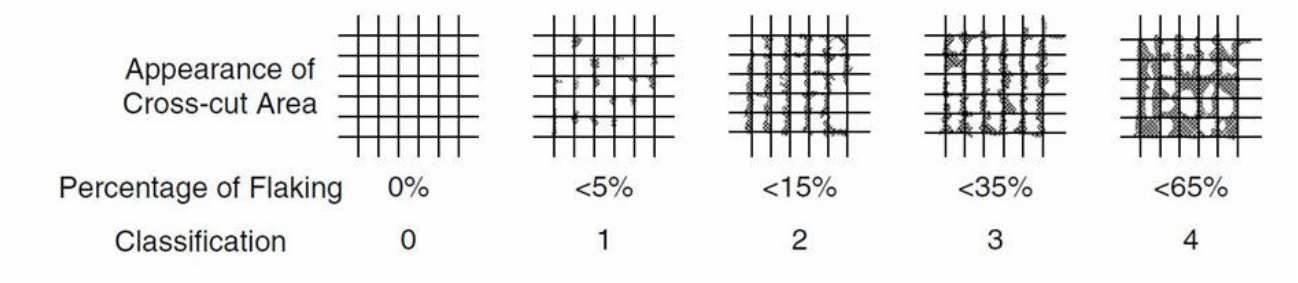

Figure 1: Principle of classifying paint film adhesion in the cross-cut test based on the percentage of flaking.(Source: Zorll 2007)

2.3.3 Abrasion

The abrasion resistance test following Koleske (2006) is a scrub resistance test for the coating (ASTM D2486). Basically, it shows the resistance to changes of its original appearance and structure due to the influence of ablating actions such as rubbing, erosion, and scrapping. For this test, the number of brushing cycles over the same area were accounted until the coating was damaged and surface was exposed.

2.3.4 Hardness

The final test is based on the hardness of the coating (ASTM D3363) where a number of different pencil grade (6B to 6H) was used to try to cut the coat. The eventual result is based on the grade of pencil that could not scratch the surface, just before the pencil grade that could, stipulating the grade of the surface hardness based on the pencil grading.

RESULTS AND DISCUSSION

Raw material plays an important role in the production of any products, especially in the lignocellulosic segment. Abundant and renewable resources such as raw *Acacia mangium* pulp are rarely being prioritized as the primary cellulosic material due to the presence of other impurities such as lignin and hemicellulose, despite undergoing the mechanical and chemical alteration from the pulping processes, compared to cotton. Certain application that ignores the presence of impurities is proven to be at a disadvantage, such as the production of paper that shows a drawback in appearance and strength. However, the hidden novel usage of these impurities may contribute positively to the properties of certain products such as shown in the AMCA lacquer production.

The effectuation of the mechanical performance of both CCA and AMCA lacquer was observed based on the impact, adhesion, abrasion, and hardness quality. Based on Figure 2, AMCA lacquer block sample that underwent the impact test has shown a slightly superior resistance towards impact compared to the CCA lacquer, as circular indentation and moderate cracking appeared on the CCA lacquer blocks, rather than just circular indentation appearing on the former. The presence of lignin may be the main contributor to the better performance in impact resistance as lignin is known to provide physical support on most lignocellulosic materials and serves as a retainer for the structure (Kakroodi & Sain, 2016).

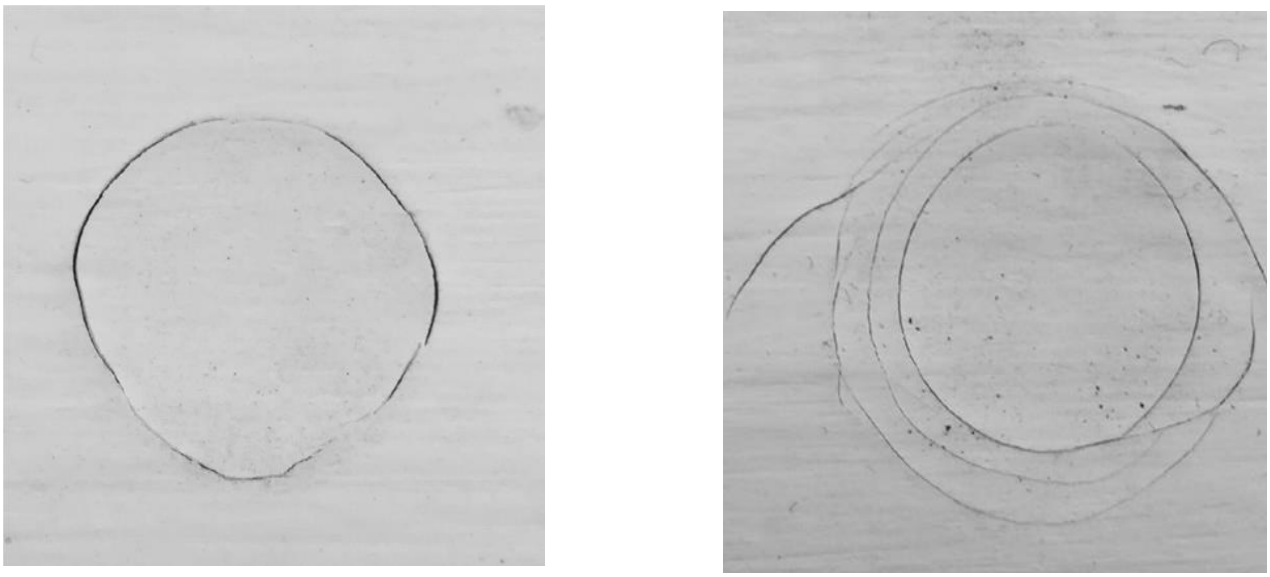

(a) (b)

Figure 2: Circular indentation (a) AMCA lacquer blocks; (b) CCA lacquer

Based on the chemical composition of *Acacia mangium* pulp by Gilbert *et al.* (2013), a near-absolute 95% of its content is cellulose, where the remaining 5% of its content consists of hemicellulose, lignin, and extractives. Due to the difference in raw material used, the AMCA which was developed from raw *Acacia mangium* pulp contains a lot more impurities as compared to the CCA, which has the content of an absolute cellulose purity. These impurities may contribute to the more advantageous performance on all three properties such as for the impact resistance, as shown in the overall results in Table 2.

Table 2: Mechanical performance of commercial cellulose acetate (CCA) lacquer compared to the *Acacia mangium* cellulose acetate (AMCA) lacquer

Lacquer	CCA	AMCA
Impact (Rate)	3 Moderate cracking	4 Two circulars around the edge of indentation
Adhesion (Percentage of flaking)	1 < 5%	2 < 15%
Abrasion (cycle)	271	288
Hardness (Pencil grade)	2H	3H

The adhesion performance for the AMCA lacquer was the only one lower than the CCA lacquer, with the CCA lacquer only obtaining less than 5% flaking covered to opposed of the 15% for the AMCA's in Figure 3. The adhesion or inter-crosslink between the coating and the surface or substrate is presumed lower than that of the CCA, in which the optimal layer thickness determination plays a great role in providing the higher strength of the bonded substrate, where the film thickness of the CCA lacquer is proven to be thicker and adhere more than that of the AMCA lacquer. Higher thickness provides better adhesion performance in coatings and adhesives (Müller *et al*., 2006).

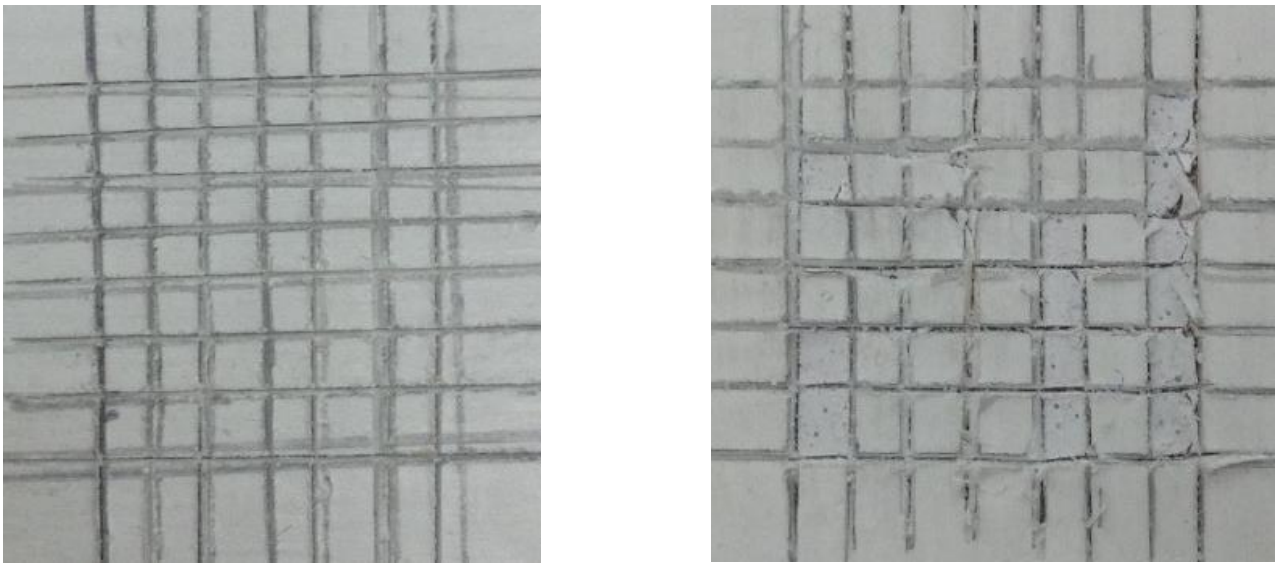

(a) (b)

Figure 3: Flaking percentage (a) AMCA lacquer; (b) CCA lacquer

However, despite the disadvantage of a lower adhesion property for the AMCA lacquer, the abrasion resistance is showed in Figure 4 to be higher than the CCA lacquer with 288 cycles compared to 271, respectively. The intra-crosslink or cohesion between the AMCA in its molecular level is higher compared to the CCA, resulting in a higher abrasion resistance. This could be contributed by the

presence of hemicellulose acetate, which increases the tensile strength of the product as demonstrated from the production of hemicellulose plasticizers in films, where in the sugarcane bagasse-cellulose acetate production study, increases the tensile strength up to three to four times from 14 MPa to 61 MPa (Shaikh *et al*., 2009). The tensile strength includes the ability of the materials to resist permanent deformation such as breaks or ruptures.

This is also evident based on the pencil hardness test, where the AMCA lacquer is shown to have a higher level of tolerance towards scratching compared to the CCA lacquer, where only the pencil grade of 3H or higher was able to scratch the surface of the AMCA coating, with the latter showing a slightly lower hardness with 2H. The AMCA lacquer has a higher resistance towards permanent change in shape compared to the CCA lacquer due to the very same reason of the abrasion, which is the higher tensile strength provided by the hemicellulose and lignin presence. In the production of printable hemicellulose-based films, cellulose alongside hemicellulose are proven to complement each other by enhancing the tensile sand contributes to the strength of the coatings (Ma *et al*., 2017). The resistance of the coat breaking may also be due to the plasticizing effect of hemicellulose, which is commonly absence in industrial grade cellulose acetate, compared to the homemade AMCA that contains traces of hemicellulose and lignin from its pulp source (Shaikh *et al*., 2009). Apart from that, a higher cohesion force may as well contribute to the resistance.

(a) (b)

Figure 4: Abrasion resistance on the (a) AMCA lacquer is higher than the (b) CCA lacquer, with 288 and 271 cycles, respectively.

CONCLUSION

The impact and abrasion resistance for the AMCA lacquer is higher than the commercial CCA lacquer, which strictly underwent gruesome formulation uniformity to avoid bias. The hardness test result also shows a higher deforming resistance for the AMCA lacquer, with hemicellulose, lignin, and other impurities surprisingly bestowing an upper hand in the properties of the lacquer.

REFERENCES

ASTM. (2005). *D3363 Standard Test Methods for Film Hardness by Pencil Test*. United States: ASTM International

ASTM. (2012). *D2486 Standard Test Methods for Scrub Resistance of Wall Paints*. United States: ASTM International

ASTM. (2012). *D3359 Standard Test Methods for Measuring Adhesion by Tape Test*. United States: ASTM International

Cheng, H. N., Dowd, M. K., Selling, G. W., & Biswas, A. (2010). Synthesis of Cellulose Acetate from Cotton Byproducts. *Carbohydrate Polymers* Vol. 80 (2): Pg. 449-452.

Egot, M. P. & Alguno, A. C. (2018). Preparation and Characterization of Cellulose Acetate from Pineapple. *Key Engineering Materials* 772:8-12.

Gilbert, M. S., Palle, I, Liew, K. C. & Md. Salim, R. (2013). Chemical Composition of Acacia mangium Wood Fiber and Pulp. *Proceedings of the International Forestry Graduate Students' Conference.* Pg. 84-86.

Gilbert, M.S. & Palle, I. (2013). Cellulose Acetate Production from *Acacia mangium* Pulp. *International Proceedings of Chemical, Biological and Environmental Engineering* Vol. 58. Pg. 115-119

Indian Standard. (2002). *IS 5807 Part 6: Methods of Test for Clear Finishes for Wooden Furniture.* Painting, Varnishing, and Allied Finishes Sectional Committee. India: Indian Standards Institution.

Kakroodi, A. R. & Sain, M. (2016). Lignin-Reinforced Rubber Composites. *Lignin in Polymer Composites*. Pg. 195-206.

Ma, R., Pekarovicova, A., Fleming III, P. D., & Husovska, V. (2017). Preparation and Characterization of Hemicellulose-Based Printable Films. *Cellulose Chemistry and Technology Vol. 51 (9-10)*. Pg. 939-948.

Ma, X. M., Lu, R., & Miyakoshi, T. (2014). Application of Pyrolysis Gas Chromatograph/Mass Spectrometry in Lacquer Research: A Review. *Polymers* Vol. 6: Pg. 132-144.

Müller, M., Hrabě, P., Chotěborský, R., Herák, D. (2006). Evaluation of Factors Influencing Adhesive Bond Strength. *Research in Agricultural Engineering* Vol. 52 (1). Pg. 30-37.

Shaikh, H. M., Pandare, K. V., Nair, G., Varma, A. J. (2009). Utilization of Sugarcane Bagasse Cellulose for Producing Cellulose Acetates: Novel Use of Residual Hemicellulose as Plasticizer. *Carbohydrate Polymers* Vol. 76 (1). Pg. 23-29.

Swain, R. C., & Adams, P. (1940). Cellulose Acetate Coating Compositions. *U.S. Patent No. 2426379*: United States Patent Office.

Zorll, U. (2006). *Adhesion Testing*. Coatings Technology: Fundamentals, Testing, and Processing Techniques. United States: CRC Press.

BorneoScience
The Journal of Science & Technology
Volume 40 Issue 1 : March 2019
Online ISSN : 2231-9085 | ISSN : 1394-4339

PHYSICO-CHEMICAL PROPERTIES, CARBON DIOXIDE EMISSIONS AND CARBON STOCK IN PEAT SOIL USED FOR TURMERIC CULTIVATION AT KUALA LANGAT SELATAN, SELANGOR, MALAYSIA

Wan Mohd. Razi, I.[2], *A.R. Sahibin[1], L. Tukimat[2], A.R. Zulfahmi[2], M. S. Mohd. Nizam[2,3], T. Fredolin[2] & T. C. Teng[2]

[1]Environmental Science Program, Faculty of Science and Natural Resources, Universiti Malaysia Sabah, Jalan UMS, 88400, Kota Kinabalu, Sabah

[2]Center for Earth Sciences and Environment, Faculty of Science and Technology, UKM 43600 Bangi, Selangor

[3]Climate Change Institute, UKM, 43600 Bangi, Selangor
*Corresponding author: sahibin@ums.edu.my

Received 11st February 2019; accepted 11st February 2019
Available online 29th March 2019
Doi: https://doi.org/10.51200/bsj.v40i1.

ABSTRACT. *Measurement of carbon dioxide emissions in peat soil was done in a turmeric cultivation area on August 2009 and January 2010 at Kampung Tumbuk Darat, Kuala Langat Selatan, Selangor. The objective of this research was to determine the quantity of CO_2 emissions from peat soil as well as the carbon stock that is stored in the peat soil. Other parameters that were investigated included soil pH, soil temperature, soil bulk density, soil organic carbon, soil fresh water content, organic matter, humic acid and fulvic acid content. A total of 30 carbon dioxide emission sampling points in rectangular grid arrangement was prepared in a survey plot of 1 hectare. The survey plot was further divided into sub-plots of size 20 m x 25 m. Soil samples were randomly taken at the depth of 0-15 cm to 50-65 cm using an auger. Sampling of CO_2 emissions was done using the static alkali absorption method (Kirita Method). The organic carbon content was determined using the Walkley-Black method, while the humic and fulvic acid content was determined using the basic molecule isolation method. Other soil properties were determined using standard methods of determination. The surface temperature of peat soil was between 28^oC and 30^oC. The bulk density of the area was as low as 0.20 g cm^{-3}. On the other hand, the soil fresh water content, soil organic matter, and peat soil humic acid was very high. The minimum quantity of CO_2 emissions in the peat soil on August 2009 and January 2010 was 40.92±21.62 t CO_2 ha^{-1} yr^{-1} (467.10±246.86 mg CO_2 m^{-2} hr^{-1}) and 41.51±13.41 t CO_2 ha^{-1} yr^{-1} (473.86±153.12 mg CO_2 m^{-2} hr^{-1}), respectively. Carbon stock for the month of August 2009 and January 2010, respectively was 297.70 t ha^{-1} and 456.60 t ha^{-1}. T test showed that there were significant ($p<0.05$) differences in many of the soil parameters such as the pH, water content and organic carbon. Correlation analysis showed that CO_2 is influenced by the organic matter, water content and temperature.*

KEYWORDS. *Humic and fulvic acid, CO_2 emissions, carbon stock, peat soil, turmeric*

INTRODUCTION

Carbon dioxide is a primary greenhouse gas with 60% contributing to the amount of greenhouse effect. Soil is a major source of carbon dioxide in the atmosphere. If there is an increased threat of global warming caused by greenhouse gas emissions, the reduction of carbon dioxide emissions originating from the soil is essential (Monika et al., 2002). Carbon dioxide is released from the soil through various processes, i.e. soil respiration, the evolution of carbon dioxide in the soil, and the outflow of carbon dioxide. The rate of carbon dioxide released into the atmosphere from the soil is controlled by the production rate of carbon dioxide in the soil (Raich & Shlesinger 1992). Good airflow in the soil optimizes the oxidation of organic matter by microbes and the release of excess carbon dioxide into the atmosphere. The nature of the carbon dioxide loss in the soil is seasonal and changes with different activities (Liikanen et al., 2006) and it depends strongly on factors such as the surrounding temperature, the type of soil, soil cavities, and soil water content (Chow et al., 2006;

Fenner et al., 2005; Silvola et al., 1996). Outflow of carbon dioxide from the Earth's surface into the atmosphere is biologically produced from plant roots and microbial respiration, with microbial respiration as the major contributor. Plant roots respiration contributes to the change of organic carbon acquisition in the soil, camouflaging the true role of soil respiration in global warming (Cheng et al., 2005; Kuzyakov, 2002a, 2002b). As the flow of carbon dioxide from the soil into the atmosphere has significant effects to global warming, many studies on the method of measuring soil respiration have been done. However, soil respiration is difficult to measure precisely because it deals with uncertainties in various methodologies, uses a large amount space, presence of temporary variables within the soil respiration, environmental factors and so on (Norman et al., 1997). This research paper discuss on the carbon dioxide emissions and carbon stock in peat soil planted with turmeric at Tanjung Tumbuk, Kuala Langat Selatan, Selangor, Malaysia.

MATERIALS AND METHODS

Study Area

The study area is located in Kampung Tumbuk Darat at Tanjung Tumbuk, Kuala Langat Selatan, Sepang. The type of soil is peat soil which has been used as an agricultural area for the cultivation of turmeric. Sampling was carried out during 20 to 21 August 2009 (Thursday and Friday) and 18 to 19 January 2010 (Monday and Tuesday). There was heavy rain during the days of sampling. The study site is located at coordinates 02°41'09.3"N and 101°35'18.1"E (Figure 1).

Figure 1: Location of study site at Kampung Tumbuk Darat, Kuala Langat Selatan, Selangor (adapted from Jabatan Pemetaan Malaysia)

Sampling Of Carbon Dioxide

Thirty (30) sponges measuring 9.5 cm x 15 cm x 2 cm were prepared and placed in plastic containers of the same length and width (9.5 cm x 15 cm x 5 cm). The sponges were tied with a thread so that it sticks on the inside at the top of the plastic containers. A total of 40 mL of 2 N KOH was prepared and poured onto each sponge. The containers were closed immediately and tightly. Upon reaching the site, each cover of the containers was reopened and placed upside down on top of the soil at the selected sampling points. Three sampling for 'blank' was also performed in which the container lids were not opened and placed at random. After 24 hours, the plastic containers which were labelled CO_2 emissions sampling points were collected. All plastic containers were closed tightly and placed in a black plastic bag for laboratory analysis of the samples.

Analysis of Carbon Dioxide

Carbon dioxide (CO_2) content in the soil samples was determined using static alkali absorption method (Kirita, 1971). The sponge was removed from the container and squeezed into a beaker immediately to obtain a KOH solution containing CO_2 (sample A). A total of 5 mL sample was

taken from the beaker and added with 3 point phenolphthalein indicator. This mixture was then titrated with 0.2 N HCl until the pink colour disappeared. After that, 3-methyl orange indicator point was added to the mixture. This new mixture was titrated with HCl until a light pink colour was obtained at the end point. Blank test (sample B) and KOH solution which was not used (sample C) for sampling was carried out using the same method (Kirita, 1971). During the course of this analysis the researcher needs to wear a mask to avoid inhalation of the carbon dioxide.

Soil Sampling and Analysis

Topsoil samples (0-15 cm) and sub-soil samples (50-65 cm) were collected using Dutch Auger. Soils collected were kept in a labelled plastic bag and transported to the laboratory. In the lab, the soil samples were dried in a room temperature by spreading them on a newspaper. Upon drying the soil samples were pounded and sieve to pass through 2 mm sieve opening. This 2 mm sieved soil is ready for analysis. Soil pH value was determined in distilled water with distilled water: soil ratio at 2.5: 1 and then determined using a pH meter (Mettler Toledo model Delta 320). The soil fresh water content and organic matter content was determined by gravimetric analysis (Tan, 2005). Soil temperature was determined by *in situ* method using a thermometer pushed at 10 cm depth. Organic carbon content was determined using Walkley and Black method (Walkley, 1947). Humic and fulvic acid content were determined using the basic molecular separation method (Tan, 2005). The bulk density was determined using the metal ring method (Patiram *et al.*, 2007). Data obtained were analysed using ANOVA, t-test, regression and correlation test in excel environment.

RESULTS AND DISCUSSION

Soil Temperature

The mean soil temperature range of the five sampling points are between 28^{o}C to 30^{o}C (Figure 2) with an average and standard deviation of 29 ± 0.28^{o}C. This value of mean temperature did not show any significant difference between the sampling stations ($p > 0.05$). This value is within the temperature interval as in the study of Fujii *et al.*, (1998) which reported that the soil temperature at the surface and subsurface is between 12^{o}C to 33^{o}C (0.15-0.5 m depth) and 13^{o}C to 27^{o}C (1.5-2.0 m depth) respectively. Temperatures that are too high can prevent microbial respiration caused by inactivity of biological oxidation systems (Monika *et al*., 2002).

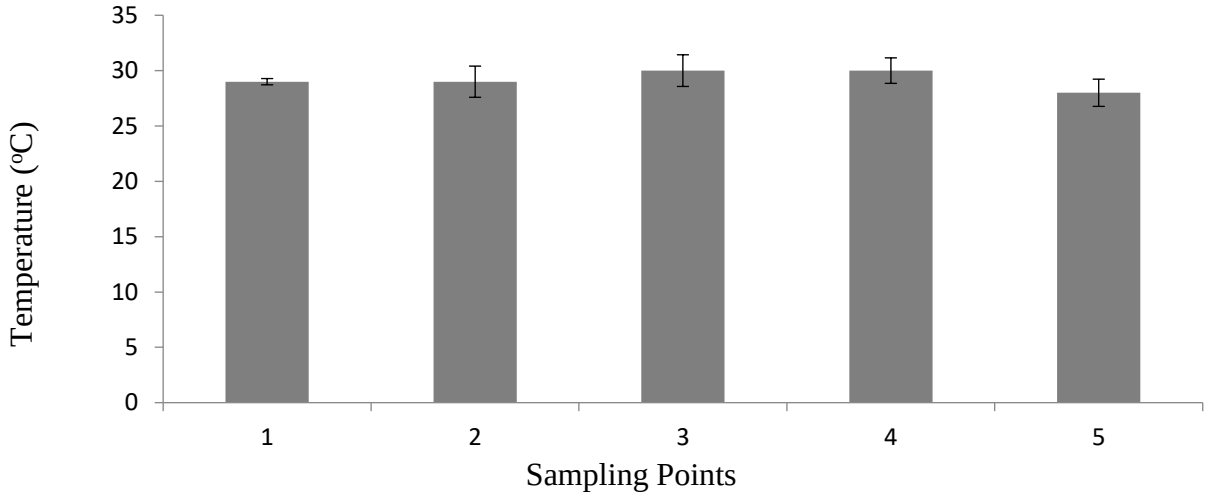

Figure 2: Mean (± standard deviation) soil temperature at the various sampling points

Soil pH

Mean range of soil pH observed at the sampling points at depth 0-15 cm is between 3.07 to 3.12 while the pH at a depth of 50-65 cm is 2.98 to 3.39 (Figure 3). The pH increases with depth at S1, S2 and S4, but decreases with depth at S3 and S5. However, ANOVA test shows that changes in pH between stations are not significantly difference ($p>0.05$). The pH value observed by month (Figure 4) shows a higher value in January compared to August. Paired t tests on soil pH showed a significant difference between the mean of August and January, with $p = 0.000$. In peat soil pH is influenced by the decomposition of organic matter directly by microorganisms into organic acids, carbon dioxide and water, thus creating carbonic acid (Kirschbaum, 1995). Acid interacts with calcium carbonate and magnesium carbonate in the soil to form dissolved bicarbonate and which result in acidic soil (Wu *et al.*, 2003). The soil was more acidic in August compared to the month of January due to heavier rain in August. When rainwater moves through the soil, the base cations such as calcium and magnesium would be leached and replaced at the adsorption sites by acid cations. In the rainy season or in areas with high rainfall the soil is usually more acidic (Guo & Gifford, 2002).

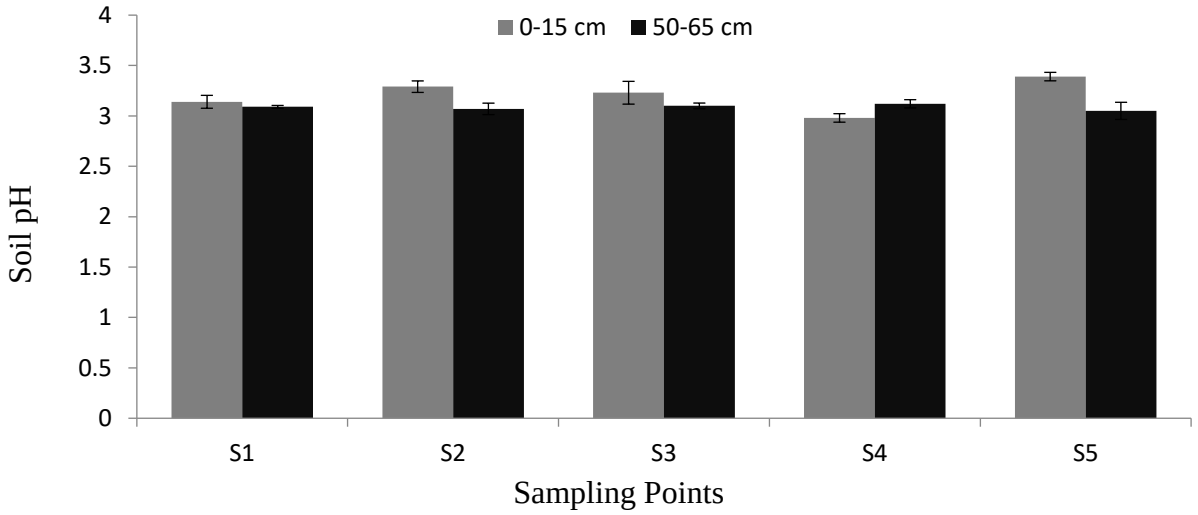

Figure 3: Mean (± standard deviation) soil pH with respect to sampling points and depths

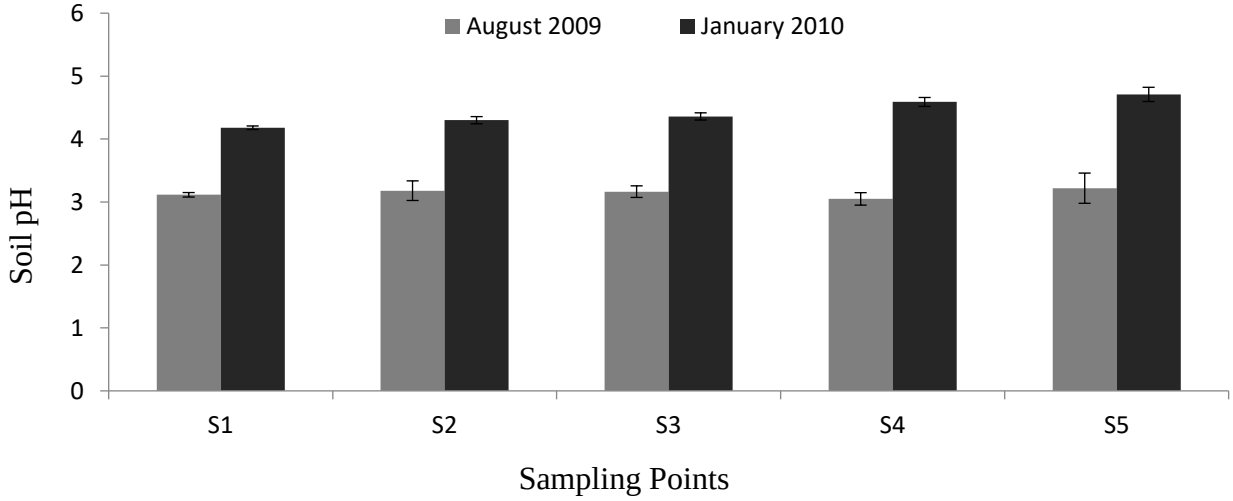

Figure 4: Mean soil pH of sampling points in August 2009 and January 2010

Soil Bulk Density

The range of soil bulk density was observed between 0.19 g cm^{-3} to 0.22 g cm^{-3} (Figure 5) with a mean and standard deviation 0.20 ± 0.000 g cm^{-3}. Paired t tests showed that the bulk density did not show significant differences in August and January sampling ($p = 0.612$). Low bulk density values at all sampling points showed that peat soil has high volume and cavity space. The high organic content leads to aggregated soil which causes the soil to become loose and lowering the bulk density of the soil (Lal, 2002).

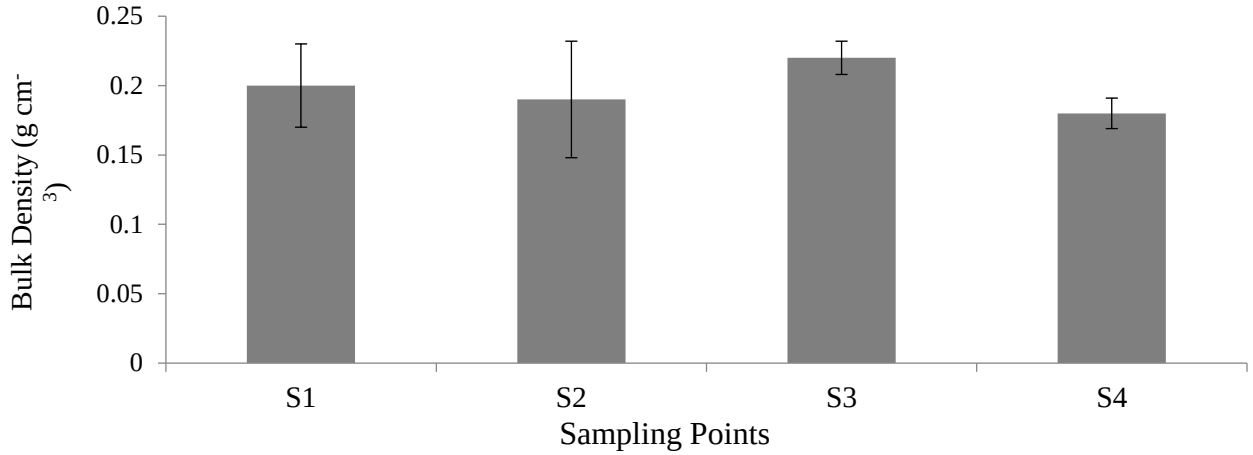

Figure 5: The mean (± standard deviation) bulk density of the various sampling point (sampling depth 0-15 cm)

Soil Water Content

Mean range of soil fresh water content recorded at all sampling points was between 73.58% and 80.57% at a depth of 0–15 cm (Figure 6). At a depth of 50-65 cm in the mean range of soil fresh water content was between 79.39% and 84.17%. Soil fresh water content showed significant differences with their depths. Figure 6 also shows an increase in the water content of the soil with depth for all sampling points. Peats soils have a high water level therefore the water content in the sub-soil are usually higher.

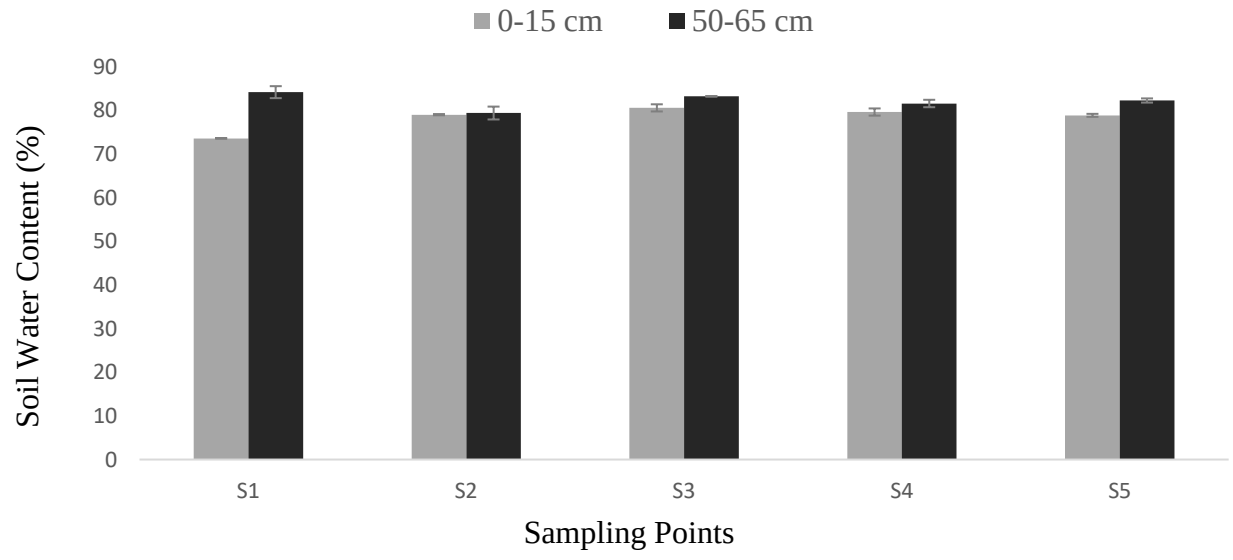

Figure 6: The mean (± standard deviation) water content with respect to sampling points and depths

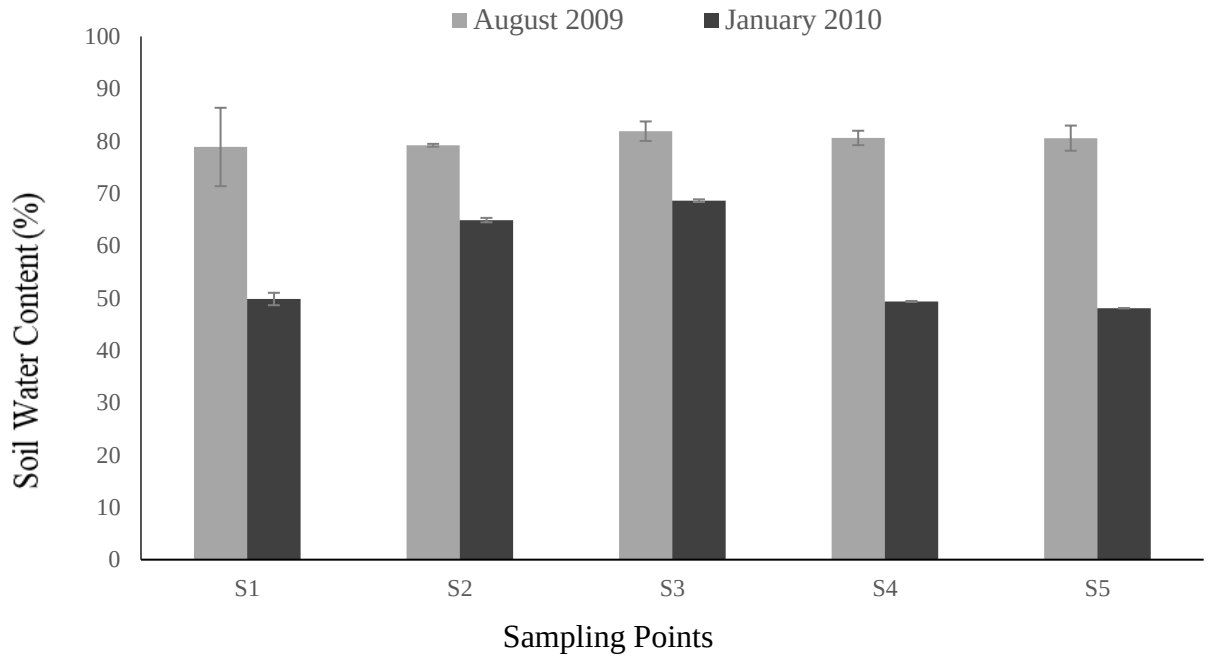

Figure 7: The mean soil water content of sampling points in August 2009 and January 2010

Soil Organic Matter

Mean range of soil organic matter content observed at a depth of 0 cm is from 84.78% to 97.95% (Figure 8), while the mean range of soil organic matter content observed at a depth of 50 cm is from 96.40% to 99.94%. This clearly shows the mean value of soil organic matter increases with depth. Figure 9 shows the mean value of soil organic matter in August 2009 and January 2010. The mean value of soil organic matter in August (95.9 ± 2.82%) was higher than in January (92.47 ± 0.16%). T test ($p = 0.267$) on soil organic matter showed no significant difference between the mean of August and January.

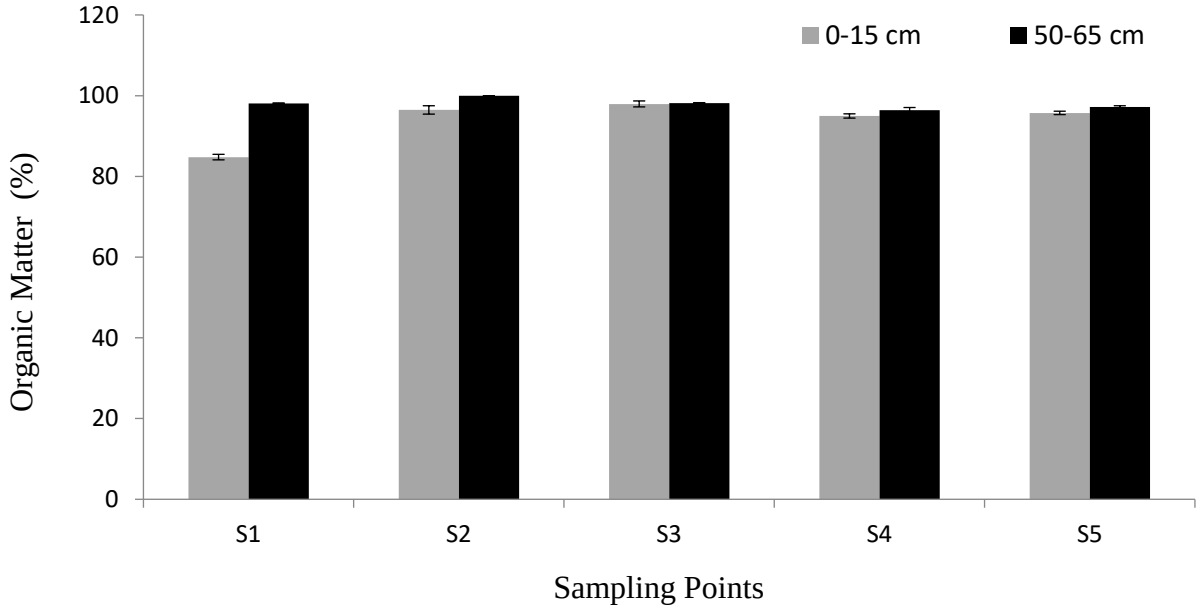

Figure 8: The mean (± standard deviation) organic matter with respect to sampling points and depths

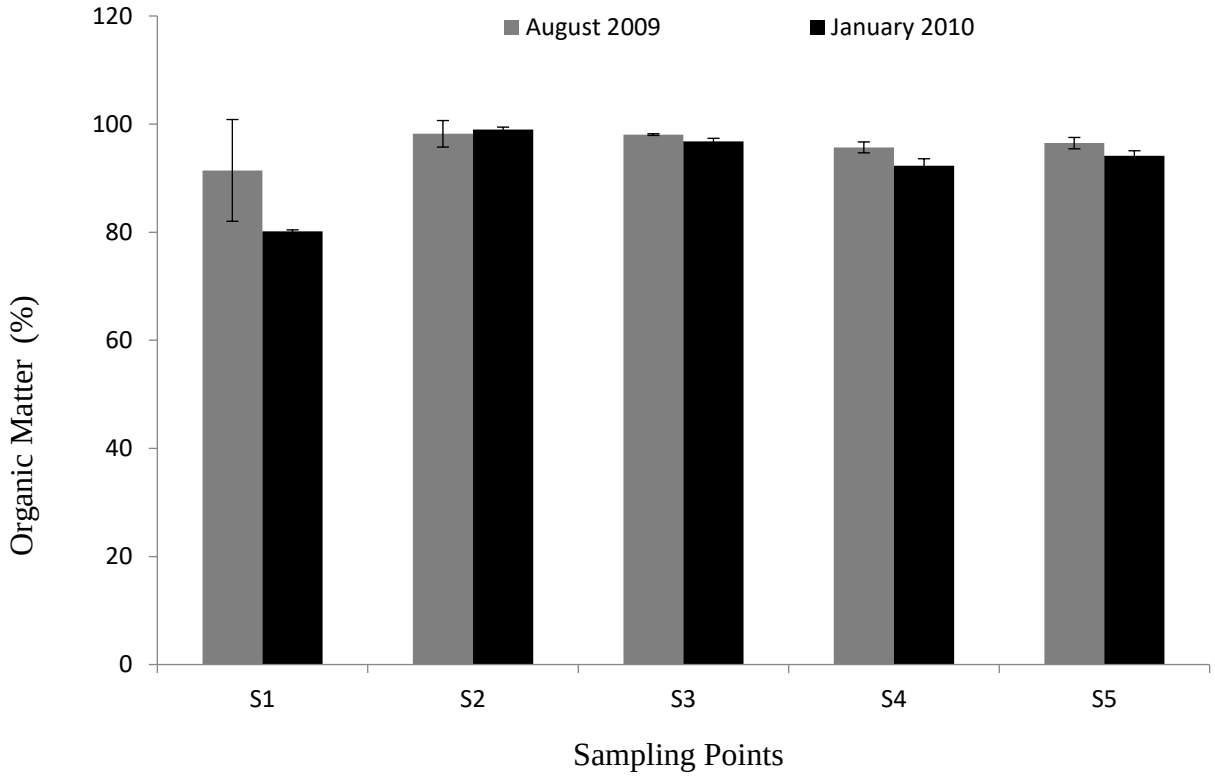

Figure 9: The mean soil organic matter of sampling points in August 2009 and January 2010

High water content reduces ventilation or oxygen concentration in the soil. The decrease of oxygen content in the soil will decrease the mineralization rate causing organisms to be inactive or dead. This will increase the organic matter content in the soil (Bot & Benites, 2005). Good drainage in peat soil allowed water from the heavy rainfall that occurred in August 2009 to drain into the soil more easily.

Soil Organic Carbon

Figure 10 shows the mean soil organic carbon content at different depths. At a depth of 0-15 cm, the mean range of soil organic carbon observed at all sampling points was between 42.64% and 46.43%. Mean range of soil organic carbon observed at a depth of 50-65 cm was between 29.24% and 38.79%. The soil organic carbon content in the soil increases with depth at each sampling point. Figure 11 shows soil organic carbon content in August 2009 and January 2010. The organic carbon content was higher in January. The average value of the organic carbon content in January was 45.66 ± 1.19% and in August 39.77 ± 6.66%. T test ($p = 0.004$) showed organic carbon content of soil in August and in January differ significantly.

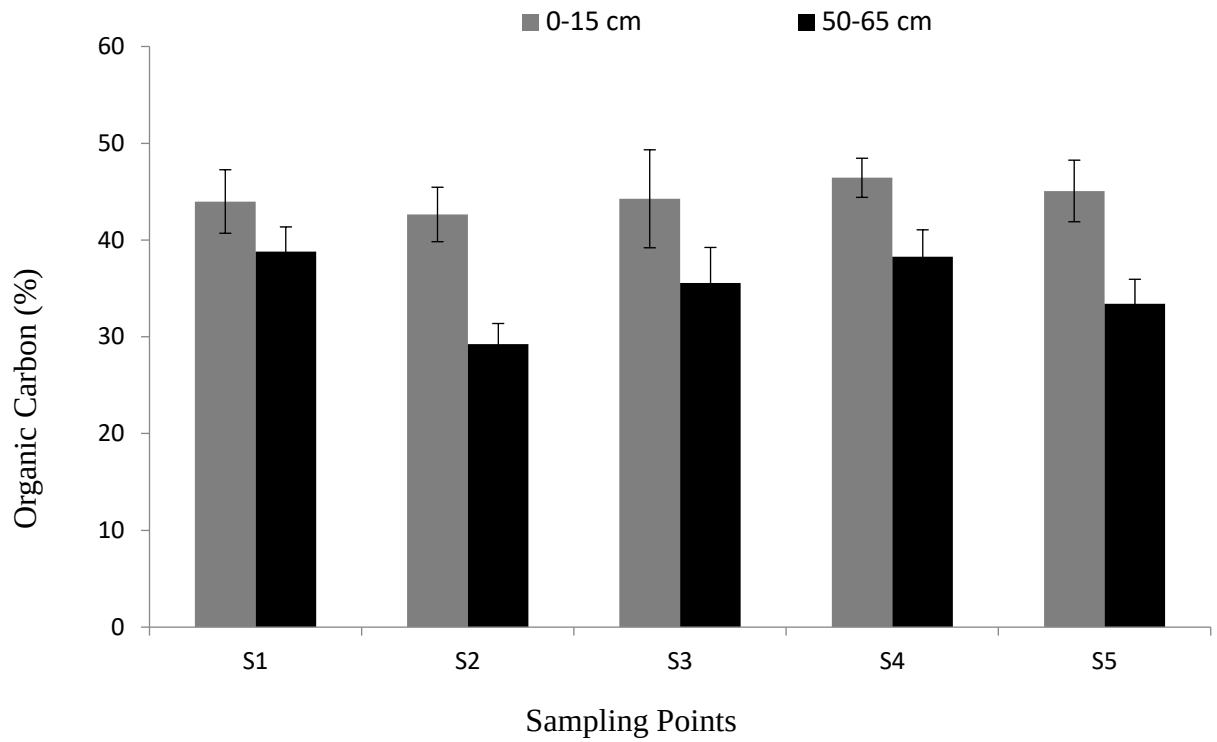

Figure 10: The mean (± standard deviation) organic carbon content with respect to the sampling points and depths

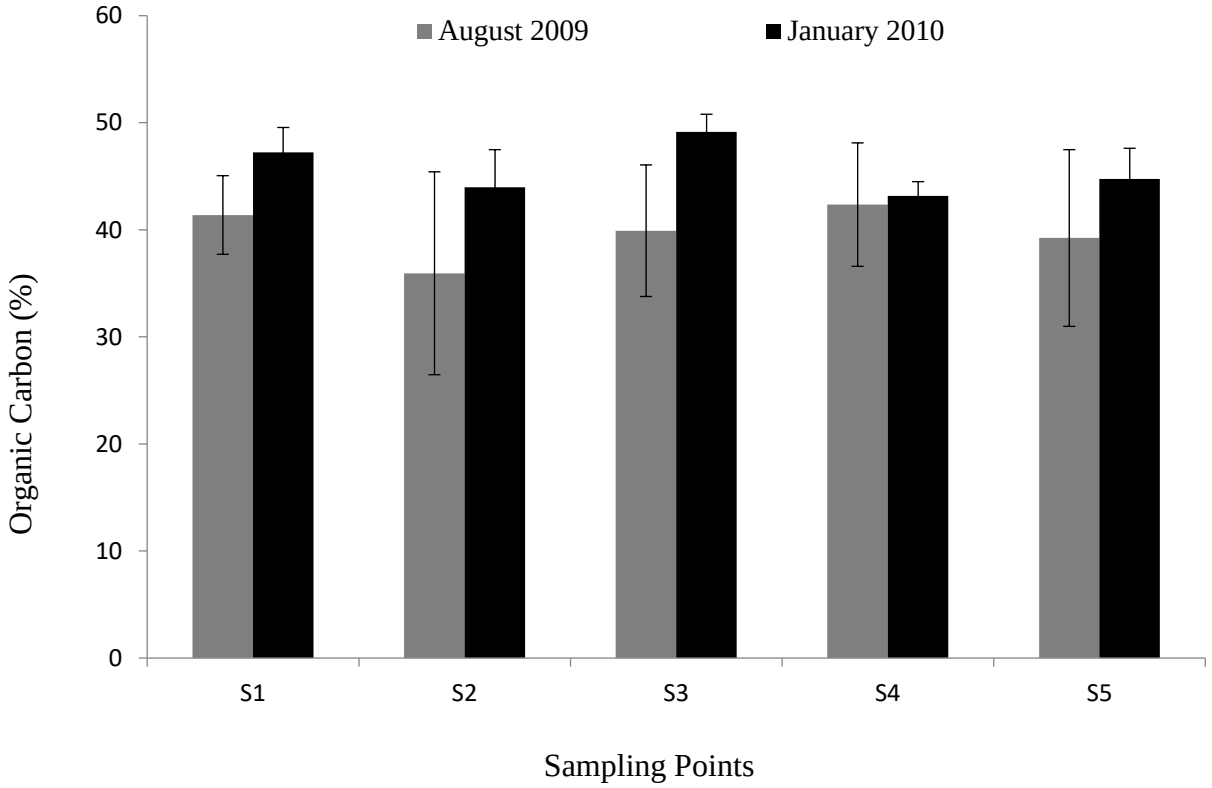

Figure 11: Mean soil organic carbon content of sampling points in August 2009 and January 2010

The organic carbon content was higher on the surface and decreases with depth. This is due to the organic carbon being dissolved easily by water movement. At depths greater than 50 cm the water content is higher, therefore organic carbon dissolves more readily and were driven into groundwater resulting in reduced organic carbon content. Thus, a lot of carbon is present in the soil nearer to the surface and reduces deeper in the soil (Davidson & Ackerman, 1993). The carbon content in the soil near the surface is also attributed by the supply of new humus from decomposed plant waste (Houghton & Hackler 2000). Bot and Benites, (2005) explained that high amount of rainwater can reduce the decomposition of soil organic matter. Decomposition of organic matter will reduce the content of organic carbon in the soil.

Humic Acid

Figure 12 shows that at a depth of 0-15 cm, the mean range of humic acid content observed at all sampling points was between 42.8 mg g^{-1} soil up to 55.3 mg g^{-1} soil. In contrast, the mean range of humic acid content that was observed at a depth of 50-65 cm at all sampling points was between 41.2 mg g^{-1} soil up to 50.3 mg g^{-1} soil. Humic acid content decreased with soil depth at each sampling point except for sampling point S2. Figure 13 shows the mean humic acid content in

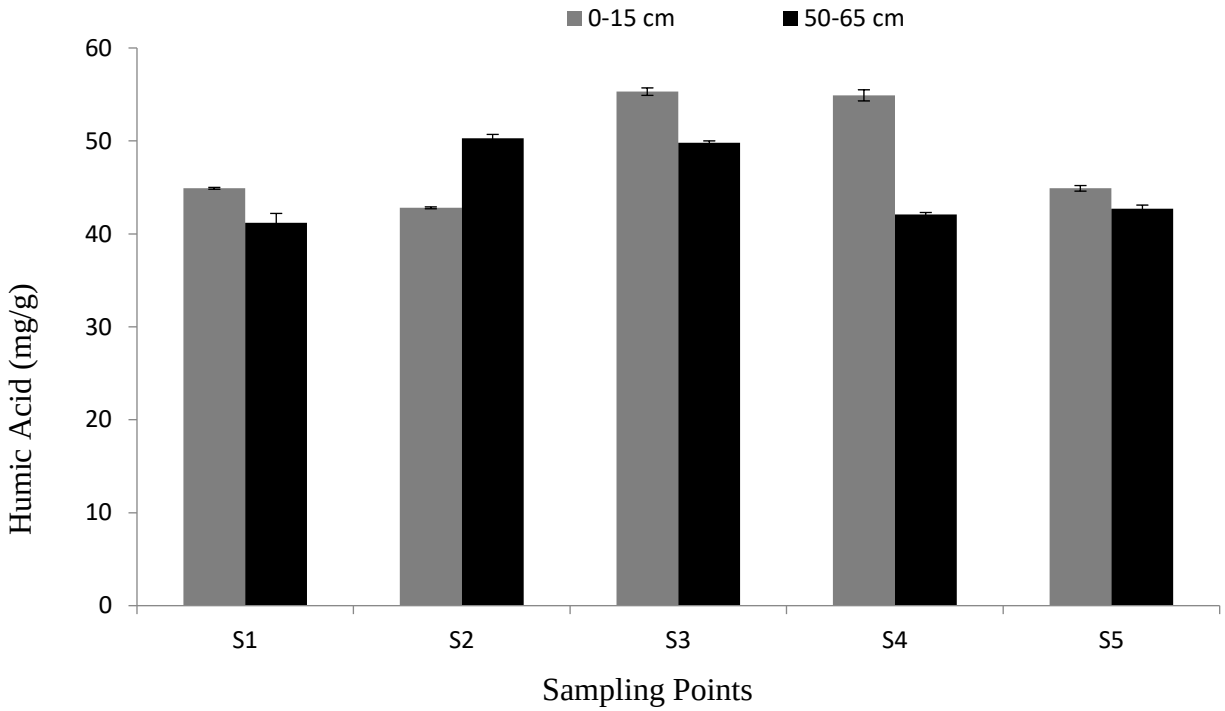

Figure 12: The mean (± standard deviation) humic acid with respect to point sampling and depth

August 2009 and January 2010 at each sampling point. The average in August and January was 48.57 ± 0.184 mg g^{-1} soil and 28.56 ± 0.085 mg g^{-1} soil, respectively. T test ($p = 0.055$) indicates that humic acid content in the soil was not significantly difference ($p>0.05$) between the mean of August and January. Humic acid content reduced substantially with depth of the soil, due to decreasing carbon content deeper into the soil. Low humic acid content at depth of more than 50 cm showed that humic acid seeps away from soil through water movement at a lower depth. Thus, there is an abundance of humic acid in the top layer whereas in the sub-soil it is scarce (Davidson & Ackerman, 1993). In addition, high humic acid content in the soil surface can also be caused by the

use of fertilizers (Houghton & Hackler, 2003). Humic acids can stimulate the microorganismsactivity in the soil by supplying carbon as a food source for the microorganisms, and thus promoting their growth and activity. These microorganisms play roles in dissolving key nutrients such as phosphorus for absorbtion by humic acid and made readily available for use by plants (Zeller *et al.*, 2001). The presence of carbonate in organic soil accelerates the humification process which leads to the formation of humic acid (Puget *et al.*, 2005).

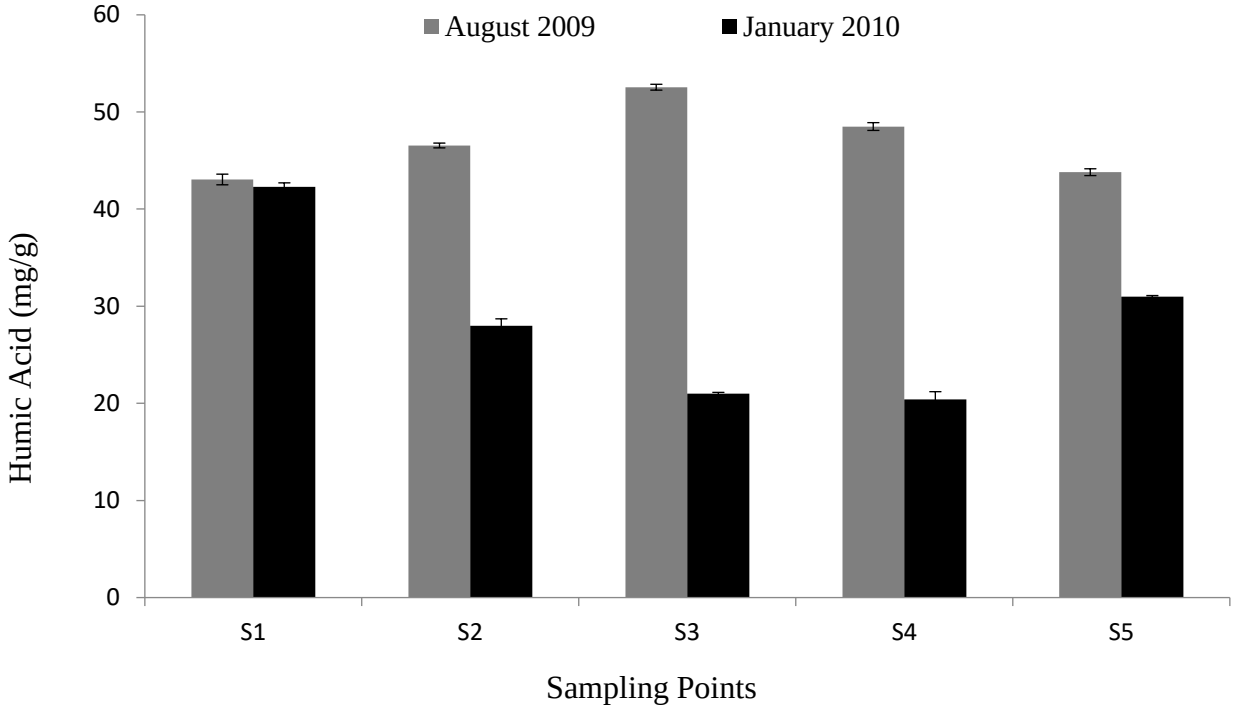

Figure 13: The mean soil humic acid of sampling points in August 2009 and January 2010

Fulvic Acid

Figure 14 shows that at a depth of 0-15 cm, the mean range of fulvic acid content observed at all sampling points was between 8.00 mg g^{-1} soil to 20.00 mg g^{-1} soil. In contrast, the mean range of fulvic acid content observed at a depth of 50-65 cm at all sampling points was between 9:00 mg g^{-1} soils to 23.00 mg g^{-1} soil. The mean value of fulvic acid content increases with depth of soil at all sampling points, except at S5 which showed a decrease. Figure 15 shows the mean value of fulvic acid content in August 2009 and January 2010. The mean value of fulvic acid content was higher in January compared to August. The average in August was 13.90 ± 0.14 mg g^{-1} soil while in January it was 15.70 ± 0.14 mg g^{-1} soil. Paired t tests ($p = 0.181$) showed that the soil mean fulvic acid content in August and January did not differ significantly. The fulvic acid content in the soil surface varied. This may have been caused by the use of fertilizers, particularly high amounts of nitrate fertilizer and pesticides in agricultural areas which have affected the life of microorganisms in the soil, causing disruption to the production of fulvic acid (Jacot *et al.*, 2000). Fulvic acid is soluble in water therefore it can get into the bottom part of the soil by water movement (Davidson & Ackerman, 1993), which led to an increase in the fulvic acid content at a depth of more than 50 cm.

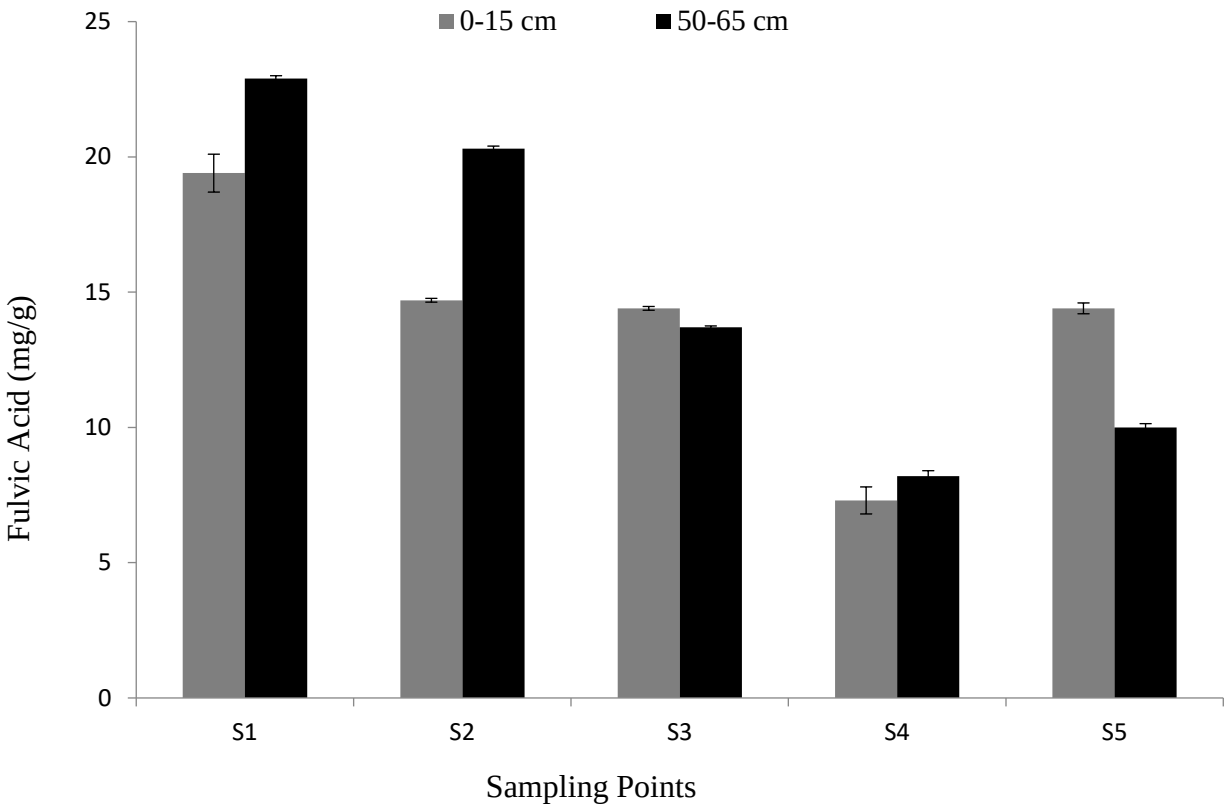

Figure 14: The mean (± standard deviation) fulvic acid in soil with respect to sampling points and depths

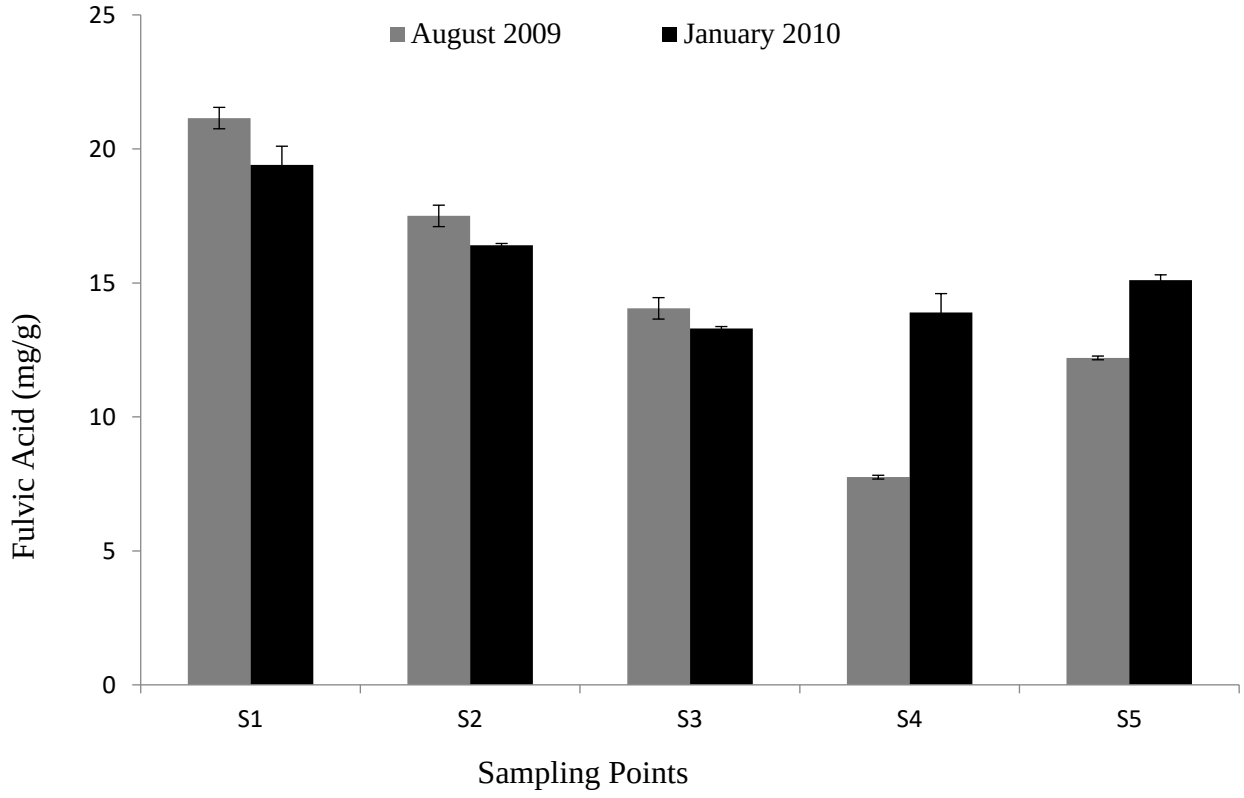

Figure 15: The mean fulvic acid of sampling points in August 2009 and January 20

Quantity of Carbon Dioxide Emissions

The mean range of CO_2 emissions was between 10.71 t CO_2 ha^{-1} yr^{-1} to 84.35 t CO_2 ha^{-1} yr^{-1} in August 2009 with an average and standard deviation of 40.92 ± 21.62 t CO_2 ha^{-1} yr^{-1} (467.10 ± 246.86 mg CO_2 m^{-2} hr^{-1}. In January 2010, the mean range of CO_2 emissions was between 12.07 t CO_2 ha^{-1} yr^{-1} to 81.31 t CO_2 ha^{-1} yr^{-1} with the average and standard deviation of 41.51 ± 13.41 t CO_2 ha^{-1} yr^{-1} (473.86 ± 153.12 mg CO_2 m^{-2} hr^{-1}). Mean CO_2 emissions from the soil between the two months showed no significant difference. The CO_2 emission in the two months of sampling was similar to the CO_2 emissions (CO_2 6.9 ± 483 mg / m^2 J) recorded in the Örke peat soil in Sweden (Berglund, *et al*., 2008). CO_2 emissions measured in peat soil in Southern Quebec recorded by Glenn, *et al.* (1993) was 16.4-127.4 kg CO_2 ha^{-1} day^{-1} (1.4-11.2 t CO_2 ha^{-1} yr^{-1}). CO_2 emissions recorded by Melling *et al*., (2005) on peat soil area planted with oil palm in Sarawak was 46 to 335 mg CO_2 m^{-2} hr^{-1}. Recent study by Ishikura *et al.*, (2019) shows that carbon dioxide emission from peat forest in Maludam National Park, Sarawak range from 891 ± 476 g C m^{-2} y^{-1} to 926 ± 610 g C m^{-2} y^{-1}). CO_2 emission recorded in this study (467.10 ± 246.86 mg CO_2 m^{-2} hr^{-1} in August and 473.86 ± 153.12 mg CO_2 m^{-2} hr^{-1} in January) was slightly higher than that recorded by Melling, *et al*. (2005). This situation occurred because 1) the different type of agricultural activity, where in Sarawak the soil was planted with oil palm while in Kg. Tumbuk the soil was planted with turmeric. 2) Method of determining CO_2 emissions in Kg.Tumbuk was absorption method (Kirita, 1971) where the change in CO_2 content is very sensitive to sample handling while Melling *et al.*, (2005) used the Closed-Chamber Method (Crill, 1991) to collect samples of CO_2 emissions which were then measured using Infrared Gas Analyzer (Fuji Electric ZFP-5) which is a neater method of sampling. Melling *et al*., (2005) also recorded CO_2 emissions in forest ecosystems and sago in Sarawak which was 100 to 533 mg CO_2 m^{-2} J^{-1} and 63 to 245 mg CO_2 m^{-2} J^{-1}, respectively. This shows that the type of land use can affect CO_2 emissions in peat soil. Yew *et al*., (2010) also reported that in the tropics the average carbon dioxide emission was 51,500 kg ha^{-1} yr^{-1} (51.5 t ha^{-1} yr^{-1}).

Correlation between Carbon Dioxide Emissions Soil Parameters

The correlation results in Table 1 show the relationship between CO_2 emissions and other tested soil parameters. The results show that CO_2 emission had a significant positive correlation ($p < 0.001$, r = 0.919***) with soil organic matter (SOM), ($p < 0.01$, r = 0.846**) with soil water content (FW) and ($p < 0.05$, r = 0.666*) with temperature (T). CO_2 emission correlation with pH, bulk density, content of humic acid and fulvic acid was not significant.

Table 1: Correlation between carbon dioxide emissions (CO_2) and soil parameters

	CO_2	Fresh Water	Organic Matter	Temperature	Bulk Density	pH	HA	FA
CO_2	1							
FW	0.846**	1						
OM	0.919***	0.965***	1					
Temp	0.666*	0.317	0.477	1				
BD	-0.199	0.125	0.003	-0.277	1			
pH	0.370	0.126	0.198	0.319	-0.005	1		
Humic Acid	0.293	0.519	0.355	-0.289	-0.022	-0.276	1	
Fulvic Acid	-0.387	-0.726*	-0.615*	0.269	-0.097	-0.055	-0.622*	1

n=10; r≥0.602*, p=5%; r≥0.735**, p=1%; r≥0.847***, p=0.1%

The effect of organic matter and soil water content to CO_2 emission shown in Figure 16 was high with regression coefficients of 84.45% and 71.5%, whereas the temperature effect was not very high, even though significant, with regression coefficient of 44.3%.

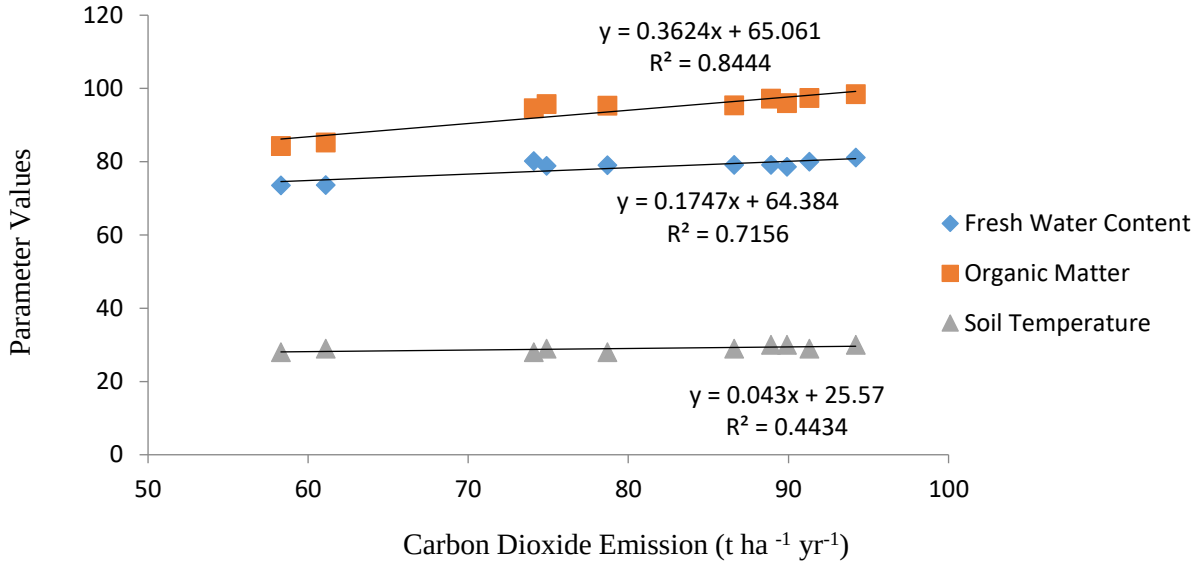

Figure 16: Regression chart showing soil parameters that affects CO_2 emission

The quantity of CO_2 emissions from soil is the total root respiration and the heterotrophic decomposition of soil organic matter (Savage & Davidson, 2001) as well as microbial respiration and oxidation of organic matter (Tan, 1994). CO_2 emission also varies with the ecosystem (Raich & Tufekcioglu, 2000), season, the quantity and quality of organic matter (La Scala *et al.*, 2000) and environmental factors such as temperature, humidity (Mosier, 1998; Kies & Butterbach-Bahl, 2002), and pH (Tan, 1994). The correlation results in Table 1 for the study area showed a similar relationship. The high content of organic matter in the soil with an average value of 92.47% to 95.90% acted as a quality source of CO_2. CO_2 emission produced from the oxidation of organic matter and respiration activity of microbes that live on the abundant organic matter. Carbon dioxide can also be produced through the process of mineralization and decomposition of organic matter where the end products are CO_2 and water (Tan, 1994). When there is more organic matter present in the soil, more CO_2 is produced. The peat soil of the study area has a large stock of organic carbon (397.70 to 456.60 t ha^{-1}), making it a major CO_2 reservoir as well.

Silvola *et al.*, (1996) found that temperature is a significant controlling factor of CO_2 production in the soil, while Lafleur *et al.*, (2005) reported that temperature is the only factor that controls soil respiration. Temperature has a clear impact on the evolution of CO_2 emission from the soil. The temperature of the soil in the study area has a low fluctuation range of 2°C, with the temperature gap between 28-30°C. This temperature range is able to influence the increase in CO_2 emissions, despite minor as shown in the graph slope of CO_2 emission versus temperature (Figure 16) which is 0.043 only. A 1°C increase in temperature can cause loss of as much as 10% of carbon mentioned in Monika *et al.*, (2002) which was higher than the loss of carbon in the study area at 4.3%. Wiant, (1967) found that the evolution of the CO_2 increases logarithmically at temperatures between 20°C to 40°C and decreases rapidly at temperatures above 50°C. CO_2 emission increases at

20-40^{o}C interval can be attributed to increased activity of roots and decaying organic matter (Bunt & Rovira, 1954). The average soil temperature at 29^{o}C in the study area was within the interval where the activity of roots and decaying organic matter increases, which can contribute to increased CO_2 emissions from the soil.

Soil moisture affects the soil respiration and CO_2 emission. Normally, an increase in soil moisture will increase CO_2 emissions to the optimum level. This is because in dry soil microbial activity occurs slowly and increases when the soil gets wet. The water content of soil in the study area based on the weight of the soil is high with mean values of 77.07% in the top soil and 81.78% in the sub soil. However, based on volume, water content in the top soil is 15.41% (v / v) and sub-soil is 21.26% (v / v) which showed pore space in the soil was mostly filled by air. Therefore, microbial life favours a state that has a good balance between air and water in the soil. Correlation analysis shown for CO_2 emission with water content in Table 1 was significantly positive ($p<0.01$), which shows increased CO_2 emission with increasing soil moisture content.

The quantity of CO_2 emission is very little in acidic soils, and increases with higher pH. Low pH conditions negatively impact soil microbial activity by lowering respiration rate and further reduce CO_2 emission (Pol van Dasselaar *et al.,* 1998). The pH value in the study area was low in August at 3.14 and slightly higher in January at 4.43. CO_2 emission data showed slightly higher values in January compared to August. This corresponds to the slightly higher pH value in January.

Changes in the physical characteristics of the soil caused by ploughing activities can increase the quantity of CO_2 emission when compared to non-ploughed soil. This is because ploughing will break down soil aggregates, helping the soil to mix with organic particles, increases water infiltration and soil's ability to retain water, ultimately causing an increase in CO_2 production (Monika *et al*., 2002). Turmeric cultivation activities on the study site need to go through a ploughing process to provide bedding for seeding. CO_2 emission recorded in the turmeric cultivation area is slightly higher than the carbon emission in oil palm estates as reported by Melling *et al.,* (2005).

The supply of organic fertilizers to agricultural soil to supply nutrients to plants may also increase the quantity of CO_2 emission. Organic carbon from dissolved organic fertilizer in the soil is a source of carbon that can promote the growth of microorganisms which in turn increases CO_2 emissions from the soil (Monika *et al*., 2002).

CARBON STOCK

Carbon Stocks in August

The study site has a length and width of 100 m each and the depth of soil at the study site is 0.5 m. The average percentage of carbon content and an average bulk density of the soil is 39.77% and 0.20 g cm^{-3}, respectively.

The calculation of carbon stock is as follows: -

Soil volume = 100 m x 100 m x 0.5 m = 5000 m^3

= 5000 000 000 cm^3

Soil mass = 0.20 g cm^{-3} x 5000 000 000 cm^3 = 1000 000 000 g

= 1000 t ha^{-1} soil

Soil carbon stock = 39.77% x 1000 t

= 397.70 t ha^{-1} carbon

So, the soil mass at the study site with measurements 100 m long, 100 m wide and 0.5 m deep is 1000 t ha^{-1} while the carbon stock for this site is 397.70 t ha^{-1}.

Carbon Stocks in January

The study site has a length and width of 100 m respectively. Mean percentage of carbon content and means bulk density of soil at a depth of 0.5 m was 45.66% and 0.20 g cm^{-3}, respectively.

The calculation of carbon stock is as follows: -

Soil volume = 100 m X 100 m X 0.5 m = 5000 m^3

= 5000 000 000 cm^3

Soil mass = 0.20 g cm^{-3} X 5000 000 000 cm^3 = 1000 000 000 g

= 1000 t ha^{-1} soil

Soil carbon stock = 45.66% X 1000 t

= 456.60 t ha^{-1} carbon

The soil mass at the study site measuring 100 m long, 100 m wide and 0.5 m deep with bulk density of 0.20 g cm^{-3} is 1000 t ha^{-1} while the carbon stock at this size is 456.60 t ha^{-1}. The content of carbon stock was higher in January 2010 than in August 2009. The difference in carbon stock at the two samplings period was due to the differences in soil organic carbon content which were determined at different times. However, the difference was not significant. Previous studies in peat soil not far from this study area by Sahibin, *et al.* (2011) showed that carbon stock in the same size of land is slightly higher with 872.72 t ha^{-1} measured at a depth of 0.8 m and a higher bulk density of 0.26 g cm^{-3}. Carbon stock in peat soil is much higher than carbon stock in the mountain area of Fraser's Hill which recorded a carbon stock range of 217.90 t ha^{-1} to 223.24 t ha^{-1} (Mohamed *et al.*, 2016).

CONCLUSION

Peat soil used for the cultivation of turmeric in Kampung Tumbuk Darat, Kuala Langat Selatan had CO_2 emission similar to other peat soil areas in Malaysia. The average quantity of CO_2 emissions obtained in August was 467.10 ± 246.86 mg CO_2 m^{-2} hr^{-1} (40.92 ± 21.62 t CO_2 ha^{-1} yr^{-1}) while January had an average emission of 473.86 ± 153.12 mg CO_2 m^{-2} hr^{-1} (41.51 ± 13.41 t CO_2 ha^{-1} yr^{-1}). CO_2 emission recorded by Melling, *et al.* (2005) in the peat soil area in Sarawak oil palm cultivation is 46 to 335 mg CO_2 m^{-2} hr^{-1}. This shows that the CO_2 absorption principle in Kirita method can be used to determine CO_2 emission from the soil.

One hectare study area with a depth of 0.5 m has 397.70 t ha^{-1} carbon stock in August, 2009, while in January, 2010 the total carbon stock is 456.60 t ha^{-1}. The volume of soil to an area of one hectare to a depth of 0.5 m that is calculated is 5000 m^3, with average bulk density of 0.20 g cm^{-3} and soil mass 1000 t ha^{-1}.

The average surface temperature of peat soil in the study site is 29ºC. Average pH in peat soil was acidic with a pH value in August and January at pH 3.14 and pH 4.43, respectively. Soil fresh water content when sampling in August and January were respectively 80.22% and 56.15% with heavy rainfall in the sampling in August. Organic content of soil in both months is very high, which is at 95.97% and 92.47%. Organic carbon content, humic acid and fulvic acid in the soil in January were higher compared with August.

It was found that CO_2 emissions in soil in the study area was influenced by organic matter content, soil water content and soil temperature.

ACKNOWLEDGEMENT

This study was conducted under the Project UKM-GUP-ASPL-07-05-004, UKM-AP-PI-18-2009/2 and LRGS/TD/2001/UKM/PG/01. The author would like to thank the Faculty of Science and Technology, the National University of Malaysia in the award of research grant and provision of the infrastructure to ensure the success of this research.

REFERENCES

Berglund, Ö. Berglund, K. & Klemedtsson, L. 2008. A lysimeter study on the effect of temperature on CO2emission from cultivated peat soils. Geoderma, 54(3-4): 211-218.

Bot, A. & Benites, J. 2005. The Importance of Soil Organic Matter: Key to Drought-resistant Soil and Sustained Food Production. Rome: Food and Agriculture Organization of The United Nations

Bunt, J. S. & Rovira, A. D. 1954. Oxygen uptake and carbon dioxide evolution of heat sterilized soil. Nature, 173, 1242.

Cheng, W., Fu, S., Susfalk, R.B. & Mitchell, R.J. 2005. Measuring tree root respiration using carbon natural abundance: rooting medium matters. New Phytologist 167: 297–307.

Chow, A.T., Tanji, K.K., Gao, S. & Dahlgren, R.A. 2006. Temperature, water content and wet–dry cycle effects on DOC production and carbon mineralisation in agricultural peat soils. Soil Biol. Biochem. 38: 477–488.

Crill, P. M. 1991. Seasonal patterns of methane uptake and carbon dioxide release by a temperate woodland soil. Global Biogeochem. Cycles 5, 319–334.

Davidson, E.A. & Ackerman, I.L. 1993. Changes in soil carbon inventories following cultivation of previously untilled soils. Biogeochemistry 20: 161-193.

Fenner, C., Freeman, C. & Reynolds, B. 2005. Observation of a seasonally shifting thermal optimum in peatland carbon-cycling processes: implications for the global carbon cycle and soil enzyme methodologies. Soil Biol. Biochem. 37: 1814–1821.

Fujii, R., Ranalli, A.J., Aiken, G.R., and Bergamaschi, B.A. 1998. Dissolved organic carbon concentrations and compositions, and trihalomethane formation potentials in water from agricultural peat soils, Sacramento-San Joaquin Delta, California: Implications for drinking-water quality. U. S. Geological Survey. Water Resources Investigation Report 98-4147.

Glenn, S., Heyes, A. & Moore, T. R., 1993. Methane and carbon dioxide fluxes from drained peatland soils, southern Quebec. Global Biogeochem Cycles, 1993, 7, 247– 258.

Guo, L.B. & Gifford, R.M. 2002. Soil carbon stocks and land use change: a meta analysis. Global Change Biology 8: 345-360

Houghton, R.A. & Hackler, J.L. 2000. Changes in terrestrial carbon storage in the United States. 1. The roles of agriculture and forestry. Global Ecology and Biogeography 9: 125-144.

Houghton, R.A. & Hackler, J.L. 2003. Sources and sinks of carbon from land-use change in China. Global Biogeography Cycles 17: 1034.

Ishikura, K., Hirata, R., Hirano, T., Okimoto, Y., Wong, G. X., Melling, L., Aeries, E. B., Kiew, F., Lo, K. S., Musin, K. K., Waili, J. W. & Ishii, Y. 2019. Carbon Dioxide and Methane Emissions from Peat Soil in an Undrained Tropical Peat Swamp Forest. Ecosystems. Pp 1-17.

Jacot, K.A., Lucher, A., Nosberger, J. & Hartwig, U.A. 2000. Symbiotic nitrogen fixation of various legume species along an altitudinal gradient in the Swiss Alps. Soil Biology & Biochem 32: 1043-1052.

Kiese, R. & Butterbach-Bahl, K. 2002. N2O and CO2 emission from three different tropical forest sites in the wet tropics of Queensland, Australia. Soil Biol. Biochem. 34, 975–987.

Kirita, H. 1971. Re-examination of The Absorption Method of Measuring Soil Respiration Under Field Conditions: An Improved Absorption Method Using A Disc of Plastic Sponge As Absorbent Holder. Journal of Ecology 21: 3.4

Kirschbaum, M.U.F. 1995. The temperature dependence of soil organic matter decomposition and the effect of global warming on soil organic carbon storage. Soil Biology & Biochemistry 27: 753-760.

Kuzyakov, Y. 2002a. Review: factors affecting rhizosphere priming effects. Journal of Plant Nutrition and Soil Science 165: 382-396.

Kuzyakov, Y. 2002b. Separating microbial respiration of exudates from root respiration in non-sterile soils: a comparison of four methods. Soil Biology and Biochemistry 34: 1619–1629.

Lafleur, P.M., Moore, T.R., Roulet, N.T., & Frolking, S. 2005. Ecosystem respiration in a cool temperate bog depends on peat temperature but not water table. Ecosystems 8(6): 619–629.

Lal, R. 2002. Encyclopedia of Soil Science. United States: Marcel Dekker. Inc.

La Scala, N., Marques, J., Pereira, G. T. & Cora, J. E. 2000. Carbon dioxide emission related to chemical properties of a tropical bare soil. Soil Biol. Biochem. 32, 1469–1473.

Liikanen, A., Huttunen, J. T., Karjalainen, S. M., Heikkinen, K., Vaisanen,T. S. , Nykänen H. & Martikainen, P. J. (2006). Temporal and seasonal changes in greenhouse gas emissions from a constructed wetland purifying peat mining runoff waters. Ecological Engineering 26: 241-251.

Melling, L., Hatano, R. & Goh, K. J. 2005. Soil CO2 flux from three ecosystems in tropical peatland of Sarawak, Malaysia. Tellus (2005), 57B, 1–11

Mohamed, A. A., Abd Rahim, S., Aitman, D. A., & Kamarudin, M. K. A. 2016. Analisis kandungan karbon organik tanah secara bermusim di hutan bukit Jeriau, Fraser Hill, Pahang. Malaysian Journal of Analytical Sciences, 20(2), 452-460.

Monika, R., Singh, S. & Pathak, H. 2002. Emission of carbon dioxide from soil. Current Science 82 (5): 510-517.

Mosier, A. R. 1998. Soil processes and global change. Biol. Fertil. Soils 27, 221–229.

Norman, J.M., Kucharik, C.J., Gower, S.T., Baldocchi, D.D., Crill, P.M., Rayment, M., Savage, K. & Striegl, R.G. 1997. A comparison of six methods for measuring soil-surface carbon dioxide fluxes. J. Geophys. Res.102: 28771 – 28777.

Patiram, B., Thakur, N.S.A. & Ramesh, T. 2007. Soil Testing and Analysis: Plant, Water and Pesticide Residue. New Delhi: New India Publishing Agency.

Pol-van Dasselaar A, Corre W J, Prieme A, Klemedtsson A K, Weslien P, Stein A, Klemedtsson L and O.Oenema 1998 Spatial variability of methane, nitrous oxide, and carbon dioxide emissions from drained grasslands. Soil Sci. Soc. Am. J. 62, 810–817

Puget, P., Lal, R., Izaurralde, C., Post, M. & Owens, L.B. 2005. Stock and distribution of total and corn-derived soil organic carbon in aggregate and primary particle fractions for different land use and soil management practices. Soil Science 170: 256-279.

Raich, J.W. & Shlesinger, W.H. 1992. The global carbon dioxide flux in soil respiration and its relationship to vegetation and climate. Tellus 44B: 81-99.

Raich, J. W. & Tufekcioglu, A. 2000. Vegetation and soil respiration: correlations and controls. Biogeochemistry 48, 71–90.

Sahibin Abd. Rahim, Zulfahmi Ali Rahman, Mohd Nizam Mohd Said, Wan Mohd Razi Idris, Tukimat Lihan, Lee Yook Heng, Tajudin Mahmud & Cho Wai Keat. 2011. Kandungan Karbon Organik dan Stok Karbon dalam Tanih Gambut, Persekitaran Pertanian Kelapa Sawit, Kuala Langat Selatan, Selangor. Jurnal e-Bangi 6(2): 156-167.

Savage, K. E. & Davidson, E. A. 2001. Interannual variation of soil respiration in two New England forests. Global Biogeochem. Cycles 15 (2): 337–350.

Silvola, J., Alm, J., Ahlholm, U., Nykanen, H. & P.J. 1996. Martikainen, CO2 fluxes from peat in boreal mires under varying temperature and moisture conditions. Journal of Ecology 84: 219–228.

Tan, K. H. 1994. Environmental Soil Science. New York: Marcel Dekker Inc.

Tan, K.H. 2005. Soil Sampling, Preparation, and Analysis. Ed ke-2. United States: CRC Press.

Walkley, A. 1947. A critical examination of a rapid method for determining organic carbon m soils: Effect of variations in digestion conditions and of inorganic soil constituents. Soil Sci. 63:251-263.

Wiant, H. V. Jr., 1967. Influence of temperature on the rate of soil respiration. J. For., 65, 489–490.

Wu, H.B., Guo, Z.T. & Peng, C.H. 2003. Land-use induced changes of organic carbon storage in soils of China. Global Change Biology 9: 305-315.

Yew, F.K., Sundram, K. & Yusof, B. (2010). Estimation of GHG Emissions from Peat Used for Agriculture with Special Reference to Oil Palm. Journal of Oil Palm & Environment 1: 1-17.

Zeller, V., Bardgett, R.D. & Tappeiner, U. 2001. Site and management effects on soil microbial properties of subalpine meadows: a study of land abandonment along a north-south gradient in the European Alps. Soil Biology & Biochem 33: 639-649.

BorneoScience
The Journal of Science & Technology
Volume 40 Issue 1 : March 2019
Online ISSN : 2231-9085 | ISSN : 1394-4339

SOLAR CAR: BRIEF REVIEW AND CHALLENGES

Ag Sufiyan Abd Hamid*[12] and Halim Razali[2]

[1]Faculty of Science and Natural Resources, Universiti Malaysia Sabah, Jalan UMS, 88400 Kota Kinabalu, Sabah, Malaysia.
[2]Solar Energy Research Institute, Universiti Kebangsaan Malaysia, 43600 Bangi, Selangor, Malaysia

*Corresponding author: pian@ums.edu.my

Received 11st March 2019; accepted 11st March 2019
Available online 2nd Sept 2019
Doi: https://doi.org/10.51200/bsj.v40i1.4431

ABSTRACT. *Solar energy is known as renewable and clean source of energy. This tremendous amount of energy is widely used from small portable application to gigawatt size power plant generation. It has been utilized for various off grid or standalone applications including for vehicles. However, the progress of Solar Car (SC) was unsatisfied. Unlike Hydrogen Car (HC) and Pure Electric Vehicle (PEV), there is no commercialize SC marketed yet. Many strategies contributed to the successful of HC and PEV such as supportive policy, taxation, facilities and private involvement. The main component of SC can be simplified and consists of the structure, photovoltaic (PV) module, rechargeable battery pack, electric motor and power management unit. Main issue for SC is how to match between energy require and supply. Researchers are trying to find multiple solution from various aspects. Thirty SC prototypes were developed globally by numerous parties and most of them from academic bodies or universities. The purpose of the development is for solar car racing and to break commercialization boundary. As far as technology is concern, to achieve self-powered SC is quite challenging. The nearest potential solution can be learned from HC and PEV. All these potential solutions must be balance with the other side factor and come with a cost.*

KEYWORDS. Solar car; Electric vehicle; Solar energy, Standalone photovoltaic.

INTRODUCTION

Solar energy consists of Solar Photovoltaic (PV), solar thermal (Hamid *et al*., 2019) and solar photovoltaic-thermal (Ibrahim *et al*., 2011). Solar photovoltaic system can be divided into two categories: grid connected and off grid (standalone) system. Grid connected system usually used by solar farm and small system without battery bank as its energy storage. The electricity produced was supplied into the grid attached. The net metering is one of the examples used in grid connected system. The second system was isolated from the grid and require battery bank as energy storage. This system is suitable at remote area and for vehicles. Usually the capacity and load are small, and simpler compared to grid connected system. Several issues related to environment awareness and modernization of automobile industry contribute to emerging of Solar Car (SC). Transportation emitted the highest greenhouse gas emission by Internal Combustion Engine (ICE). **Figure 1** shows amount of carbon dioxide release approximately 1800 million metric tons.

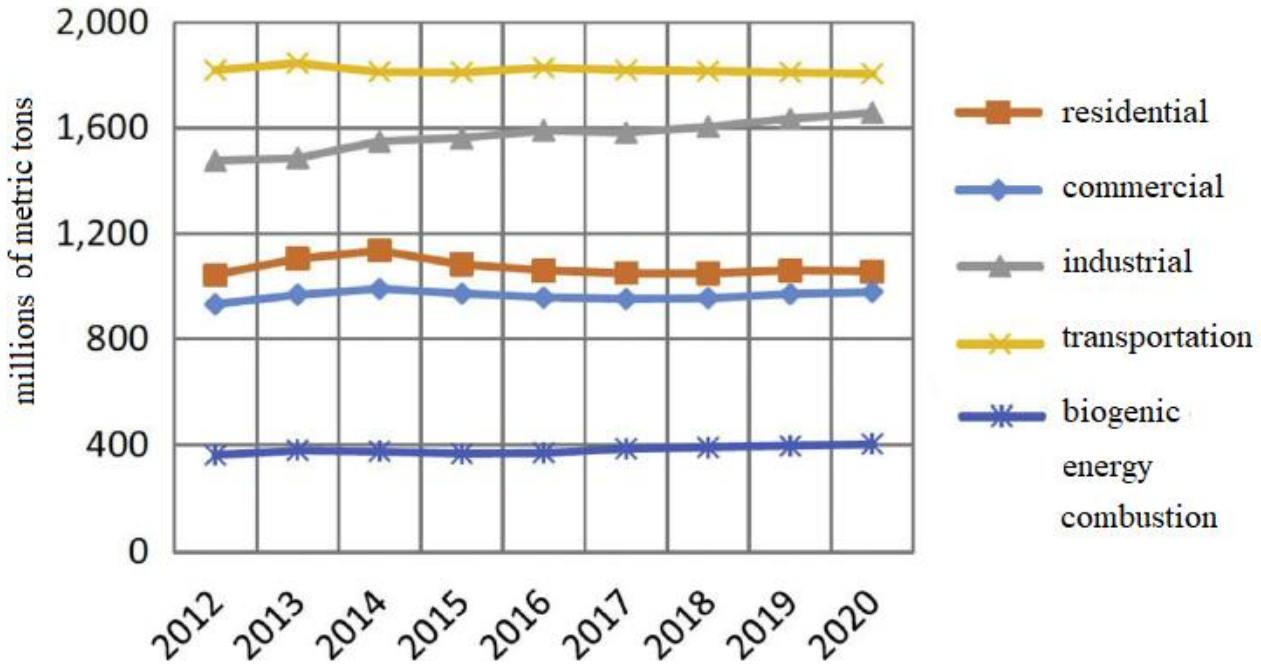

Figure 1 Survey and prediction of carbon dioxide for various sectors between 2012 – 2020 (Das *et al*., 2017).

Research shows by just installing PV module on conventional car, CO_2 emission can be reduced by 1-3%. The module estimated received 58% of solar irradiance available (Lodi *et al*., 2018). The hope from the implementation of SC can reduce even more and significant amount of pollutant by replacing the Internal Combustion Engine (ICE) with clean and renewable transportation vehicle.

It was estimated there are more than 900 million vehicles today and 1.1 billion by 2020. A review report divided electric car under three categories: battery powered car, fuel cell car and hybrid electric car (Wilberforce *et al*., 2017). However, authors would like to introduce the characterization of vehicle (car) based on the energy source (fuel) and type of engine as shown in **Figure 2**. The description of **Figure 2** is shown in **Table 1**.

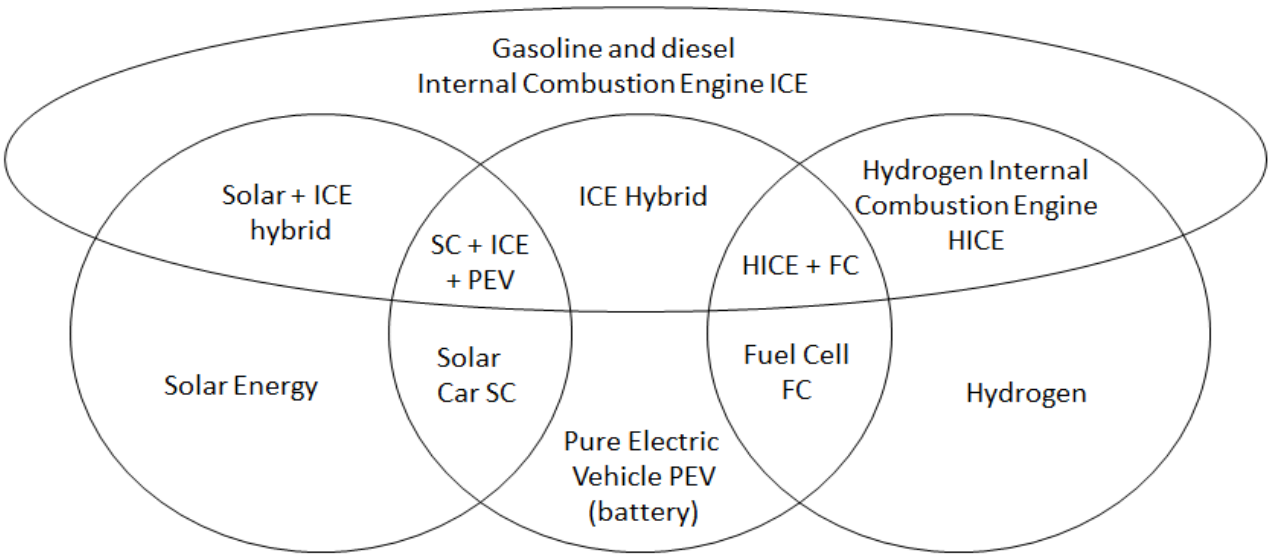

Figure 2 The characterization of car based on the fuel and type of engine.

Table 1 Description of car characterization based on fuel and engine technology.

	Type	Description
1	Internal Combustion Engine (ICE)	conventional (gasoline and diesel)
2	Hydrogen Internal Combustion Engine (HICE)	used hydrogen as mixture in ICE
3	Pure Electric Vehicle (PEV)	using battery + electric motor. Charge by electric grid
4	Fuel Cell (FC)	utilize FC technology
5	HICE + FC	the car is on dual mechanism (mechanical from HICE and electric motor from FC). The hydrogen divides to ICE and FC.
6	ICE hybrid	dual mechanism. Charging battery from grid
7	Solar Car (SC)	electric car. Charging battery from solar energy
8	SC + ICE + PEV	dual mechanism and the battery charged by solar energy
9	Solar + ICE hybrid	dual mechanism without battery

THE SOLAR CAR

Solar car basically use PV technology to convert sunlight spectrum to electricity. The electricity then used to power motor to create movement. Battery acts as energy storage to maintain power supply especially during low level or absence of sunlight. Power management unit will configurate charge and discharge process. **Figure 3** shows the diagram and components of SC.

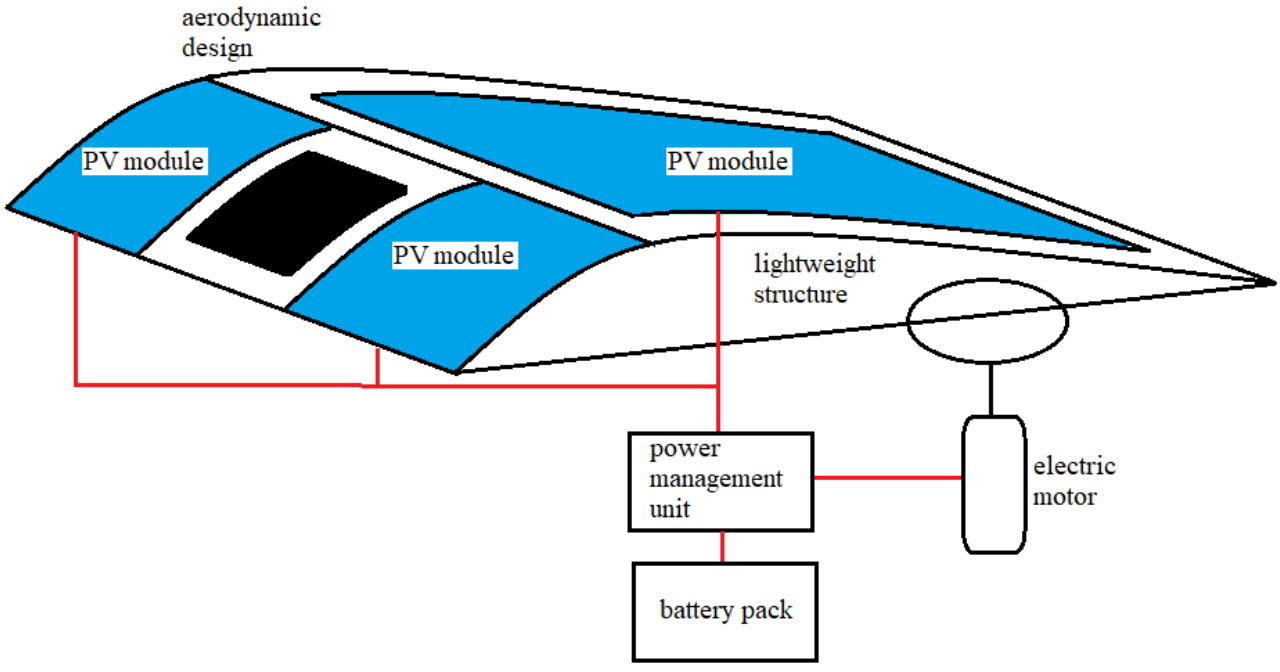

Figure 3 Solar car diagram and components.

To achieve pure solar car or self-powered solar car, the car should be able to generate its own energy from the sun. However, in practical so far almost all prototype SC need electric socket from grid for (plug-in) charging. The energy converted is insufficient due to small PV area and high energy require by the car.

1. Solar Photovoltaic PV Module

Energy conversion from direct sunlight spectrum into electric energy was done by using PV technology. The main characteristic of PV output can be referred to its voltage and current. These values can be manipulated into various parameters such as I-V (current-voltage) curve and P-V (power-voltage) curve. Shading will reduce PV module output. Unlike stationary PV installation, SC will experience inconsistence sunlight due to shading effect from tree, building and other terrestrial structures. Study estimates PV mounted car expose to only 58% of solar radiation available (Lodi *et al*., 2018). Choosing travelling path and parking spot are important for SC in order to reach direct sunlight as much as possible. This situation has already been studied by using Solar Car optimized Rout Estimation SCORE scheme (Hasicic *et al*., 2017). The SCORE gathered weather information (historical and forecast) and configurated the best path and spot for the car. Sunlight exposure will create temperature effect. Higher temperature will reduce module output. Research found that low temperature by using surface laminar H_2O method performed better than standard module. The improvement of power output and efficiency achieved are 9.74 W and 3.7 % respectively (Sukarno *et al*., 2017). The latest invention of flexible solar module enables designer of SC to create aerodynamic shape. The advantages of flexi solar are light weight, can be manufactured in roll, higher yield production, capable to bend and can be used as textile (Idris *et al*., 2018). Amorphous silicon and other thin film photovoltaic are capable to flex. However, poor bending radius and cost limited the potential (Schubert and Werner, 2006). Flexible solar cell based in carbon nanomaterial including dye sensitized, organic and perovskite solar cells have also been investigated. Several factors contribute to use carbon nanomaterials as flexible solar cell such as transparency, conductivity, durability, bendability and adjustable energy level (Fu *et al*., 2018). Research on fabrication, mechanical tolerant and stability of flexible perovskite solar was done at different condition. The result from the test successfully achieved 17.3 % efficiency of flexible perovskite solar cell (Idris *et al*., 2018).

2. Structure and Design

Solar car structure is important as body to attach all the component together. The structure must be light weight and strong for energy saving and safety purposes. Most of SC prototype aerodynamically designed to create less friction and smooth airflow all over the body. Light weight composite such as fiberglass and carbon fiber have advantages and potential to replace aluminum and steel in the automobile sector. Various supercars used increasing percentage of the composite such as Lamborghini, Ford GT, McLaren, Koenigsegg, Ferrari and Corvette (Howell *et al*., 2018). Teijin Group and Toho Tenax developed material and technology for SC. The ultra-light carbon fiber can be fabricated as thin as 0.06 mm and used as the cars body layer and the windows made from panlite polycarbonate resin. The fiber is 5 times lighter and has 8 times strength (tensile strength) of steel (Teijin 2018). **Figure 4** shows SC from Japan developed by Kogakuin University. The material was supplied by Teijin Group.

Figure 4 Solar car developed by Kogakuin University Japan for the Bridgestone World Solar Challenge race in Australia. (Source: Teijin 2018)

The aerodynamic design of solar car not only reduces the air drag but also increases PV module output. Better module performance is the result of heat removal by the airflow (Vinnichenko *et al*., 2014).

3. Energy Storage

Energy generated must be stored in order to sustained energy supply during low radiation or at night. Three type of rechargeable battery available for SC which are lithium-ion battery (li-ion), nickel metal hydride battery (NiMH) and lead-acid battery. Brief comparison shows specific energy for li-ion, NiMH and lead-acid are 100-265 Wh/kg, 60-120 Wh/kg and 33-42 Wh/kg respectively. Average energy density also estimated as 471.5 Wh/L, 220 Wh/L and 85 Wh/L respectively. The lowest specific power is lead-acid 180 W/kg, followed by li-ion 250-340 W/kg and NiMH 250-1000 W/kg. Charging and discharging efficiency also identified for li-ion ranging between 80-90 %, NiMH 66-90 % and lead-acid 50-95 % (Kim *et al*., 2019; Morris and Tosunoglu, 2012; Bukhari *et al*., 2015).

The battery suitable for SC has the same criteria with battery that use in standalone PV system and electric car. Researchers are focusing on li-ion battery and are trying to optimize the performance in many aspects. The temperature of the battery increases drastically during discharge. Cooling process was investigated by applying several configuration of phase changes material PCM round the battery. Result showed two PCM configurations reduced maximum temperature by 20.9 K and 23.2 K (Moraga *et al*., 2016). Investigation on battery requirement concluded that the possibility of using home and public charger station, battery technology is the bottleneck to electric car implementation and the relevant of charging infrastructure service to reduce the required battery range (Shi *et al*., 2019). Lithium ion battery supply chain is also important. A study has proposed a strategy from development and remanufacturing aspects related to li-ion battery to maximize the profit. Outcome from the study estimated 9.81 % higher profit can be achieved by considering several selected key factors (Li *et al*., 2018). Another study experimented on load optimization to reduce the cost. The

result showed 12.7 % cost reduction compared to original battery pack setup from the factory (Cardenas *et al*., 2018).

4. Power Management Unit

The process of charging from PV to battery and discharging from battery to motor must be in optimized condition. Generally, in PV system, power management configurated by charge controller. Charge controller divided into maximum power point tracker and pulse width modulation. In solar or electric car, the configuration is more complex due to variation of charge and load condition. Some features such as additional load for computation and brake-charging push the need for more dynamic controlling capabilities. Power management unit or battery management system BMS act like charge controller in PV system. The function of BMS for SC is illustrated in **Figure 5** (Hoquea *et al*., 2017).

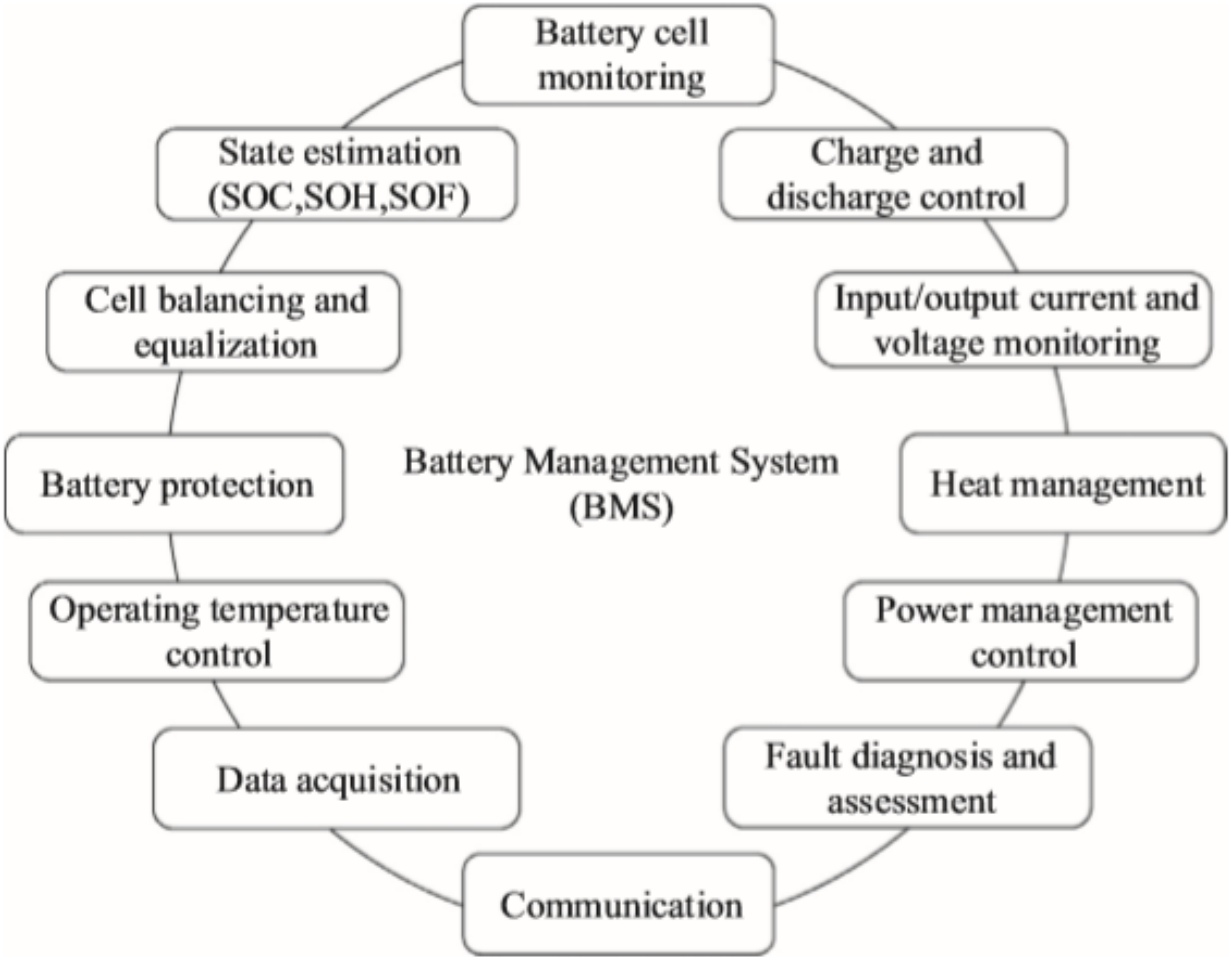

Figure 5 The functions of battery management unit in solar car (Hoquea *et al*., 2017).

5. The Electric Motor

Solar car movement is created by electric motor. Efficient motor is crucial to minimize energy loss from the battery. Type of electric motor available are Permanent Magnet Synchronous Motor (PMSM), direct current motor and induction motor. The main issues related to electric motor for vehicle are inconsistent drive cycle, high torque and power, some main component failure in backup system, durability and wide range of speed control (Chi-lan *et al*., 2011). For PMSM, motor needs to

match the requirements of the external characteristics as shown in **Figure 6**, such as start-stop, climbing and acceleration maneuver which require constant torque at low-speed. Another maneuver is for high speed which requires constant power at low torque (Wang *et al*., 2018).

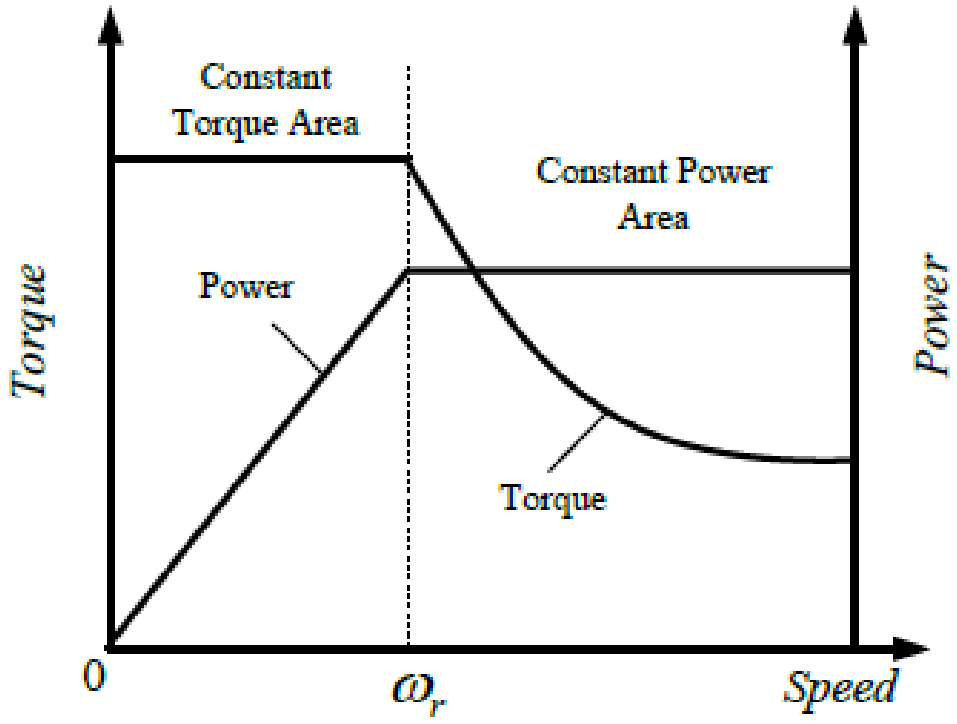

Figure 6 The external characteristic of PMSM (Wang *et al*., 2018).

The application of electric motor for solar car becomes interesting by discovering more concepts such as in-wheel component, using multiple motor and charge-braking features. In-wheel motored vehicle was tested and simulated, focusing on yaw stability control. Results simulated the advantages of control methodology during maneuver on slippery road (Ren *et al*., 2016). A comparison between single and dual motor input was also discussed. The outcome shows dual motor powertrain produced higher overall efficiency compared to single motor (Wu *et al*., 2018). The capability of charging by braking was also discovered and discussed. Regeneration charge was produced by several method such as DC-DC converter, ultracapacitors and electronic gearshift technology. The testing on brushless DC motor was analyzed from simulation and experimental data (Godfrey and Sangkaranarayanan, 2018).

RECENT PROGRESS AND CHALLENGES

The achievement of SC can be measured by the number of cars commercialize in the market. So far, not a single SC marketed yet. In comparison, hydrogen car has already launched 5 models: two hydrogen internal combustion engine models (BMW hydrogen 7 and Aston Martin Rapid S) and three fuel cell models (Honda clarity, Hyundei Nexo and Toyota Mirai).

The current status of SC remains as prototype. Various parties already come out with their SC concept. However, none of them successfully achieve market commercialization. The prototype

list is shown in **Table 3**. Most of them were produced by universities or academic body and involved in solar car racing. Meaning that SC is still under R&D and heavily funded.

Table 3 The model, developer and origin of the SC prototype.

No	Solar car model	Developer	Origin
1	Sunswift V (eVe)	University of New South Wales	Australia
2	Solar Spirit 3	TAFE institute	
3	e.coTech Solar version	HiTech Electric	Brazil
4	Schulich Delta	University of Calgary	Canada
5	"Chen Shungui"	-	China
6	Hochschule Bochum: Open World	Hochschule Bochum	Germany
7	PowerCore SunCruiser	Hochschule Bochum	
8	Sion	Sono Motors	
9	SolarWorld GT	Hochschule Bochum	
10	ThyssenKrupp SunRiser	Hochschule Bochum	
11	SolarMobil	Manipal University	India
12	P-Mob	Fiat	Italy
13	Emilia 4	University of Bologna	
14	Kaiton II	Goko High School	Japan
15	OWL	Kogakuin University	
16	Venturi Astrolab	Venturi Automobiles	Monaco
17	Venturi Eclectic	Venturi Automobiles	
18	Stella	Eindhoven University	The Netherlands
19	Stella Lux	Eindhoven University	
20	Stella Vie	Eindhoven University	
21	Twente One	University of Twente and Saxion University	
22	UltraCommuter	University of Waikato	New Zealand
23	ECO1, ECO1GL and ECO3GL	Muhammad Aslam Azaad	Pakistan
24	Metron 7	Andrej Pecjak and his Metron team	Slovenia
25	Superpiki	Yuneec & Metron	
26	Icare	Icare	Switzerland
27	Solar Taxi	Lucerne University and University of Applied Sciences Northwestern Switzerland	
28	Apollo Solar Cruiser Car	National Kaohsiung University of Applied Sciences	Taiwan
29	Daedalus	University of Minnesota	USA
30	Eos	University of Minnesota	

Most significant SC race is Bridgestone World Solar Challenge held in Australia. The racetrack between Darwin and Adelaide is estimated to be 3000 km. The racing class is divided into three: challenger, cruiser and adventure class.

The main hurdle to implement self-powered SC is insufficient power generated to tackle energy demand for the motor and other appliances. The fundamental problem emerged from several aspects such as power supply, weight and PV area. To achieve full charge for average typical battery vehicle, 4.5 peak sun hour with 7.5 kW array required. Meaning that 7500 m^2 PV and additional of 800 kg weight needed which is not practical for SC. In comparison, the car must be able to overcome 6.25 times PV power, 4 times weight and 1250 times PV area. Other issues are PV efficiency, shading and cost. Flexible solar cell only achieved 17.3 % (Idris *et al*., 2018), exposed to 58 % (Lodi *et al*., 2018) sunlight available and cost is extremely high (4 times electric car and 15 times conventional car). A case study (Sukarno *et al*., 2015) determined the limitation of solar source estimated that the average and maximum irradiance intensity were 500 W/m^2 and 1000 W/m^2 respectively. These factors will add even more challenges to construct practical SC in term of SC energy balance and structure design.

In order to overcome the deficit energy. Main solar array can be off set from the car and construction of solar charging station might be helpful. Applying wireless charging road enables SC to maintain travelling without stopping while charging its battery. Many strategies can be learned from hydrogen car and electric vehicle. Japan as leading country in hydrogen development has invested great effort in many sectors such as facilities, economy, R&D and public involvement program. Japan provides many hydrogen stations for hydrogen car. In economy, 12.3 billion USD was invested in hydrogen development. The country also patented around 25 000 patents on fuel cell and selected several cities to implement hydrogen energy as their main energy source (Behling *et al*., 2015).

CONCLUSION

This report briefly concludes the importance to revolutionize transportation sector and applying SC as part of transportation mode. The basic of SC and its components were also discussed. As far as technological concern, fundamental hurdle and other technology aspect contribute to slow progress of SC compared to hydrogen car and battery electric vehicle. Not a single commercial self-powered solar car yet to be marketed indicates that many more must be done and there is a need for government and private support. However, it is optimistic that SC can be implemented in the future by proceeding to discover solution for current issues.

ACKNOWLEGEMENT

Authors would like to acknowledge Solar Energy research Institute, Universiti Kebangsaan Malaysia (STPD6083 program) for initiating this work. Authors also would like to acknowledge Faculty of Science and Natural Resources, Universiti Malaysia Sabah for supporting this work.

REFERENCES

Hamid, A.S.A, Ibrahim A, Mat S, Sopian K (2019) Experimental Evaluation on Large Scale Solar Dryer for Drying Natural Fiber in Malaysia. *International Journal of Renewable Energy Research* Vol.9(2): 598-604.

Ibrahim A, Othman M.Y, Ruslan M.H, Mat S, Sopian K (2011) Recent advances in flat plate photovoltaic/thermal (PV/T) solar collectors. *Renewable and Sustainable Energy Reviews*, V15(1):352-365.

Das S.H, Tan C.W, Yatim A.H.M (2017) Fuel cell hybrid electric vehicles: a review on power conditioning units and topologies, *Renew Sustainable Energy Rev*:268–91.

Lodi C, Seitsonen A, Paffumi E, Gennaro M. D, Huld T, Malfettani S (2018) Reducing CO2 emissions of conventional fuel cars by vehicle photovoltaic roof, *Transportation Research Part D* 59, 313–324.

Wilberforce T, El-Hassan Z, Khatib F. N, Al-Makky A, Baroutaji A, Carton J. G, Olabi A. G (2017) Developments of electric cars and fuel cell hydrogen electric cars, *International Journal of Hydrogen Energy 42*, 25695–25734.

Hasicic M, Bilic D, Siljak H (2017) Criteria for Solar Car Optimized Route Estimation, *Microprocessors and Microsystems 51*, 289–296.

Sukarno K, Hamid A. S. A, Razali H, Dayou J (2017) Evaluation on Cooling Effect on Solar PV Power Output Using Laminar H2O Surface Method, *International Journal of Renewable Energy Research Vol.7* No.3 1213 – 1218.

Idris K. Popoola, Mohammed A. Gondal, T. F. Qahtan (2018) Recent progress in flexible perovskite solar cells: Materials, mechanical tolerance and stability, *Renewable and Sustainable Energy Reviews 82*, 3127–3151.

Schubert M. B, Werner J. H (2006) Flexible solar cells for clothing, *Material Today 9(6)*, 42–50.

Fu X, Xu L, Li J, Sun X, Peng H (2018) Flexible solar cells based on carbon nanomaterials, *Carbon 139*, 1063 – 1073.

Howell E, Neal D, Kieffer D (2018) Changing the paradigm of transportation: Lightweight composites used in solar car in intercollegiate competition, *Reinforced Plastics* Vol 62, No 4.

Teijin supplies materials for solar car (2017) *Reinforced Plastics*. Vol 61, Number 5.

Vinnichenko N. A, Uvarov A. V, Znamenskaya I. A, Ay H, Wang T. H (2014) Solar car aerodynamic design for optimal cooling and high efficiency, *Solar Energy* 103, 183–190.

Kim J, Oh J, Lee H (2018) Review on battery thermal management system for electric vehicles, *Applied Thermal Engineering* 149, 192–212.

Morris M, Tosunoglu S (2012) Comparison of Rechargeable Battery Technologies, *ASME Early Career Technical Journal*. ASME Early Career Technical Conference, ASME ECTC. November 2-3, Atlanta, Georgia USA.

Bukhari S. A. S, Maqsood J, Baig M. Q, Ashraf S, Khan T. A (2015) Comparison of Characteristics - Lead Acid, Nickel Based, Lead Crystal and Lithium Based Batteries, *17th UKSIM-AMSS International Conference on Modelling and Simulation*. DOI 10.1109/UKSim.2015.69, 2015

Moraga N. O, Xamán J. P, Araya R. H (2016) Cooling Li-ion batteries of racing solar car by using multiple phase change materials, *Applied Thermal Engineering 108*, 1041–1054.

Shi X, Pan J, Wang H, Cai H (2019) Battery electric vehicles: What is the minimum range required?, *Energy 166*, 352-358.

Li L, Dababneh F, Zhao J (2018) Cost-effective supply chain for electric vehicle battery remanufacturing, *Applied Energy 226*, 277–286.

Cárdenas B, Garvey S. D (2018) Load optimization for reducing the cost of an electric vehicle's battery pack, *Journal of Energy Storage 20*, 254–263.

Hoquea M. M, Hannan M. A, Mohameda A, Ayob A (2017) Battery charge equalization controller in electric vehicle applications: A review, *Renewable and Sustainable Energy Reviews 75*, 1363–1385.

Chi-lan C, Xiao-gang W, Yue-wei B, Yan-chun X, Kai L (2011) Key Technologies of EV Motor Drive System Design, *Procedia Engineering 16*, 356 – 362. 2011

Wang W, Fu R, Fan Y (2018) Electromagnetic Parameters Matching of Permanent Magnet Synchronous Motor for Hybrid Electric Vehicles, *IFAC papers online 51-31*, 407-414.

Ren B, Chen H, Zhao H, Yuan L (2016) MPC-based yaw stability control in in-wheel-motored EV via active front steering and motor torque distribution, *Mechatronics 38*, 103–114.

Wu J, Liang J, Ruan J, Zhang N, Walker P. D (2018) Efficiency comparison of electric vehicles powertrains with dual motor and single motor input, *Mechanism and Machine Theory 128*, 569 – 585.

Godfrey A. J, Sankaranarayanan V (2018) A new electric braking system with energy regeneration for a BLDC motor driven electric vehicle, *International Journal of Engineering Science and Technology*, 21, 704–713.

Sukarno K, Hamid A. S. A, Dayou J, Makmud M. Z. H, Sarjadi M. S. (2015) Measurement of Global Solar Radiation in Kota Kinabalu Malaysia, *ARPN Journal of Engineering and Applied Sciences*, Vol. 10, No. 15, 6467-6471.

Behling N, Williams M. C, Managi S (2015) Fuel cells and the hydrogen revolution: Analysis of a strategic plan in Japan, *Economic Analysis and Policy 48*, 204–221.

BorneoScience
The Journal of Science & Technology
Volume 40 Issue 1 : March 2019
Online ISSN : 2231-9085 | ISSN : 1394-4339

PERFORMANCE OF KAPOK FIBER REINFORCED POLYVINYL ALCOHOL BICOMPOSITE BY ALKALI TREATED

Muhammad Danial Jamat, Jahimin Asik[a]

[a]Faculty Science and Natural Resources, Universiti Malaysia Sabah, Jalan UMS, 88400 Kota Kinabalu, Sabah, Malaysia

*Corresponding author email: jthan@ums.edu.my

Received 23rd April 2019; accepted 23rd April 2019
Available online 2nd Sept 2019
Doi: https://doi.org/10.51200/bsj.v40i1.4429

ABSTRACT. *Raw Kapok (Ceiba pentandra) fibre was initially washed and dried before undergoes chemical treatment. Upon dried, the kapok fibre was bleached and delignified at room temperature, in an acidic solution containing 6% of sulphuric acid and 4% hydrogen peroxide to remove hemicellulose and wax. The treated kapok was filtered and washed thoroughly with distilled water and vacuum dried at 60 ^oC for 10 hours. Finally, the treated kapok was converted to alpha-cellulose (α-cellulose) by alkali treatment. In this step, treated kapok was immersed in 17.5% of sodium hydroxide solution for 30 minutes at a temperature of 50 ^oC to remove alkali-soluble components. The obtained α-cellulose, termed as alkali-treated kapok fiber (AKTF) was filtered, washed thoroughly with distilled water until pH is neutral and vacuum dried at 60 ^oC for 10 hours. In this stage, a certain weight of ATKF (0%, 10%, 20%, 30%, and 40%) were mixed with a hot solution of PVA and dried at room temperature. In the mechanical test, ATKF – PVA biocomposite shows an increase in tensile strength and elastic modulus up to 30% content of kapok fibre but drop at 40% kapok loading. The result shows that both ATKF – PVA biocomposite film (30%) were having the highest mechanical properties among the others and was chosen for next characterizations. It is evidence in FTIR spectra that the composites indicate the formation of new hydrogen interaction between kapok fibre and PVA which might help to improve the mechanical properties. As for XRD analysis, the ATKF – PVA biocomposite film (30%) blend was found to be a heterogeneous as the peaks of diffractogram were overlap each other. This is supported by SEM micrograph in which ATKF – PVA biocomposite (30%) show a heterogeneous phase. Additionally, in the TGA data, ATKF – PVA biocomposite (30%) was founded less thermally stable than raw kapok and pure PVA is the least thermally stable among other samples.*

KEYWORDS. PVA; Kapok fiber; Biocomposite; Mechanical Properties

INTRODUCTION

Kapok tree or *Ceiba pentandra* is belong Bombacaceae family which mostly grows in Asia, West Africa and Central America region. Kapok also refers to the fluffy cotton-like that obtained from seed pods. The

physical appearance of kapok is silky, yellowish or brownish colour (Zheng *et a*l., 2015). According to Fengel and Przyklenk (1986), main composition of kapok fiber consists of cellulose, lignin and xylan. Their composition percentage however, were *inconsistently reported. A study conducted by* Kobayashi *et al*., (1977) has revealed that kapok fibre is composed of about 64% of cellulose, 13% of lignin and 23% of pentosan on a weigh basis, while another study found that kapok fiber composed of cellulose (35 %), xylan (22%), and lignin (21.5%) (Hori *et al*., 2000). Recent study shows that cellulose content in the kapok fiber is 50.7% (Tye *et al*., 2012). Kapok fibre is mostly used as filling material in mattresses, pillows or as oil absorbing materials (Abdullah *et al*., 2010) and water-safety equipment due to its excellent buoyancy (Zhang *et al*., 2013).

Polyvinyl Alcohol (PVA) is a water-soluble synthetic polymer which widely used as a matrix in the composite. It possesses many excellent properties such as non-toxic, biocompatible, good mechanical properties and good film-forming capability (Srinivasa *et al*., 2003). PVA also water-soluble and hydrophilic in nature (Qiu, & Netravali, 2013) make it easier to work on. Compared to other man-made polymer such as polyvinyl chloride (PVC) and polyethylene (PE) which are non-biodegradable, PVA can be considered as biodegradable synthetic polymer due to the hydroxyl groups that presence on carbon atoms and its degradability can be improved by hydrolysis process (Gaaz *et al*., 2015). PVA has the idealized formula $[CH_2CH(OH)]n$ and can be combined compatibly with organic or inorganic materials due to the presence OH groups and formed hydrogen bond to form PVA composites. Multiple studies showed PVA based composite was successfully applied in tissue scaffolding, filtration material, protective coveralls and pharmaceutical applications (Abdulkhani *et al*., 2013). Many previous researches were using PVA as matrix in combination with different fillers such as seaweed, cotton and kenaf. For example, Puttaswamy *et a*l., (2017) has fabricated PVA reinforced cellulose microfibers from jatropha seed shell in his research. He found that the tensile strength of the composite was increasing as filler content increase. Another study by Laxemeshwar *et al*., (2012) using microcrystalline cellulose blend with PVA, shows that the tensile strength of modified cellulose to PVA, 95 + 05 is the strongest while 10 + 90 is the weakest.

METHODOLOGY AND MATERIALS

1. Materials

Chemicals used in this research were of analytical grade. They were purchased from Aldrich Co. and used without further purification. Kapok fiber was purchased locally at Kota Kinabalu Sabah market. Before chemical treatment, all the impurities such as leaves, fruit skin and seed was manually removed.

2. Preparation of Kapok Fiber

a) Delignification and Bleaching

About 7 g of raw kapok fiber was heated in 100 ml of solution (a combination of 25 ml of 4% hydrogen peroxide, H_2O_2 and 75ml of 6% sulphuric acid, H_2SO_4) (Asik et al., 2016). The solution was stirred and heated at 70 ^oC for 1 hour. In order to recover the loss of solution during heating process, 100 ml of the

solution was added into the solution every 20 minutes. Next, the slurry was vacuum filtered by using polyester cloth and then washed with distilled water several times until the pH of the filtrate reaches a neutral condition at pH 7. Finally, the wet cellulose was vacuum dried for 10 hours at 60 ^{o}C.

b) α-Cellulose Conversion

The slurry obtained from section 3.4.1 was further treated again with 17.5% of sodium hydroxide, NaOH to obtain α-cellulose. The solution was stirred for 30 minutes at 50 ^{o}C until the colour of the mixture turn to milky white. The slurry was vacuum filtered using polyester cloth and then washed with distilled water several times until the pH reaches 7. Lastly, the wet α- cellulose was vacuum dried for 10 hours at 60 ^{o}C. The cellulose obtained in this section was termed as alkali treated kapok fibre (ATKF).

c) Preparation of Kapok Fiber/PVA Biocomposite

A series amount of an alkali treated kapok fibre (ATKF) was weighed and soften by addition of 2 ml of boiling water. Meanwhile, PVA solution was prepared by dissolving 4% of PVA pallets in 100 ml distilled water which make the concentration of PVA solution produced is 4 wt % (w/v). PVA solution is heated at 75 ^{o}C and stirred with magnetic stirrer to ensure PVA solid is fully dissolved. Next, the wetted alkali treated kapok fiber (ATKF) was mixed and stirred for 10 minutes until the mixture became homogenous. The mixture was casted on metal tray and let it dried in fume hood for 24 hours at room temperature. The dried ATKF biocomposite was peeled, cut into size and subjected for characterization.

3. Characterization of Kapok Fibre - PVA Biocomposite Film

a) Mechanical Properties of Kapok Fibre - PVA Biocomposite

The tensile test was carried out using universal testing machine (Gotech AI-7000M) according to ASTM and all testing was done at room temperature. Tensile strength was expressed as the maximum tensile strength divided by the initial cross-sectional area. The specimens were cut at dimension 110 mm (L) x 30 mm (W) x 0.5 mm (T). Each test was repeated 3 time with different specimens and the average value was calculated.

b) Functional Group Determination of Kapok Fibre - PVA Biocomposite

Fourier Transform Infrared Spectroscopy (FTIR) was used to detect the presence of functional group in kapok/PVA biocomposite thin film. 2 mg of sample was weighed and analyzed with FTIR (100 series, Perkin –Elmer) and pressed onto disc with 1 mm thickness. The range of absorption band recorded in between 600 – 4000 cm^{-1}.

c) CrystallinityDetermination of Kapok Fibre - PVA Biocomposite

X-ray diffraction (XRD) is a method in determination of crystallinity of a compound. The X-ray diffraction measurement were carried out using Expert Pro (Philipes EW3040/60) with Cu Kα radiation operating at 40 kV. The scattering angle covered the range from 2Θ of 5^{o} to 60^{o} and the samples were cut into 3 x 3 cm dimension for length and width.

d) Morphology Behavior of Kapok Fibre - PVA Biocomposite

The study on morphology of dried samples were carried out using field electron scanning electron microscopy model LEO SUPRA 55, Carl Zeiss. The sample was cut into small dimension and coated with gold coating to improve electrical conductivity. All the samples images were taken at 15 kV of accelerating voltage with various magnification image of the samples.

e) Thermal Behavior of Kapok Fibre - PVA Biocomposite

The thermal behaviour of kapok fibre was determined using Thermogravimetric Analysis (TGA) using Perkin-Elmer model 4000. About 8-12 mg of kapok fiber was heated at rate of 10 ^{o}C/min in nitrogen atmosphere and temperature for each samples were set from 30 - 700 ^{o}C. Derivative Thermogravimetry (DTG) analysis was carried out in the same way.

RESULTS AND DISCUSSION

1. Sample Selection

The composition of ATKF biocomposite shown in Table 1. Selection of best biocomposite for further characterizations was based on mechanical test results.

Table 1: The composition of ATKF biocomposite.

Sample	1	2	3	4	5
Polyvinyl alcohol (g)	4	4	4	4	4
Kapok (%)	0	10	20	30	40

2. Mechanical Properties

Figure 1 indicate tensile strength and elongation at break results while figure 2 show result of elastic modulus for pure PVA and ATKF biocomposite thin film composite. It reveals that pure PVA shows the highest percentage of elongation to break (48.05%) compared other samples. It was found that the tensile strength of ATKF biocomposite increases as kapok content increased to 30% (17.11 MPa). The highest tensile strength with the value of 17.11 MPa was obtained when 30% kapok is added. The increase of tensile strength probably because of strong interfacial interaction between kapok fiber and matrix which is PVA thus inhibit crack formation. The ability of fibers to restrict matrix mobility also contributed to tensile strength improvement (Zainuddin *et al*., 2013).

However, the tensile strength of ATKF biocomposite started to decrease when it reaches 40% kapok loading. This observation might be due the possible aggregation of kapok fibre that could reduce tensile strength of the ATKF biocomposite as described by Lu *et al.*, (2008). In other words, kapok cellulose was not dispersed homogeneously in the PVA matrix at 40% content that lead the decline of tensile strength (Cho & Park, 2011). Increasing kapok loading resulted in increased elastic modulus of

ATKF biocomposite until reached 30% (177.89 MPa) but declined as kapok loading increase further until 40%. Pure PVA show the lowest elastic modulus with the value 15.24 MPa which supported from previous research by Puttaswamy *et al*., (2017), also have the lowest elastic modulus results among the samples for pure PVA.

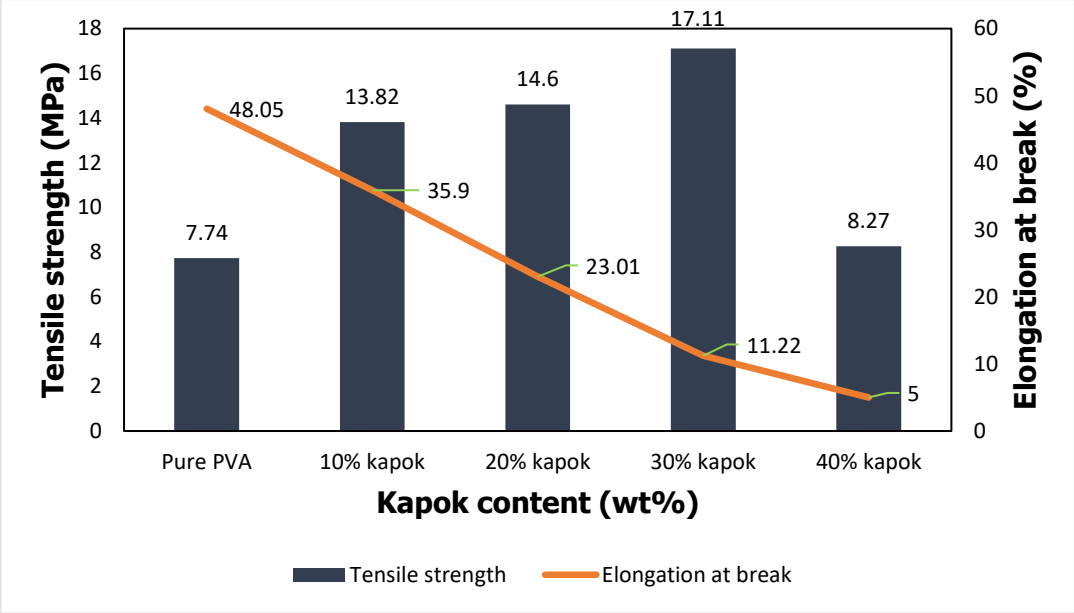

Figure 1: Tensile strength and elongation at break of ATKF biocomposite thin film.

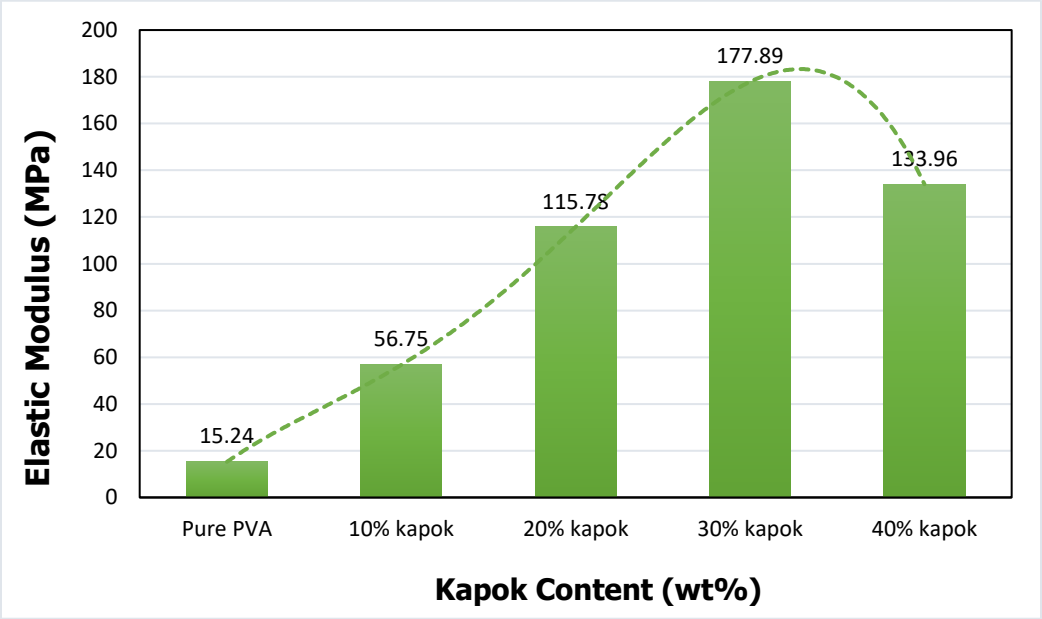

Figure 2: Elastic modulus of ATKF biocomposite thin film.

3. Fourier Transform Infrared (FT-IR) Spectroscopy

FTIR spectra of ATKF, ATKF – PVA biocomposite (30%), pure PVA and raw kapok were shown in figure 3. Strong and broad peak at 3341 cm^{-1} showed hydrogen bonded O – H stretching vibration due to existence of water. The intramolecular hydrogen bonds inside the PVA cause O – H stretching vibration while the formation of this peak are responsible by intermolecular hydrogen bonding between hydroxyl groups of PVA and kapok fiber (Jahan *et al*., 2018). Weak peak at 2900 and 2901 cm^{-1} was assigned C – H stretching vibrations of alkyl group. Absorption band at 1368 cm^{-1} attributed to C – H bending and peak 1737 cm^{-1} reveal the C = O group and esters in lignin and acetyl ester groups in xylan which can be seen at raw kapok spectre (Matuana *et al*., 2001). Theoretically, carbonyl group (C=O) should not exist in pure PVA spectrum at peak 1716 cm^{-1} since PVA chemical formula only consists hydroxyl group (OH). However, there are maybe some remaining of acetate group which contain C=O group exist in the PVA batch since PVA is prepared from PVAc. This statement can be proved by the presence of carbonyl group (C=O) at band 1723 cm^{-1} (Campos *et al.*, 2013). The absorption band at 896 cm^{-1} is showing the typical structure β-glycoside linkage at raw kapok spectrum and ATKF wavenumber of C–O–C stretching at peak 1159 cm^{-1}.

ATKF – PVA biocomposite film (30%) bands reveal the interaction between O – H bonding kapok/PVA composite at peak of 1422 cm^{-1} (Prachayawarakorn *et al*., 2013). ATKF band show O-H bending of adsorbed water is observed at peak 1629 cm^{-1}. Even ATKF cellulose undergoes drying process, however the peak of adsorbed water still presence. This is due to the cellulose-water interaction make the water in the cellulose molecules difficult to be extracted (Moran *et al*., 2008). As studies by Tiwari *et al*. (2013), absorption peaks in raw kapok at 1595 cm^{-1} and 1426 cm^{-1} shows the presence of lignin compound corresponding to the aromatic skeletal vibration. Based on the FTIR spectrum of ATKF, hemicellulose and lignin peaks were found to completely vanish. The lignin removal from kapok fibre was encouraged by loss of peaks at 1426 cm^{-1} in ATKF (Bono *et al*., 2009; Draman *et al*., 2013).

The FT-IR composites material interaction between matrix and filler can be identified by band position shifting to a lower wavenumber in the spectra which indicates the interaction of hydrogen bonding between the composites (Wu *et al*., 2009). From the FT-IR spectre below, the hydrogen bonded hydroxyl peak at 3350 cm^{-1} for raw kapok and 3301 cm^{-1} for pure PVA has shifted to lower wavenumber at 3290 cm^{-1} for ATKF – PVA biocomposite (30%). This results lead to the new hydrogen bond formation between kapok and PVA during composite preparation (Jumaidin *et al*., 2017). The peak shifting revealed the good compatibility between matrix filler interaction while hydrogen bonding formation in composite materials probably supported with mechanical properties enhancement of the materials (Jumaidin *et al*., 2017).

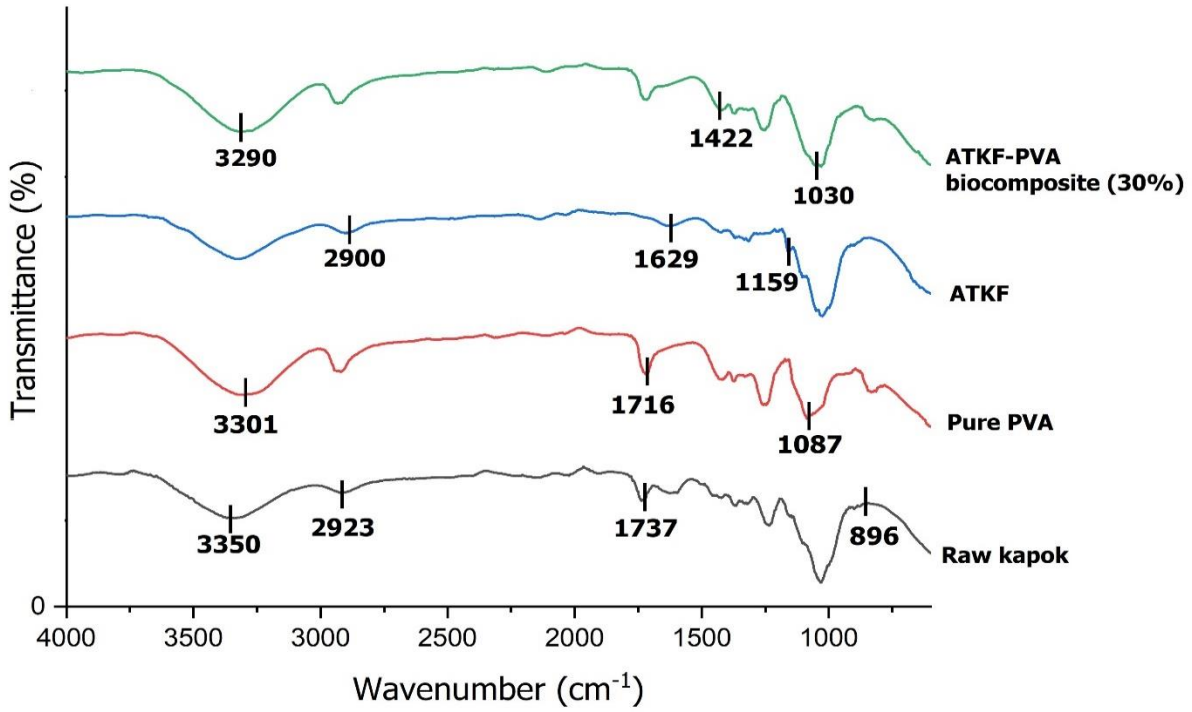

Figure 3: FT-IR spectre of ATKF – PVA biocomposite (30%), ATKF, pure PVA and raw kapok.

4. X – Ray Diffraction (XRD) Analysis

Figure 4 demonstrated x-ray diffractogram of ATKF, ATKF – PVA biocomposite (30%), pure PVA and raw kapok. From the results, pure PVA show typical a peak with high intensity at range 2θ = 19.89º which are same from the previous researches by Hajeeassa *et al*., (2018) and Jahan *et al*., (2018). The crystallinity index obtained for pure PVA was 53.45% similar to Jahan *et al*., (2018) which the crystallinity index for their PVA membrane around 53%. On the other hand, it can be interpreted PVA reveal a semicrystalline structure because of the high affinity to form hydrogen bond (Hajeeassa *et al*., 2018). Meanwhile, raw kapok shows small peak at 17.37º and broad peak at 2θ = 23º. The crystallinity index (CI) of raw kapok fibre was 32% which is slightly lower as reported by Purnawati *et al*., (2018**)** which the kapok fibre crystallinity index was 35.65%. The peak 17.37º represents the presence amorphous parts of kapok such as lignin, hemicellulose, wax and other impurities (Ma *et al*., 2015).

When raw kapok fibre was treated with 17.5 NaOH solution, there is change occur in the result. The peak intensity incline compares to raw kapok due to the removal of lignin and hemicellulose. The sharp peak at region 2θ = 22.1º and weak peak show in region 2θ = 16.8 and 12.3º in diffractrogram represent typical crystalline cellulose peak (Bondsen *et al*., 2006). The crystallinity index of ATKF is expected to be increased up to 64% which also similar result reported by Liu & Wang (2009) where the dewaxed fiber crystallinity index was 63%. On the other hand, the diffractogram pattern of ATKF -PVA composite (30%) indicated 2 overlap peak at region 20º and 23º. No new peak produced from the ATKF -PVA composite (30%). It can be concluded that ATKF -PVA composite (30%) is a heterogeneous composite phase.

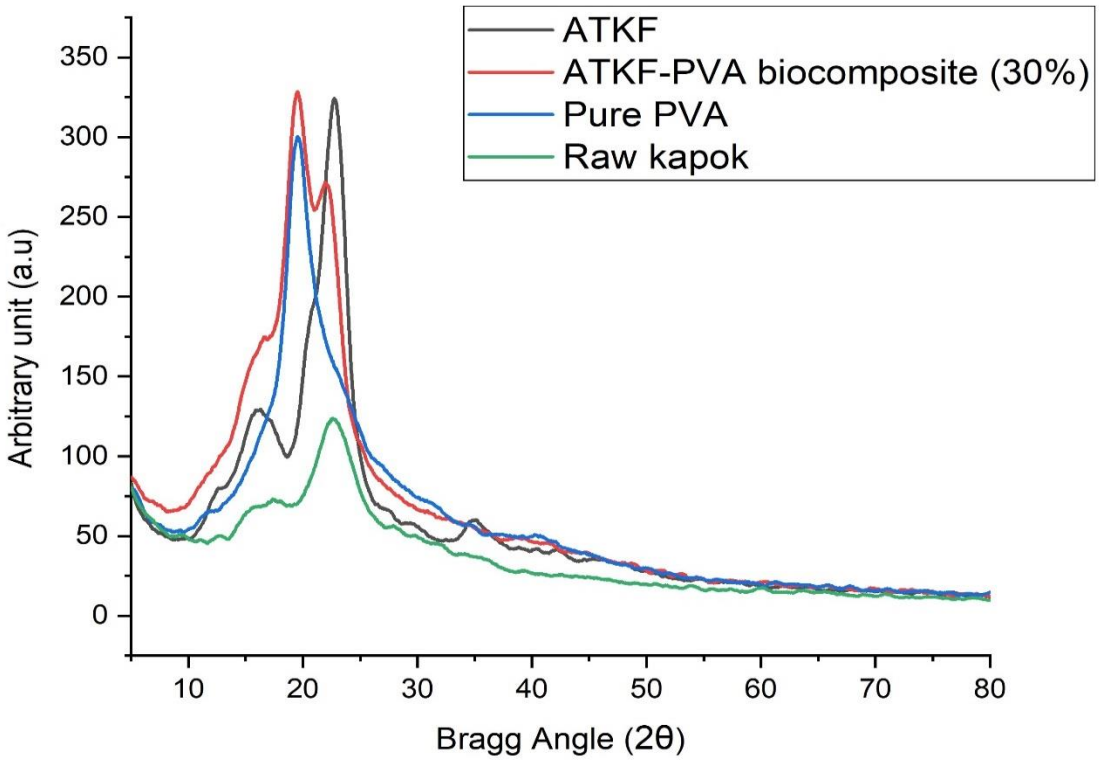

Figure 4: XRD diffractogram of ATKF, ATKF – PVA biocomposite (30%), pure PVA and raw kapok.

5. Scanning Electron Microscopy (SEM)

Scanning electron micrographs of raw kapok fibres, cross section of kapok fibre, ATKF, pure PVA, surface of ATKF – PVA biocomposite (30%) and cross section ATKF – PVA biocomposite (30%). A silky appearance, smooth surface (Draman *et al.* 2013) and tangled like structure can be seen in raw kapok fiber as shown in Figure 5a. The average diameter for raw kapok is 28.7 µm which slightly larger than reported by Purnawati *et al*., (2018) in the range 17.59 µm. Meanwhile, kapok fibre cross section on Figure 5b shows a large lumen with hollow tube shape of and thin fibre wall of kapok fibre cross section. The cell wall thickness of kapok fiber obtained an average of 1.16 µm which similar to Purnawati *et al*., (2018) meanwhile the average lumen diameter obtained was 14.51 µm which larger from a previous finding by Mwaikambo and Bisanda, (1999) and Kang *et al*., (2007).

ATKF in Figure 5c indicate the kapok fiber look a rougher than raw kapok fiber and also the structure turned out to be totally flattened with strip like shape (Draman *et al.* 2013). ATKF image also show the different length from raw kapok fibers which the length was drastically reduced after chemical treatment (Sonia & Dasan, 2013). The average width estimated is around 19.5 µm which is in the range as reported by Draman *et al.,* (2013) were 18.5 to 23.1 µm the width obtained from kapok treated with NaOH. As for pure PVA image (Figure 5d), the plain image shows as expected which alike from previous research from El-Kheir *et al*., (2015). The situation in Figure 5e was a difference where the ATKF and PVA matrix form a uniform layer composite. It can be seen the ATKF merge into PVA matrix and form a good adhesion interaction. However, data from XRD reveal that the layer formed was heterogenous. The alkali treatment attests that the hydrogen bonding interaction between PVA and ATKF was improved as indicated in FTIR analysis.

.

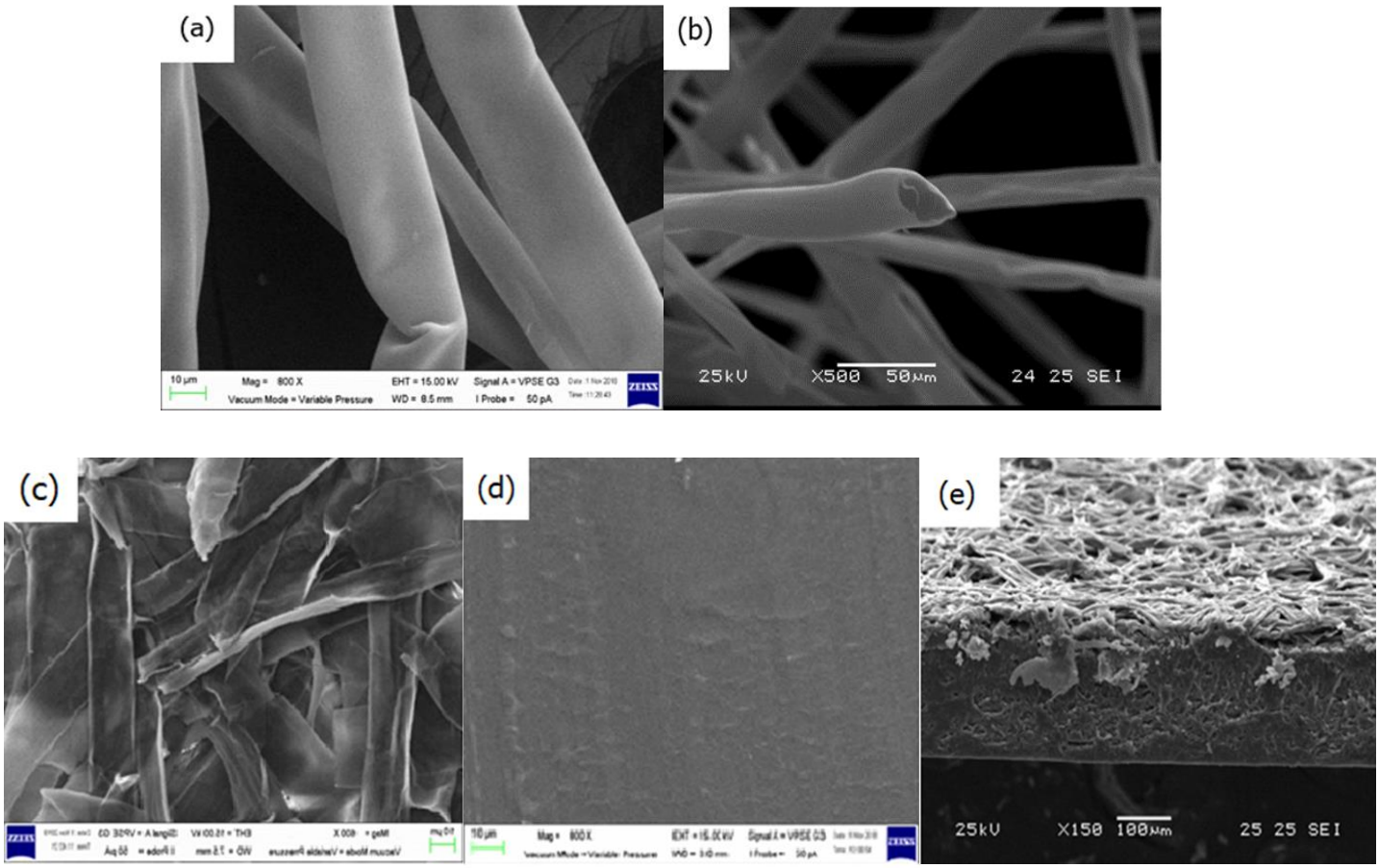

Figure 5: SEM images of (a) raw kapok fibre; (b) cross section of kapok fibre; (c) ATKF; (d) pure PVA; (e) cross section ATKF – PVA biocomposite (30%).

6. Thermogravimetric Analysis

Figure 6 and 7 below shows the thermograms of TGA and DTG respectively. The starting degradation temperature was observed to be 350 ^{o}C, 359 °C, 394 °C and 360 °C for raw kapok, pure PVA, ATKF and ATKF – PVA biocomposite film (30%) respectively. The initial weight loss for all samples begins from 50 to 150 °C due to removal of moisture content in the samples by evaporation.

Raw kapok exhibits two major degradation stages. The raw kapok degradation temperature started at 350 ^{o}C. At this stage, polysaccharides, i.e. cellulose and hemicelluloses were started to be degraded (Draman *et al*., 2014) and proceed until it reaches the completion decomposition temperature at 550 ^{o}C (Brebu and Vasile, 2010). Meanwhile, for ATKF, the moisture evaporation occurs at 56 ^{o}C and decomposition temperature started at 352 ^{o}C. During this stage, cellulose in ATKF was almost burnt because of oxidative thermal degradation and crystallite structure deterioration (Yeng *et al*., 2015).

Pure PVA also have 2 major degradation stages. The first weight loss occurs at temperature range 103 – 106 °C due to removal of moisture in the samples by evaporation which causes 5% mass loss from the original weight. Kim *et. al.*, (2008) published that the cause of this first weight loss is related to the evaporation of both water and also glycerol. As the temperature increased, the decomposition of PVA

started at 360 to 370 ^{o}C. At this stage, the hydroxyl and methyhydroxyl groups were stated to be eliminated. The degradation continues until it reaches the completion decomposition at 480 – 500 ^{o}C where the polymer C – C backbone has been destroyed completely (Ahad *et al.*, 2012).

For ATKF – PVA biocomposite film (30%), it showed an expected result which 2 steps of mass loss. The first weight loss was definitely due to evaporation of moisture content in the sample that occur at ranges of 90 –110 ^{o}C. The drastic mass loss that start at 360 ^{o}C might be due to the disintegration of intra- and intermolecular of hydrogen bonds between PVA and cellulose (El-Kheir *et al*, 2017). The completion decomposition at 500 ^{o}C has indicated that PVA and cellulose main chain have been completely degraded (Othman *et al.*, 2011).

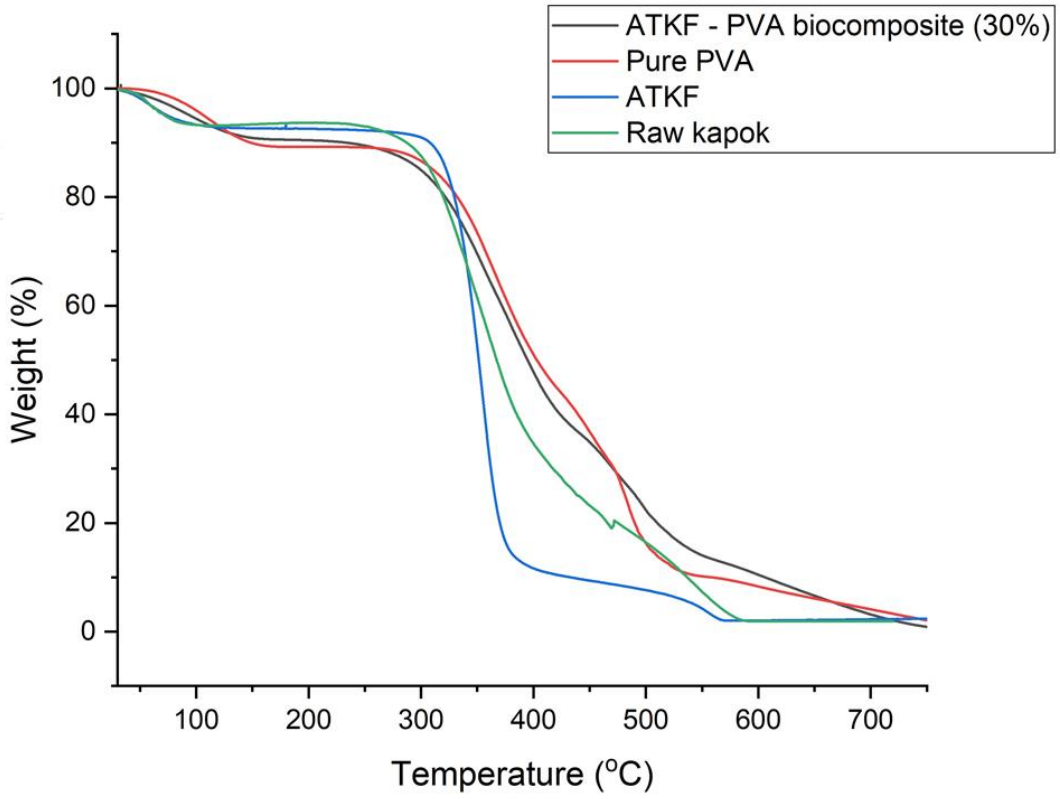

Figure 6: The TGA thermograms obtained from ATKF – PVA biocomposite film (30%), pure PVA, ATKF and raw kapok.

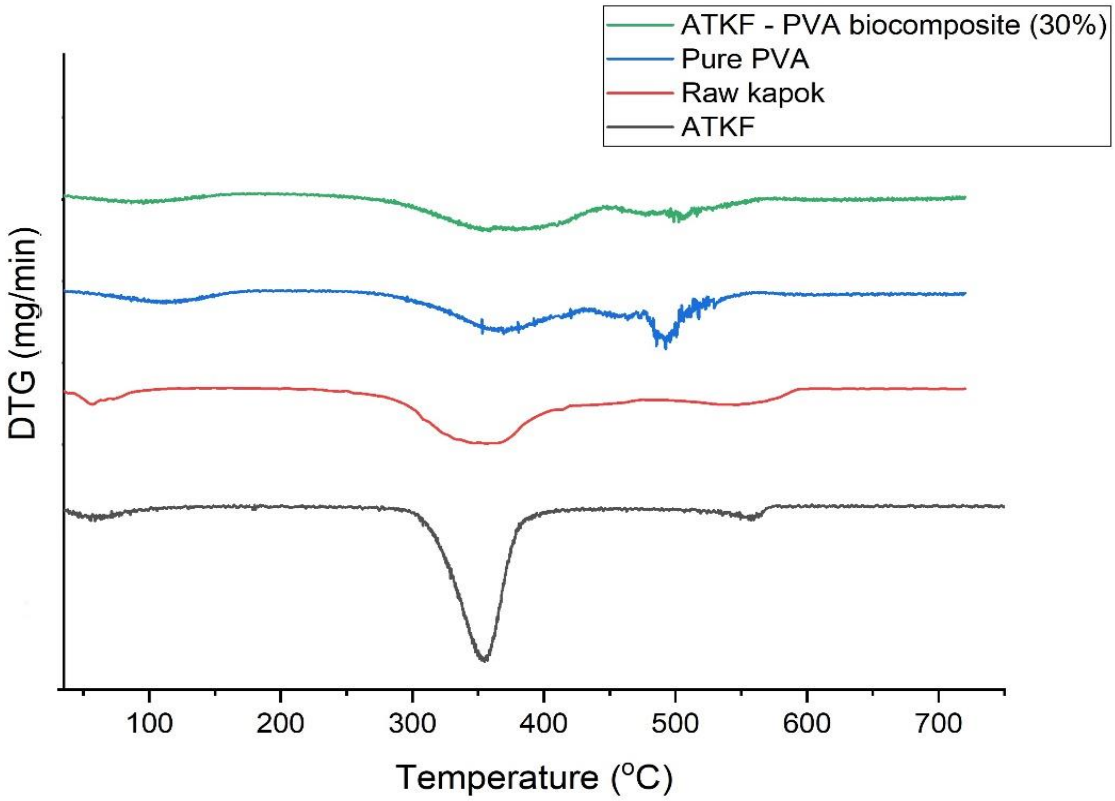

Figure 7: DTG thermogram of ATKF – PVA biocomposite film (30%), pure PVA, ATKF and raw kapok.

CONCLUSION

This study has shown the improvement in tensile strength of ATKF – PVA bicomposite until it reaches 30% kapok loading and decrease when it reaches 40% kapok loading. FTIR spectra indicates interaction of ATKF with PVA matrix produce new hydrogen interaction which helps improve the mechanical properties. As for XRD analysis, the result reveals ATKF – PVA biocomposite film (30%) was heterogeneous which in diffractogram, the peaks of kapok/PVA (30%) overlap each other that supposedly new peak formed for the composite. SEM micrograph shows ATKF – PVA biocomposite (30%) film form a heterogeneous layer. However, ATKF – PVA bicomposite (30%) interaction is more smooth and uniform which give advantage in mechanical properties. From the TGA data, ATKF – PVA bicomposite (30%) was founded less thermally stable than raw kapok and pure PVA is the least thermally stable among other samples.

ACKNOWLEDGEMENTS

The authors are grateful for financial support from Universiti Malaysia Sabah under UMS Great Grant for their financial support during research have been conducted.

REFERENCES

Abdulkhani, A., Hojati, M. E., Ashori, A., Hamzeh, Y., Karimi, A. N. (2013). Preparation of Cellulose/Polyvinyl Alcohol Biocomposite Films Using1-n-butyl-3-Methylimidazolium Chloride. *International Journal of Biological Macromolecules*, 62, 379– 386.

Abdullah, M. A., Rahmah, A. U., Man, Z. (2010). Physicochemical and Sorption Characteristics of Malaysian *Ceiba pentandra (L.) Gaertn*. as a Natural Oil Sorbent. *Journal Hazardous Materials*, 177, 683–691.

Ahad, N., Saion, E., & Gharibshahi, E. (2012). Structural, Thermal, and Electrical Properties of PVA-Sodium Salicylate Solid Composite Polymer Electrolyte. *Journal of Nanomaterials*, 2012, 1–8.

Asik, J., Aziz, F. A., Idris, R. (2016). *Mercerized Natural Cellulose Based-Solid Polymer Electrolyte. Borneo Science*, 37(2), 48 – 60.

Bondsen, D., Mathew, A., Oksman, K. (2006). Optimization of the nanocrystal from microcrystalline celluloses by acid hydrolysis. *Journal of Cellulose*, 13, 171–180.

Bono, A., Ying, P.H., Farm, Y. Y., Muei, C.L., Sarbatly, R., Krishnaiah, D. (2009). Synthesis and characterization of carboxymethyl cellulose from palm kernel cake. *Advances in Natural and Applied Sciences*, 3, 5-11.

Brebu, M., Vasile, C. (2010). Thermal degradation of lignin – A review. *Cellulose Chemistry and Technology*, 44, 353–363.

Campos, E., Coimbra, P., Gil, M. H. (2013). An improved Method for Preparing Glutaraldehyde Cross-linked Chitosan–Poly(vinyl Alcohol) Microparticles. *Polymer Bulletin*, 70, 549 – 561.

Cho, M. J., Park, B. D. (2011). Tensile and thermal properties of nanocellulose-reinforced poly(vinyl alcohol) nanocomposites. *Journal of Industrial and Engineering* Chemistry, 17: 36 – 40.

Draman, S. F. S., Daik, R., Abdul Latif, F., El-Sheikh, Said. M. (2013). Characterization and Thermal Decomposition Kinetics of Kapok (Ceiba pentandra L.)–Based Cellulose, *BioResources*, 9(1), 8 – 23.

El-Kheir, A., A., Popescu, C., Mowafi, S., Salama, M., El-Sayed, H. (2015). Physico-chemical Properties of Keratin-polyvinyl Alcohol Composite. Fibers and Polymers, 16(3), 537 – 542.

Fengel, D., & Przyklenk, M., (1986). Studies on Kapok. *Holzforschung*, 40 (6), 325–330.

Gaaz, T. S., Sulong, A. B., Akhtar, M. N., Kadhum, A. A. H., Mohamad, A. B., Al-Amiery AA. (2015). Properties and Applications of Polyvinyl Alcohol, Halloysite Nanotubes and Their Nanocomposites. *Molecules*, 20, 22833–22847.

Hajeeassa, K. S. Hussein, M. A., Anwar, Y. Tashkandi, N., Y. and Zahra M Al-amshany. (2018). Nanocomposites containing polyvinyl alcohol and reinforced carbon-based nanofiller: A super effective biologically active material. *Nano Biomedicine*, 5, 1–12.

Hori, K., Flavier, M. E., Kuga, S., Lam, T. B. T., & Iiyama, K. (2000). Excellent Oil Absorbent Kapok [Ceiba pentandra (L.) Gaertn.] Fibre: Fibre Structure, Chemical Characteristics, and Application. *Journal Wood Science*, 46 (5), 401–404.

Jahan, Z., Niazi, M. B. K., Hägg, M.-B., & Gregersen, Ø. W. (2018). Cellulose nanocrystal/PVA nanocomposite membranes for CO_2 /CH_4 separation at high pressure. *Journal of Membrane Science*, 554, 275–281.

Jumaidin, R., Sapuan, S. M., Jawaid, M., Ishak, M. R., Sahari, J. (2017). Effect of seaweed on mechanical, thermal, and biodegradation properties of thermoplastic sugar palm starch/agar composites. *International Journal of Biological Macromolecules*, 99, 265 –273.

Kang, P. H., Jeun, J. P., Yeoup Chung, B. Y., Kim, J. S., & Nho, Y. C. (2007). Preparation and Characterization of Glycidyl Methacrylate (GMA) Grafted Kapok Fiber by Using Radiation Induced-grafting Technique. *Journal of Industrial and Engineering Chemistry*, 13, 956-958.

Kim, G. M., Asran A. S., Michler G. H., Simon P., Kim, J. S. (2008). Electrospun PVA/HAp Nanocomposites Nanofibers: Biomimetics of Mineralized Hard Tissues at a Lower Level of Complexity. *Bioinspiration & Biomimetics*, 3(4), 1-12.

Kobayashi, Y., Matsuo, R., & Nishiyama, M. (1977). Method for Adsorption of Oils.Japanese Patent, 52,138,081, November, 17, 1977.

Laxmeshwar, S. S., Viveka, S., Kumar, D. J. M., & Nagaraja, G. K. (2012). Preparation a Properties of Composite Films from Modified Cellulose Fiber-reinforced with PLA. *Journal of International Scholarly Research Network Polymer Science*, 4(1), 159-168.

Liu, J. &. Wang, F., M. (2009). Effect of Alkalization Treatment on Structure and Properties of Blended Kapok Yarn. *Journal of Xi'an University Engineering Science and Technology*. 23, 379-386.

Lu, J., Wang, T. and Drzal, L.T. (2008). Preparation and Properties of Microfibrillated Cellulose Polyvinyl Alcohol Composite Materials. Composites Part A: *Applied Science and Manufacturing*. 39, 738 – 746.

Ma, N., Liu, D., Liu, Y., & Sui, G. (2015). Extraction and Characterization of Nanocellulose from *Xanthoceras Sorbifolia* Husks. *International Journal of Nanoscience and Nano Engineering*. 2: 43-50.

Matuana, L. M., Balatinecz, J., Sodhi, R. N. S., Park, C.B. (2001). Surface characterization of esterified cellulosic fibers by XPS and FTIR Spectroscopy. *Wood Science and Technology*, 35, 191-201.

Mwaikambo, L. Y., & Bisanda, E. T. N. (1999). The Performance of Cotton Kapok Fabric Polyester Composites. Polymer Testing, 18 (3), 181–198.

Othman, N., Azahari, N. A., & Ismail, H. (2011). Thermal Properties of Polyvinyl Alcohol (PVOH)/Corn Starch Blend Film. Malaysian Polymer Journal, 6, 147–154.

Prachayawarakorn, J., Chaiwatyothin, S., Mueangta, S., Hanchana, A. (2013). Effect of jute and kapok fibres on properties of thermoplastic cassava starch composites. *Material & Design*, 47, 309–315.

Purnawati, R., Febrianto, F., Wistara, I. N. J., Nikmatin, S., Hidayat, W., Lee, S. H., & Kim, N. H. (2018). Physical and Chemical Properties of Kapok (*Ceiba pentandra*) and Balsa (*Ochroma pyramidale*) Fibres. *Wood Engineering*, 46 (4). 393-401.

Puttaswamy, M., Srinikethan, G., Shetty, K. V. (2017). Biocomposite composed of PVA reinforced with cellulose microfibers isolated from biofuel industrial dissipate: *Jatropha Curcus L*. seed shell. *Journal of Environmental Chemical Engineering*, 5, 1990–1997.

Qiu, K., Netravali, A.N. (2013). A Composting Study of Membrane-Like Polyvinyl Alcohol Based Resins and Nanocomposites. *Journal of Polymers and the Environment*, 21, 658 –674.

Sonia, A., Dasan, K. P. (2013). Chemical, morphology and thermal evaluation of cellulose microfibers obtained from Hibiscus sabdariffa. *Carbohydrate Polymers*, 92, 668 – 674.

Srinivasa, P. C., Ramesh, M. N., Kumar, K. R., & Tharanathan, R. N. (2003). Properties and Sorption Studies of Chitosan-Polyvinyl Alcohol Blend Films. *Carbohydrate Polymer*, 53, 431–438.

Tiwari, R., Rana, S., Singh, S., Arora, A., Kaushik, R., Agrawal, W., Saxena, A. K., Nain, L. (2012). Biological delignification of paddy straw and *Parthenium sp*. using a novel micromycete Myrothecium roridum. Bioresource Technology, 135, 7 – 11.

Tye, Y. Y., Lee, K. T., Abdullah, W. N. W., & Leh, C.P. (2012). Potential of Ceiba pentandra (L.) Gaertn. (Kapok Fiber) as a Resource for Second Generation Bioethanol: Effect of Various Simple Pre-treatment Methods on Sugar Production. *Bio resource Technology*, 116, 536–539.

Wu, Y., Geng, F., Chang, P.R., Yu, J., Ma, X. (2006). Effect of Agar on the Microstructure and Performance of Potato Starch Film. *Carbohydrate Polymer*, 76, 299–304.

Yue, Y. (2011). A Comparative Study of Cellulose I and II and Fibres and Nanocrystals (Master Thesis, Louisiana State University). Retrieved from https://digitalcommons.lsu.edu/gradschool_theses/764/?utm_source=digitalcommons.lsu.edu%2Fgradschool_theses%2F764&utm_medium=PDF&utm_cam paign=PDFCoverPages

Zainuddin, S. Y. Z., Ahmad, I., Kargarzadeh, H., Abdullah, I., Dufrense, A. (2013). Potential of using multiscale kenaf fibers as reinforcing filler in cassava starch – kenaf biocomposites. *Carbohydrate Polymers*, 92, 2299 – 2305.

Zhang, X.Y., Fu, W.Y., Duan, C.T., Xiao, H., Shi, M.W., Zhao, N., & Xu, J. (2013). Super Hydrophobicity Determines the Buoyancy Performance of Kapok Fibre Aggregates. *Applied Surface Science*, 266, 225–229.

Zheng, Y., Wang, J., Zhu, Y., & Wang, A., (2015). Research and Application of Kapok Fibre as an Absorbing Material: A Mini Review. *Journal of Environmental Sciences*, 27, 1-12.

BorneoScience
The Journal of Science & Technology
Volume 40 Issue 1 : March 2019
Online ISSN : 2231-9085 | ISSN : 1394-4339

FORMULATION OF POLYMERIC INHIBITOR FOR VISCOSITY REDUCTION OF CRUDE OIL

S. M. Anisuzzaman[a,b*], M. Rajin[b], D. Krishnaiah[b], E. Junny[b]

[a]Energy Research Unit (ERU),

[b]Chemical Engineering Programme, Faculty of Engineering,
Universiti Malaysia Sabah, 88400 Kota Kinabalu, Sabah, MALAYSIA.

[*]Corresponding author: anis_zaman@ums.edu.my; dr.anis.ums@gmail.com

Received 5th February2019; accepted 5th February2019
Available online 2nd Sept 2019
Doi: https://doi.org/10.51200/bsj.v40i1.4432

ABSTRACT. *Generally, waxes and asphaltenes are classified as solid category which involved with deposition of high-molecular-weighted compounds along pipelines which leads to production issues. This study presents the effect of different mixture concentration consisting of copolymer and solvent on crude oil viscosity in order to find a solution for reduction of wax and asphalthene deposition along the surface of pipelines. There were two proportions used which are ethylene-vinyl acetate 25 (EVA 25), methylcyclohexane (MCH) and paraxylene as first proportion and EVA 40, MCH and paraxylene as second proportion. EVA is a polymer that comprises of linear chain of polyethylene fragment and vinyl acetate molecule which has the ability in controlling the size of formed wax crystals. Laboratory experiments were designed by response surface methodology (RSM) specifically using central composite design (CCD) to formulate ratio and analyzed optimum percentage composition of mixture to obtain a good model. The optimum parameters were 10.02% of EVA 25, 10.00% of MCH and 79.98% of paraxylene for first proportion and 10.00% of EVA 40, 45.78% of MCH and 44.22% of paraxylene for second proportion to minimize the viscosity of crude oil.*

KEYWORDS: Crude Oil, Ethylene-vinyl acetate, Methylcyclohexane, Paraxylene, Wax, Response surface methodology (RSM)

INTRODUCTION

Wax defined as hydrocarbon containing 20 to 40 carbon atoms in a chain where those structures consists of few structural types including straight chain, branched chain and cyclic chain (Yao *et al.*, 2016). For asphaltene, it defined as saturated hydrocarbon which consists of carbon, nitrogen, oxygen, hydrogen and sulphur (Ariza-León *et. al.*, 2014). Both of wax and asphaltene involved in stability of crude oil at distributed state. Instability of temperature will caused of coagulation of wax and flocculation of asphaltene during the process of transportation of crude oil along pipelines from oil rig to the shore.

In crude oil, wax molecules exist in liquid phase where the molecules undergo crystallization when it exposed to cold condition (Oh *et. al.*, 2009). Drastic change of solubility of waxes is the main reason for deposition of waxes where this condition cause wax molecules crystallize and become a solid gel, decreasing cross sectional area of pipelines (Bai and Zhang, 2013). Thus, changes of solubility of waxes result in the formation of gel which minimizes the transportation efficiency.

There are several assumptions made because of complex nature of waxy crude oil (Aiyejina *et. al.*, 2011; Anisuzzaman *et. al.*, 2017 a,b; Luthi, 2013; Kralova et al., 2011). Those assumptions are used to highlight the oil properties that affect their flow ability in production, refining and transportation of crude oil. There are lots size of pumps and pipeline system produced by oil industries which been led by those assumptions. During cooling process, waxy crude oil encounter thermal shrinkage where the gas voids appear while the fluid turn into multiphase (Singh *et al.*, 2008). Voids in the gel occur because of decrease in volume of waxy-oil gel during that process (Chala *et al.*, 2015, Chala *et al.*, 2016; Lionetto *et al.*, 2007; Kané *et al.*, 2003). Those conditions caused in reduction of pressure which break the gel along pipelines due to non-uniform gel formation (Wachs *et al.*, 2009; Sakthipriya et al., 2015).

As time goes on, the potential of blockage on the pipelines due to wax deposition will increase during transportation of crude oil along the pipelines from the oil rig to the shore. This problem may occur due to wax coagulation which will convert to wax crystals (Anisuzzaman *et. al.*, 2019; Anisuzzaman *et. al.*, 2018; Pendersen and Rønningsen, 2003). Since the precipitations along the pipelines will result in decreasing space of inner pipelines during transportation of crude oil, it may cause blockage of path. This blockage problem will affect the transportation, production processes and cost for maintenance of the industry (Coto *et al.*, 2014). Hence, in order to prevent or reduce the problem of wax deposition along the pipelines, few modifications of flow properties of the crude oil should be implemented.

Therefore, the objective of this study was to formulate a mixture of ethylene-vinyl acetate (EVA), MCH and paraxylene at different ratios and tested for flow properties improvement of crude oil viscosity. This study was conducted using EVA with two concentrations consisting of EVA 25 and EVA 40. Meanwhile, MCH was used as a solvent for the polymer and paraxylene as the asphaltene dispersant or inhibitor. Besides, this study was also conducted using response surface methodology (RSM) specifically central composite design (CCD) type to optimize percentage composition of the sample in order to enhance flow properties. According to previous research, RSM was used to study the effect of shear rates on improvement flow properties of crude oil.

MATERIALS AND METHODS

Materials and chemicals

The crude oil used in this study was Malaysian crude oil, specifically taken from Sabah platform. Malaysian crude oil generally has very little amount of wax but high content of asphaltene (Ridzuan *et al.*, 2016; Anisuzzaman *et al.*, 2017). In order to study the effect of concentration of

polymer on viscosity of crude oil, one copolymer being selected which is EVA with two concentrations consisting of EVA 25 and EVA 40.

Preparation of chemicals and crude oil

The crude oil was heated in an oven at 90^{o}C overnight to melt any primitively formed wax crystals and asphaltene agglomerates. The spindle of viscometer, measuring cylinder and pipette was heated first for about 60^{o}C to avoid the precipitation of wax at the point of contact between the hot crude oil and cold apparatus. Prior to mixing of inhibitor, EVA, MCH and paraxylene were heated in a water bath at 50^{o}C (Anisuzzaman *et. al.*, 2017 a,b).

Preparation of inhibitor

In the preparation of the inhibitor, the reaction was conducted at 90^{o}C. The individual chemicals, EVA, MCH and paraxylene were measured separately of its respective volume and weightage in accordance to manipulate percentage composition. The total volume of inhibitor used is 0.1 mL. Care was taken to replace the micropipette tube for the both chemicals to avoid contamination. Polymer was added with MCH and paraxylene and heated at 90℃ to melt the polymer. When the inhibitor has completely melted, the crude oil was poured into the measuring cylinder. The sample was shaken for about 30 seconds to allow the mixture of the inhibitor and crude oil. Then, the samples were placed in the oven for 15 min to allow the reaction to take place.

Experimental procedure

The rheological measurements were carried out using viscometer (Brookfield Programmable Viscometer DV-II + PRO) at fixed temperature which is 25.6^{o}C. The temperature of 25.6^{o}C was chosen to stimulate the real average temperature of the seabed. The amount of each chemical had been fixed to 0.3 g of total weight respectively. The crude oil was removed from the oven and allowed to decrease about 5^{o}C from initial temperature before measurement of viscosity using viscometer. Meanwhile, the rotational speed of spindle of viscometer also had been fixed to 100 rpm (Anisuzzaman *et. al.*, 2017 a,b).

Response surface methodology (RSM) modeling

In this work, CCD of RSM was used for data analysis (Bono *et. al.*, 2014, Torgut et al., 2017). The implementation of CCD was started with design of experiment, followed by data analysis. This method was used instead of one-to-one factor in order to reduce the number of experiments. A three level, three-factor CCD has been employed in order to obtain optimum composition for the reduction viscosity of crude oil. The factors or the independent variables studied were the percentage of EVA, percentage of MCH and percentage of paraxylene and the response was viscosity.

RESULTS AND DISCUSSION

In this study, total of experimental runs required suggested by CCD was 16 for each set. Weight and volume of each chemical was calculated in accordance to ratio given in order to find viscosity of each sample. The data obtained from CCD is shown in Table 1.

Table 1: Percentage ratio from central composite design (CCD)

Run	Factor 1 A: (MCH) (%)	Factor 2 B: (EVA) (%)	Factor 3 C: Paraxylene (%)
1	19.7858	51.4160	28.7985
2	79.9914	10.0000	10.0085
3	10.0000	42.5300	47.4700
4	45.7767	10.0000	44.2232
5	10.0000	10.0170	79.9827
6	23.1321	20.0060	56.8621
7	10.0000	42.5300	47.4700
8	31.1315	58.8680	10.0000
9	33.2855	33.3800	33.3342
10	49.1917	40.8080	10.0000
11	45.7767	10.0000	44.2232
12	10.3279	70.0000	19.6720
13	79.9914	10.0000	10.0085
14	58.2104	19.0331	22.7565
15	10.3279	70.0000	19.6720
16	10.0000	10.0172	79.9827

There were few properties observed to design good model for this study. The properties including design summary, model development, ANOVA, model graphs and analysis summary. For ANOVA, analysis included variance, fit statistics and coefficient of model of chemical proportion.

Model development

A quadratic model was used to express the responses as a function of independent variables. The test of statistical significance was performed on the total error criteria, with a confidence level of 95%. The significant terms in the model were found using analysis of variance (ANOVA) for each response. The adequacy of the model was confirmed using R^2 and the adjusted R^2 values. The numerical optimization techniques of the software were used for simultaneous optimization of the multiple responses. Under this optimization, the desired goals for each variable and response were chosen within a range.

The variables and responses of viscosity obtained from experiments are listed in Tables 2 and 3. The experimental data were used to calculate the coefficients of the quadratic equation. The ANOVA of each case and the diagnostic plot was presented. Based on ANOVA analysis, RSM stated that the data entry was valid since most of the requirements to get good model were achieved. For variance, the p-value should be less than 0.005 while Lack of Fit value should be greater than 0.1. For fit statistics, value of R^2 should not be less than 0.75 and adjusted R^2 should have similarly high value to R^2. In addition, adjusted R^2 and predicted R^2 should be within 0.2.

Table 2: Data entry in RSM for proportion of EVA 25, MCH and paraxylene

Run	Factor 1 A: (MCH) (%)	Factor 2 B: (EVA) (%)	Factor 3 C: Paraxylene (%)	Response 1 Viscosity
1	19.7858	51.4160	28.7985	12
2	79.9914	10.0000	10.0085	6
3	10.0000	42.5300	47.4700	12
4	45.7767	10.0000	44.2232	6
5	10.0000	10.0170	79.9827	6
6	23.1321	20.0060	56.8621	12
7	10.0000	42.5300	47.4700	12
8	31.1315	58.8680	10.0000	12
9	33.2855	33.3800	33.3342	12
10	49.1917	40.8080	10.0000	6
11	45.7767	10.0000	44.2232	6
12	10.3279	70.0000	19.6720	12
13	79.9914	10.0000	10.0085	6
14	58.2104	19.0331	22.7565	6
15	10.3279	70.0000	19.6720	12
16	10.0000	10.0172	79.9827	12

Table 3: Data entry in RSM for proportion of EVA 40, MCH and paraxylene

Run	Factor 1 A: (MCH) (%)	Factor 2 B: (EVA) (%)	Factor 3 C: Paraxylene (%)	Response 1 Viscosity
1	19.7858	51.4160	28.7985	18
2	79.9914	10.0000	10.0085	18
3	10.0000	42.5300	47.4700	6
4	45.7767	10.0000	44.2232	12
5	10.0000	10.0170	79.9827	6
6	23.1321	20.0060	56.8621	12
7	10.0000	42.5300	47.4700	6
8	31.1315	58.8680	10.0000	12
9	33.2855	33.3800	33.3342	6
10	49.1917	40.8080	10.0000	12
11	45.7767	10.0000	44.2232	6
12	10.3279	70.0000	19.6720	12
13	79.9914	10.0000	10.0085	6
14	58.2104	19.0331	22.7565	6
15	10.3279	70.0000	19.6720	12
16	10.0000	10.0172	79.9827	6

Statistical analysis of the design model

Table 4 shows the analysis of variance of proportion MCH, EVA 25 and paraxylene. On the other hand, Table 5 shows the analysis of variance of proportion MCH, EVA 40 and paraxylene.

Table 4: Analysis of variance of proportion MCH, EVA 25 and paraxylene

Source	Sum of squares	df	Mean square	F-value	p-value	
Model	372.62	3	124.21	39.45	<0.0001	significant
A-MCH	12.58	1	12.58	4.00	0.0629	
B-EVA 25	245.58	1	245.58	77.99	<0.0001	
C-paraxylene	118.68	1	118.68	37.69	<0.0001	
Residual	50.38	16	3.15			
Lack of fit	32.38	8	4.05	1.80	0.2120	not significant
Pure error	18.00	8	2.25			
Cor total	423.00	19				

Table 5: Analysis of variance of proportion MCH, EVA 40 and paraxylene

Source	Sum of squares	df	Mean square	F-value	p-value	
Model	366.90	3	122.30	9.05	0.0010	significant
A-MCH	162.34	1	162.34	12.01	0.0032	
B-EVA 40	215.41	1	15.93	15.93	0.0011	
C-paraxylene	20.62	1	1.53	1.53	0.2346	
Residual	216.30	16				
Lack of fit	126.30	8	1.40	1.40	0.3215	not significant
Pure error	90.00	8				
Cor total	583.20	19				

Based on analysis in table 4, model F-value of 39.45 implies the model is significant. For p-value, the model is significant because the value is less than 0.005. In first proportion, EVA 25 and paraxylene are significant model terms. Meanwhile, MCH is not significant since the value is greater than 0.1. For lack of fit, F-value, the good model is a non-significant. From the result, the lack of fit, F-value is 1.80 which the value implied not significant relative to pure error. For second proportion analysis, model F-value of 9.05 implies the model is significant (Table 5). For p-value, the model is significant because the value is less than 0.005. In this experiment, MCH and EVA 40 are significant model terms. Meanwhile, paraxylene is not significant since the value is greater than 0.1. For lack of fit, F-value, the good model is a non-significant. From the result, the lack of fit, F-value is 1.40 which the value implied not significant relative to pure error.

Tables 6 and 7 showed the fit statistics for proportion MCH, EVA 25 and paraxylene and MCH, EVA 40 and paraxylene, respectively.

Table 6: Fit statistics for proportion MCH, EVA 25 and paraxylene

Standard deviation	1.77	R^2	0.8809
Mean	7.50	Adjusted R^2	0.8586
Coefficient of variation (%)	23.66	Predicted R^2	0.8046
		Adequate precision	16.2558

Table 7: Fit statistics for proportion MCH, EVA 40 and paraxylene

Standard deviation	3.68	R^2	0.6291
Mean	7.80	Adjusted R^2	0.5596
Coefficient of variation (%)	47.14	Predicted R^2	0.4242
		Adequate precision	7.5073

Based on both fit statistics above, the first proportion showed that R^2 value of 0.8809, indicating that the model can explain 88.09% of the data variation and only 11.91% of total variations were not explained by the model. R^2 value should not be less than 0.75 (Le Man *et al.*, 2010). According to Koocheki *et al.* (2009), the model can be a good one if value of adjusted R^2 is a similarly high value. Furthermore, adjusted R^2 and predicted R^2 should be within 20% to be in reasonable agreement (Rai *et al.*, 2016). For first proportion, adjusted R^2 value is 0.8586 while predicted R^2 value is 0.8046. Therefore, the model is highly significant because the experimental and predicted values of monomer conversion are in a good agreement. For second proportion, R^2 value was 0.6291. This model can explain 62.91% of the data variation and only 37.09% of total variations were not explained. In this experiment, adjusted R^2 value is 0.6291 while predicted R^2 value is 0.4242. The model is highly significant too because the experimental and predicted values of monomer conversion are in a good agreement.

Tables 8 and 9 show the coefficient of model of proportion MCH, EVA 25 and paraxylene and MCH, EVA 40 and paraxylene, respectively

Table 8: Coefficient of model of proportion MCH, EVA 25 and paraxylene

Coefficient of model	Equation
Actual	Viscosity = -3.553 ×10-6 + 0.0312A +0.1517B +0.0993C
Coded	Viscosity = 14.14+ 1.60A +7.58B + 4.96C

Table 9: Coefficient of model of proportion MCH, EVA 40 and paraxylene

Coefficient of model	Equation
Actual	Viscosity = -9.88 ×10^{-6}+ 0.1146A +0.1421+0.0414C
Coded	Viscosity = 14.90+ 5.73 +7.10B + 2.07C

The coded equation used to identify the relative impact of the factors by comparing the factor coefficients. Meanwhile, actual equation make predictions about the response for given levels of each factor. The positive signs in the models signify synergetic effects of factor while the negative sign indicates antagonistic effect.

Model graphs

Figure 1 (a, b) shows the contour plot of viscosity (%) vs EVA 25 (%), MCH (%) and EVA 40 (%), MCH (%), respectively. The contour plot depicted that the optimum ratio was determined by mixture of high percentage of paraxylene, low percentage of EVA 25 and low percentage of MCH. Based on Figure 1 (b), contour plot of second proportion, the optimum ratio was determined by mixture of medium percentage of paraxylene, low percentage of EVA 40 and medium percentage of MCH.

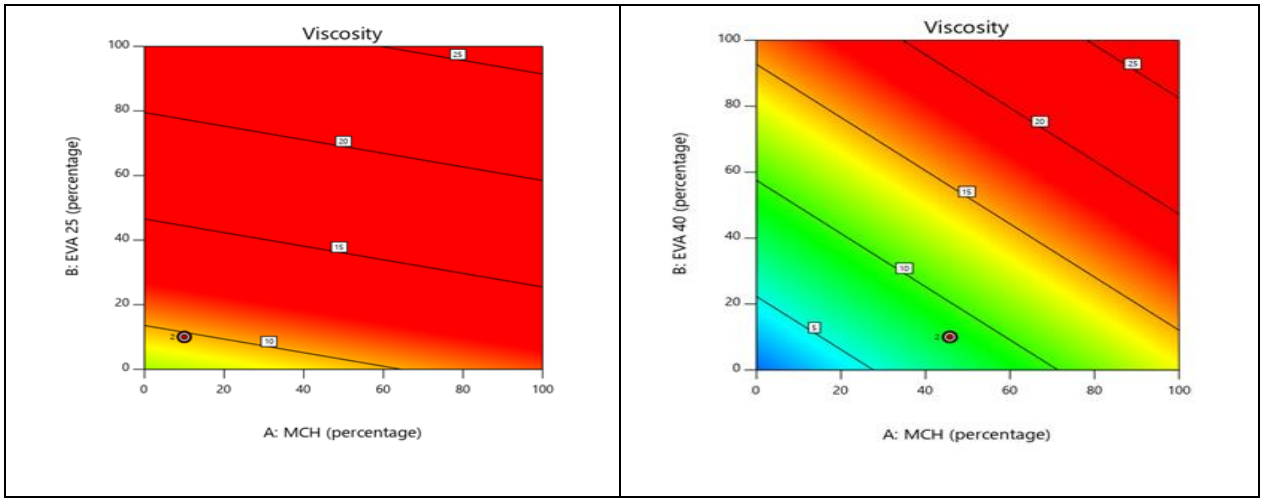

(a) (b)

Figure 1: Contour plot of viscosity (%) vs (a) EVA 25 (%), MCH (%) (b) EVA 40 (%), MCH (%)

Figure 2 (a,b) shows 3D graphs for optimization EVA 25, MCH and paraxylene and EVA 40, MCH and paraxylene, respectively. Figure 2 (a) depicted the 3D graphs for first proportion based on result of contour plot. For optimization, CCD selected experimental run 16 as the optimum ratio to obtain minimum viscosity of crude oil which is 6.0 cP.

Figure 2 (b) depicted the 3D graphs for first proportion based on result of contour plot. For optimization, CCD selected experimental run 4 as the optimum ratio to obtain minimum viscosity of crude oil which is also 6.0 cP.

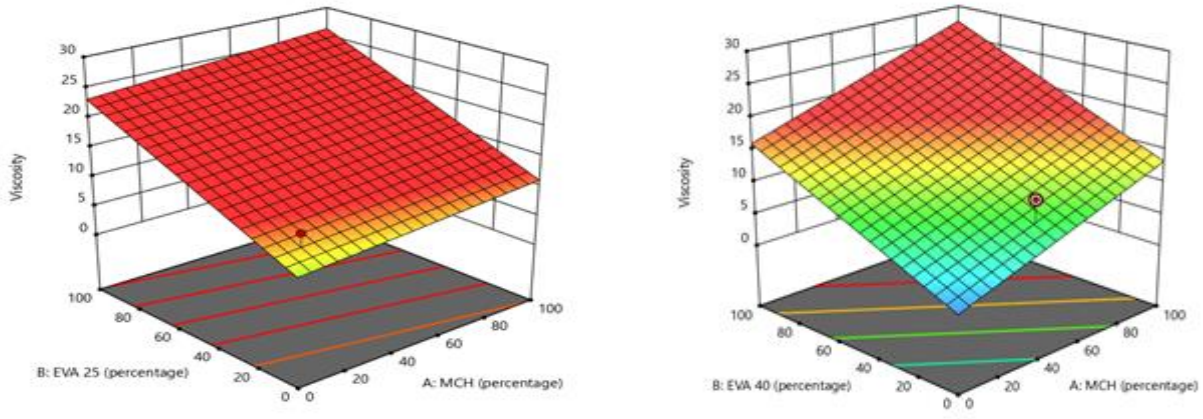

(a) (b)

Figure 2: 3D graphs for optimization (a) EVA 25, MCH and paraxylene (b) EVA 40, MCH and paraxylene

Based on Figures 1 and 2, for first proportion, contour plots and 3D graphs depicted that high percentage of paraxylene with low percentage of EVA and low percentage of MCH lead to low viscosity value. Meanwhile for second proportion, lowest viscosity value can be obtained with medium percentage of paraxylene with low percentage of EVA and medium percentage of MCH. This can be observed through the design point location in four figures above where it located far away from red area which signify high viscosity. For optimization, CCD selected experimental run 16 in first proportion consist of 10.02% of EVA 25, 10.00% of MCH and 79.98% of paraxylene as the optimum ratio for reduction of crude oil viscosity. The viscosity obtained was 6.0 cP. Meanwhile, optimum ratio for second proportion was 10.00% of EVA 40, 45.78% of MCH and 44.22% of paraxylene which in experimental run 4. The viscosity obtained was also same with first proportion which was 6.0 cP. Both of these values had desirability value of 1 which signified the most desirable predicted responses on the dependent variables.

CONCLUSIONS

CCD in RSM had provided valid ratio for chemical proportion consists of EVA 25 and EVA 40, MCH and paraxylene. The validity has been tested during analysis in RSM since the model obtained was significant in both proportions. Every ratio formulated by CCD has been tested in order to find optimum ratio for viscosity reduction of crude oil. Based on analysis in RSM, the optimum viscosity

value which is 6.0 cP which can be obtained from proportion of high percentage of paraxylene, low percentage of EVA and low percentage of MCH for first proportion. For second proportion, the optimum viscosity value was also same with first proportion which was 6.0 cP. The value can be obtained from proportion of medium percentage of paraxylene with low percentage of EVA and medium percentage of MCH. The optimum parameters were 10.02% of EVA 25, 10.00% of MCH and 79.98% of paraxylene for first proportion and 10.00% of EVA 40, 45.78% of MCH and 44.22% of paraxylene for second proportion to minimize the viscosity of crude oil. The obtained quadratic regression model is very adequate based on ANOVA test. For comparison between experimental optimization and RSM optimization, the data obtained depicted that both optimization has value of 6.0 cP as the optimum value for viscosity reduction of crude oil. In conclusion, in this study RSM specifically CCD type was used to optimize percentage composition of the sample in order to enhance flow properties and transportation of crude oil.

ACKNOWLEDGEMENTS

The authors would like to express greatest appreciation to the Centre of Research and Innovation (PPI), Universiti Malaysia Sabah (UMS) for the support to this study (Grant No. **SBK0346-2017**).

REFERENCES

Aiyejina, A., Chakrabarti, D. P., Pilgrim, A. & Sastry, M. K. S. 2011. Wax formation in oil pipelines: A critical review. International Journal of Multiphase Flow, 37(7), 671-694.

Anisuzzaman, S. M., Krishnaiah, D. & Madsah, M. 2019. Effect of various polymeric crystal modifiers and solvents formulations on the prevention of wax and asphaltene formation in crude oil pipelines. Petroleum & Petrochemical Engineering Journal, 3(2), 1-10.

Anisuzzaman, S. M., Yeow W. F. & Madsah, M. 2018. A review on various techniques and recent advances in polymeric additives to mitigate wax problems in crude oil. Journal of Advanced Research in Fluid Mechanics and Thermal Sciences, 48(1), 53-64.

Anisuzzaman, S. M., Abang, S., Bono, A., Krishnaiah, D., Karali, R. & Safuan, M. K. 2017. Wax inhibitor based on ethylene vinyl acetate with methyl methacrylate and diethanolamine for crude oil pipeline. IOP Conference Series: Materials Science and Engineering, 206(012074), 1-8.

Anisuzzaman, S. M., Abang, S., Bono, A., Krishnaiah, D., Ismail, N. M. & Sandrison, G. B. 2017. An evaluation of solubility of wax and asphaltene in crude oil for improved flow properties using a copolymer solubilized in organic solvent with an aromatic hydrocarbon. International Journal of Chemical and Molecular Engineering, 11(10), 688-695.

Ariza-León, E., Molina-Velasco, D. R. & Chaves-Guerrero, A. 2014. Review of studies on asphaltene - wax interaction and the effect thereof on crystallization. *CT&F - Ciencia, Tecnología y Futuro*, 5(5), 39-53.

Bai, C. & Zhang, J. 2013. Effect of carbon number distribution of wax on the yield stress of waxy oil gels. Industrial & Engineering Chemistry Research, 52(7), 2732-2739.

Bono, A., Anisuzzaman, S. M., & Ding, O. W. 2014. Effect of process conditions on the gel viscosity and gel strength of semi-refined carrageenan (SRC) produced from seaweed (Kappaphycus alvarezii). Journal of King Saud University Engineering Sciences, 26(1), 3-9.

Chala, G. T., Sulaiman, S. A., Japper-Jaafar, A. & Kamil, W. A. 2015. Study on influence of flow rates on voids in waxy crude oil subjected to dynamic and static cooling. Journal of Mechanical Engineering and Sciences, 9, 1586-1594.

Chala, G. T., Sulaiman, S. A., Japper-Jaafar, A. & Kamil W. A. 2016. Investigation of convective heat transfer coefficient and initial temperature of waxy crude oil on the formation of voids. International Journal of Automotive & Mechanical Engineering, 13(3), 3754-3762.

Coto, B., Martos, C., Espada, J. J., Robustillo, M. D. & Peña, J. L. 2014. Experimental study of the effect of inhibitors in wax precipitation by different techniques. Energy Science and Engineering, 2(4), 196-203.

Kané, M., Djabourov, M., Volle, J. L. , Lechaire, J. P. & Frebourg, G. 2003. Morphology of paraffin crystals in waxy crude oils cooled in quiescent conditions and under flow. Fuel, 82(2), 127-135.

Koocheki, A., Taherian, A.R., Razavi, S. & Bostan, A. 2009. Response surface methodology for optimization of extraction yield, viscosity, hue and emulsion stability of mucilage extracted from Lepidium perfoliatum seeds. Food Hydrocolloids 23(8), 2369-2379.

Kralova, I., Sjöblom, J., Øye, G., Simon, S., Grimes, B. A. & Paso, K. 2011. Heavy crude oils/particle stabilized emulsions. Advances in Colloid and Interface Science, 169(2), 106-127.

Le Man, H., Behera, S. K. & Park, H.S. 2010. Optimization of operational parameters for ethanol production from Korean food waste leachate. International Journal of Environmental Science & Technology, 7(1), 157-164.

Lionetto, F., Coluccia, G., D'Antona, P. & Maffezzoli, A. 2007. Gelation of waxy crude oils by ultrasonic and dynamic mechanical analysis. Rheologica Acta, vol. 46(5), 601-609.

Luthi, I. F. 2013. Waxy crude oil characterization and experimental study of the restart of a line blocked with gelled waxy crude. SPE Annual Technical Conference and Exhibition, Lousiana, USA, 5433-5443.

Oh, K., Jemmett, M. & Deo, M. 2009. Yield behaviour of gelled waxy oil: Effect of stress application in creep ranges. Industrial & Engineering Chemistry Research, 48(19), 8950-8953.

Pendersen K.S & Rønningsen H.P. 2003. Influence of wax inhibitors on wax appearance temperature, pour point and viscosity of waxy crude oils. Energy Fuels 17(2), 321-328.

Ridzuan, N., Adam, F., & Yaacob, Z. 2016. Evaluation of the inhibitor selection on wax deposition for Malaysian crude oil. Petroleum Science and Technology, 34(4), 366-371.

Sakthipriya, N., Doble, M. & Sangwai, J. S. 2015. Fast degradation and viscosity reduction of waxy crude oil and model waxy crude oil using *Bacillus subtilis*. Journal of Petroleum Science and Engineering, 134, 158-166.

Torgut, G., Tanyol, M., Biryan, F., Pihtili, G., & Demirelli, K. 2017. Application of response surface methodology for optimization of Remazol Brilliant Blue R removal onto a novel polymeric adsorbent. Journal of the Taiwan Institute of Chemical Engineers, 80, 406-414.

Wachs, A., Vinay, G. & Frigaard, I. 2009. A 1.5D numerical model for the start-up of weakly compressible flow of a viscoplastic and thixotropic fluid in pipelines, Journal of Non-Newtonian Fluid Mechanics, 159(1-3), 81-94.

Yao, B., Li, C., Yang, F., Zhang, Y., Xiao, Z. & Sun, G. 2016. Structural properties of gelled Changqing waxy crude oil benefitted with nanocomposite pour point depressant. Fuel, 184, 544-554.